IAEA-TECDOC-1705

Passive Safety Systems in Advanced Water Cooled Reactors (AWCRs)

Case Studies

A Report of the International Project on Innovative Nuclear Reactors and Fuel Cycles (INPRO)

IAEA
International Atomic Energy Agency

PASSIVE SAFETY SYSTEMS IN ADVANCED WATER COOLED REACTORS (AWCRs)

The following States are Members of the International Atomic Energy Agency:

AFGHANISTAN
ALBANIA
ALGERIA
ANGOLA
ARGENTINA
ARMENIA
AUSTRALIA
AUSTRIA
AZERBAIJAN
BAHRAIN
BANGLADESH
BELARUS
BELGIUM
BELIZE
BENIN
BOLIVIA
BOSNIA AND HERZEGOVINA
BOTSWANA
BRAZIL
BULGARIA
BURKINA FASO
BURUNDI
CAMBODIA
CAMEROON
CANADA
CENTRAL AFRICAN REPUBLIC
CHAD
CHILE
CHINA
COLOMBIA
CONGO
COSTA RICA
CÔTE D'IVOIRE
CROATIA
CUBA
CYPRUS
CZECH REPUBLIC
DEMOCRATIC REPUBLIC OF THE CONGO
DENMARK
DOMINICA
DOMINICAN REPUBLIC
ECUADOR
EGYPT
EL SALVADOR
ERITREA
ESTONIA
ETHIOPIA
FIJI
FINLAND
FRANCE
GABON
GEORGIA
GERMANY
GHANA
GREECE
GUATEMALA
HAITI
HOLY SEE
HONDURAS
HUNGARY
ICELAND
INDIA
INDONESIA
IRAN, ISLAMIC REPUBLIC OF
IRAQ
IRELAND
ISRAEL
ITALY
JAMAICA
JAPAN
JORDAN
KAZAKHSTAN
KENYA
KOREA, REPUBLIC OF
KUWAIT
KYRGYZSTAN
LAO PEOPLE'S DEMOCRATIC REPUBLIC
LATVIA
LEBANON
LESOTHO
LIBERIA
LIBYA
LIECHTENSTEIN
LITHUANIA
LUXEMBOURG
MADAGASCAR
MALAWI
MALAYSIA
MALI
MALTA
MARSHALL ISLANDS
MAURITANIA
MAURITIUS
MEXICO
MONACO
MONGOLIA
MONTENEGRO
MOROCCO
MOZAMBIQUE
MYANMAR
NAMIBIA
NEPAL
NETHERLANDS
NEW ZEALAND
NICARAGUA
NIGER
NIGERIA
NORWAY
OMAN
PAKISTAN
PALAU
PANAMA
PAPUA NEW GUINEA
PARAGUAY
PERU
PHILIPPINES
POLAND
PORTUGAL
QATAR
REPUBLIC OF MOLDOVA
ROMANIA
RUSSIAN FEDERATION
RWANDA
SAUDI ARABIA
SENEGAL
SERBIA
SEYCHELLES
SIERRA LEONE
SINGAPORE
SLOVAKIA
SLOVENIA
SOUTH AFRICA
SPAIN
SRI LANKA
SUDAN
SWAZILAND
SWEDEN
SWITZERLAND
SYRIAN ARAB REPUBLIC
TAJIKISTAN
THAILAND
THE FORMER YUGOSLAV REPUBLIC OF MACEDONIA
TOGO
TRINIDAD AND TOBAGO
TUNISIA
TURKEY
UGANDA
UKRAINE
UNITED ARAB EMIRATES
UNITED KINGDOM OF GREAT BRITAIN AND NORTHERN IRELAND
UNITED REPUBLIC OF TANZANIA
UNITED STATES OF AMERICA
URUGUAY
UZBEKISTAN
VENEZUELA
VIETNAM
YEMEN
ZAMBIA
ZIMBABWE

The Agency's Statute was approved on 23 October 1956 by the Conference on the Statute of the IAEA held at United Nations Headquarters, New York; it entered into force on 29 July 1957. The Headquarters of the Agency are situated in Vienna. Its principal objective is "to accelerate and enlarge the contribution of atomic energy to peace, health and prosperity throughout the world''.

IAEA-TECDOC-1705

PASSIVE SAFETY SYSTEMS IN ADVANCED WATER COOLED REACTORS (AWCRs)

CASE STUDIES

A REPORT OF THE INTERNATIONAL PROJECT ON
INNOVATIVE NUCLEAR REACTORS AND FUEL CYCLES (INPRO)

INTERNATIONAL ATOMIC ENERGY AGENCY
VIENNA, 2013

For further information on this publication, please contact:

Division of Nuclear Power – INPRO Group
International Atomic Energy Agency
Vienna International Centre
PO Box 100
1400 Vienna, Austria
Email: Official.Mail@iaea.org

Printed by the IAEA in Austria
September 2013

IAEA Library Cataloguing in Publication Data

Passive safety systems in advanced water cooled reactors (AWCRs) : case studies – Vienna : International Atomic Energy Agency, 2013.
p. ; 30 cm. – (IAEA-TECDOC series, ISSN 1011-4289 ; no. 1705)
ISBN 978-92-0-139810-9
Includes bibliographical references.

1. Nuclear power plants – Design and construction. 2. Nuclear reactors – Cooling. 3. Water cooled reactors – Safety measures. I. International Atomic Energy Agency. II. Series.

IAEAL 13-00837

FOREWORD

The International Project on Innovative Nuclear Reactors and Fuel Cycles (INPRO) was launched in 2000, on the basis of IAEA General Conference resolution GC(44)/RES/21. INPRO helps to ensure that nuclear energy is available to contribute to meeting the global energy needs of the 21st century in a sustainable manner. INPRO seeks to bring together nuclear technology holders and users to jointly consider international and national actions for desired innovations in nuclear reactors, fuel cycles and institutional approaches. As of September 2012, its members consisted of 37 countries and the European Commission.

Public concern about nuclear reactor safety has increased since the accident at TEPCO's Fukushima Daiichi nuclear power plant in 2011, which involved the loss of power to pump water for removing residual heat from the core. As a consequence, there has been special interest in designing safety systems for developing new and advanced reactors that are passive in nature. Unlike active systems, passive safety systems do not require operator intervention or active controls, relying only on physical phenomena such as natural circulation, convection, gravity and self-pressurization. The advantages of passive safety systems include simplicity and avoidance of human intervention, external power or signals. Passive safety systems, therefore, are increasingly recognized as an essential component of next generation advanced reactors.

Since 1991, the IAEA has made continuous efforts to improve the economics and safety of water cooled reactors through a variety of activities on passive safety systems. Among these efforts is the collaborative project on 'Advanced Water Cooled Reactor Case Studies in Support of Passive Safety Systems' (AWCR), implemented by the IAEA in 2008.

The AWCR collaborative project focuses on case studies of natural circulation and thermal stratification phenomena. More specifically, the project investigates important phenomena associated with these features, including stability, self-pressurization and thermal stratification over a wide range of operating conditions. The reactor systems concerned are the advanced heavy water reactor (AHWR) (India), CAREM-25 pressurized water reactor (PWR) (Argentina) and advanced power reactor plus (APR+) (Republic of Korea).

The objective of this publication is to report on the state of the art knowledge associated with natural circulation phenomena, thermal stratification relevant to the performance of the selected nuclear reactor systems and assessment of analytical tools to predict the performance of such systems. This report is intended for technical experts and scientists working in the area of advanced nuclear reactor design.

The IAEA would like to thank the participants from Argentina, India and the Republic of Korea for their contributions to the project. The IAEA officers responsible for this publication were S.B. Kim, H. Khartabil, and P.H. Park of the Division of Nuclear Power.

EDITORIAL NOTE

This publication (including the figures, tables and references) has undergone only the minimum copy editing considered necessary for the reader's assistance.

The views expressed do not necessarily reflect those of the IAEA, the governments of the nominating Member States or the nominating organizations.

The use of particular designations of countries or territories does not imply any judgement by the publisher, the IAEA, as to the legal status of such countries or territories, of their authorities and institutions or of the delimitation of their boundaries.

The mention of names of specific companies or products (whether or not indicated as registered) does not imply any intention to infringe proprietary rights, nor should it be construed as an endorsement or recommendation on the part of the IAEA.

The authors are responsible for having obtained the necessary permission for the IAEA to reproduce, translate or use material from sources already protected by copyrights.

The IAEA has no responsibility for the persistence or accuracy of URLs for external or third party Internet web sites referred to in this book and does not guarantee that any content on such web sites is, or will remain, accurate or appropriate.

CONTENTS

SUMMARY

This report presents the results from the International Project on Innovative Nuclear Reactors and Fuel Cycles (INPRO) collaborative project (CP) on Advanced Water Cooled Reactor Case Studies in Support of Passive Safety Systems (AWCR), undertaken under the INPRO Programme Area C. INPRO was launched in 2000 — on the basis of a resolution of the IAEA General Conference (GC(44)/RES/21) — to ensure that nuclear energy is available in the 21st century in a sustainable manner, and it seeks to bring together all interested Member States to consider actions to achieve innovation. An important objective of nuclear energy system assessments is to identify 'gaps' in the various technologies and corresponding research and development (R&D) needs. This programme area fosters collaboration among INPRO Member States on selected innovative nuclear technologies to bridge technology gaps.

Public concern about nuclear reactor safety has increased after the Fukushima Daiichi nuclear power plant accident caused by the loss of power to pump water for removing residual heat in the core. As a consequence, there has been an increasing interest in designing safety systems for new and advanced reactors that are passive in nature. Compared to active systems, passive safety features do not require operator intervention, active controls, or an external energy source. Passive systems rely only on physical phenomena such as natural circulation, thermal convection, gravity and self-pressurization. Passive safety features, therefore, are increasingly recognized as an essential component of the next-generation advanced reactors.

A high level of safety and improved competitiveness are common goals for designing advanced nuclear power plants. Many of these systems incorporate several passive design concepts aimed at improving safety and reliability. The advantages of passive safety systems include simplicity, and avoidance of human intervention, external power or signals. For these reasons, most advanced type of reactors have adopted passive safety systems such as gravity driven water pool, isolation condenser, accumulator and other passive heat removal systems.

Since 1991, the IAEA has made various efforts to improve economics, safety, and reliability of evolutionary or innovative reactors through the implementation of a variety of activities related to passive safety systems. In particular, the coordinated research programme (CRP) launched in 2004, titled *Natural Circulation Phenomena, Modelling and Reliability of Passive Systems*, focused on the use of passive safety systems in new generation of nuclear power plants. Following this CRP, the IAEA supported the implementation of the collaborative project on *Advanced Water Cooled Reactor (AWCR) Case Studies in Support of Passive Safety Systems* launched in 2008.

The objectives of the current collaborative project were to investigate natural circulation phenomena related to the selected AWCR systems, such as: (1) steady state, stability and startup of single-phase and two-phase natural circulation reactor systems, and (2) theoretical and experimental studies on mixing and stratification in large water pools with immersed heat exchangers. The reactor systems concerned are the advanced heavy water reactor (AHWR) of India, the Central Argentina de Elementos Modulares (CAREM-25) of Argentina, and the advanced power reactor plus (APR+) of the Republic of Korea.

During the past three years, India, Argentina, and the Republic of Korea have actively participated in implementing this project and, according to the terms of reference, each country has successfully conducted an assigned case study associated with natural circulation and thermal stratification phenomena. In-depth review and discussion on case study results

were made at the final consultants meeting held in December 2011 at the IAEA Headquarters in Vienna, Austria during which the final report was also reviewed.

In order to simulate the AHWR main heat transport system, an integral test loop (ITL) was set up at Bhabha Atomic Research Centre (BARC) and the stability state of the ITL was investigated and experiments were conducted in ITL simulating the startup procedure for different powers and pressures. In the CAREM-25 study, investigations were carried out on: a neutronic feedback mechanism using a point kinetic neutronic model, pressure feedback and self-pressurization effect, flow modelling, flashing effect, transient simulations, etc. The case study of APR+ has focused on preliminary performance analysis of a passive auxiliary feedwater system (PAFS) using RELAP5/Mod3.3 codes, computerized fluid dynamics (CFD) analysis on natural convection in a pool, and separate effect tests on PAFS.

Major findings and conclusions of the AWCR case studies are the following:

- All mechanical devices considered are able to suppress the instability in the loop and especially the spool piece with helical coil and bellow. It can be concluded that the helical coil is an effective tool to suppress instability in single-phase natural circulation systems.

- The instabilities get suppressed in both single-phase and two-phase natural circulation systems in the presence of nanoparticles in the water. The increase in the loop flow rate in the presence of nanoparticles was found to be proportional to the concentration of nanoparticles.

- A wide area in the stability map has been detected at condensation power values close to 0.75 MW in which the stability margins are considerably incremented. This region offers excellent conditions to guarantee the reactor stability for a wide range of operation conditions.

- The use of fewer shrouds gives a higher flow rate and improved inventory utilization but multidimensional effects are not accounted for in RELAP5 code simulation. Therefore, further studies on the shroud effect based on integral simulation with isolation condenser system (ICS) and CFD simulation are required.

- As per simple analyses using CFX code and the separate effect tests, a horizontal heat exchanger shows better performance regarding thermal stratification in large pools. The reason is that the horizontal heat exchanger provides a greater driving force for natural convection and hence higher circulation rates than a vertical heat exchanger.

1. INTRODUCTION

1.1. BACKGROUND

This report documents the results of the IAEA/INPRO collaborative project on *Advanced Water Cooled Reactor Case Studies in Support of Passive Safety Systems* (AWCR).

A high level of safety and improved competitiveness are common goals for designing advanced nuclear power reactors. Thus, continuing international efforts to enhance the safety and economic competitiveness of nuclear reactor systems have led to the development of a number of advanced water cooled reactors (AWCRs). Many of these systems incorporate several passive design concepts for improving safety reliability and reactor economics. The advantages of passive systems include simplicity, and avoidance of human intervention and external power. For these reasons, most advanced types of reactors have adopted such innovative features as a gravity driven water pool, an isolation condenser, an accumulator, and a passive heat removal system.

Against this backdrop, the IAEA has made continuous efforts since 1991 to improve the safety and economics of the AWCR by performing a variety of activities on passive safety systems. In particular, it is worth mentioning the coordinated research programme (CRP) launched in early 2004 titled *Natural Circulation Phenomena, Modelling and Reliability of Passive Systems* [1]. Since 2008, following this CRP, as a part of the activities of INPRO, the IAEA has been supporting the implementation of the AWCR collaborative project.

1.2. OBJECTIVE

The objectives of this project are to investigate natural circulation phenomena relevant to selected AWCR systems[1] such as:

- startup and stability of single-phase natural circulation reactor systems and two-phase natural circulation with immersed heat exchangers (AHWR, CAREM-25);

- theoretical and experimental studies on mixing and stratification in large water pools with immersed heat exchangers (AHWR, APR+).

1.3. SCOPE

The AWCR collaborative project deals with case studies of natural circulation and thermal stratification phenomena. In comparison to the previous CRP, this project focuses on innovative features such as natural circulation for core heat removal under normal, startup and shutdown conditions, and thermohydraulic phenomena in large pools to serve as heat sinks. More specifically, this collaborative project intends to investigate important phenomena associated with these features, including stability, self-pressurization, and thermal stratification over a wide range of operating conditions. Also, the theoretical models and experimental test facilities set up for evaluating such phenomena have been assessed.

[1] Selected reactor systems are the advanced heavy water reactor (AHWR), the advanced power reactor plus (APR+), and the Central Argentina de Elementos Modulares-25 (CAREM-25).

The concerned reactor systems for case studies are as follows: the advanced heavy water reactor (AHWR) of India and the Central Argentina de elementos modulares (CAREM-25) of Argentina for natural circulation phenomenon related case studies; and the advanced power reactor plus (APR+) of the Republic of Korea and also the AHWR of India for the thermal stratification phenomenon related case studies.

The work scope and the specific activities in participating countries are the following:

- Argentina: investigate analytically the influence on stability of different phenomena and feedback mechanisms in an integral self-pressurized natural circulation nuclear reactor designed to work at low quality values.

- India: investigate stability of an integral test loop (ITL) with in-house codes based on linear and nonlinear methods; conduct experiments on the startup procedure of AHWR using ITL; and study thermal stratification phenomenon in ITL with the simulated isolation condenser system (ICS) of AHWR.

- Republic of Korea: verify overall performance of passive auxiliary feedwater system (PAFS) through separate effect test and develop a numerical model to best estimate thermohydraulic code such as MARS or RELAP5.

1.4. STRUCTURE

This report consists of four main sections and a conclusion along with this introduction. Section 2 looks at a brief description of concerned AWCRs, including the general system arrangement and main features of incorporated passive systems. Section 3 covers phenomena of common interest in the case studies on natural circulation and thermal stratification. Major issues in these studies are also identified. Section 4 looks at substantial experimental results on stable and unstable two-phase natural circulation shown in AHWRs and CAREM reactors respectively. Section 5 presents case study results on the thermal stratification in large water pools. Section 6 presents the major findings and conclusions drawn from these case studies.

2. BRIEF DESCRIPTION OF AWCRS CONSIDERED

2.1. ADVANCED HEAVY WATER REACTOR (AHWR)

The Indian nuclear power programme was formulated considering the vast reserves of thorium and moderate amount of uranium in the country. To ensure long-term availability of nuclear energy in a sustainable manner and taking cognizance of its resource position, India has followed the closed fuel cycle and formulated a three-stage nuclear power programme.

The first stage comprises the set up natural uranium fuelled pressurized heavy water reactors (PHWRs) and associated fuel cycle facilities. Fifteen units of 220 MW(e) capacity and two units of 540 MW(e) PHWR are now operational and the complete fuel cycle technology has been mastered. The second stage envisages the development of fast breeder reactors using plutonium obtained from reprocessing spent fuel of the first stage. A 40 MW(th) fast breeder test reactor has been operating since 1985, at Indira Gandhi Centre for Atomic Research (IGCAR) at Kalpakkam, India. Construction of the first 500 MW(e) prototype fast breeder reactor (PFBR) is in progress. The third stage aims at the development of reactors based on uranium-233 fuel obtained from irradiated thorium. Already, a U^{233} based research reactor is operating at Kalpakkam since 1996. To expedite transition to thorium based systems as envisaged in the third stage, an AHWRis being developed in the Bhabha Atomic Research Centre (BARC).

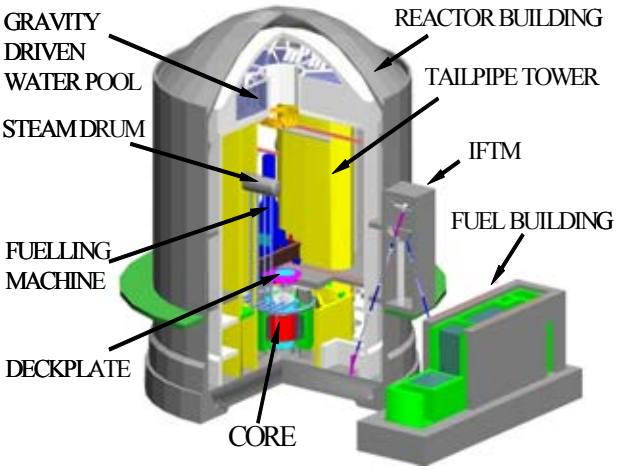

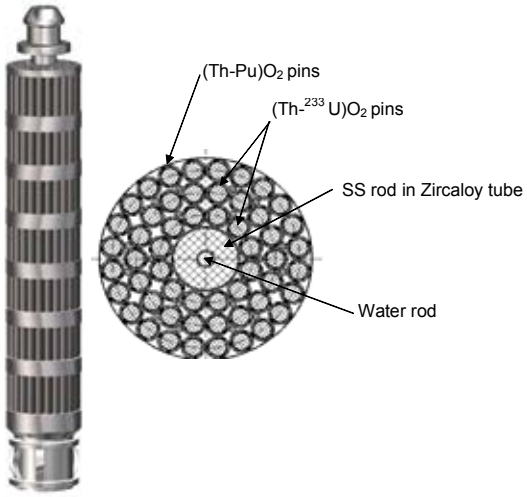

FIG. 1.(a) Schematic view of AHWR. *FIG. 1.(b) AHWR fuel cluster assembly.*

The AHWR [2] is a 300 MW(e), vertical, pressure tube type reactor cooled by boiling light water and moderated by heavy water (Fig. 1(a)). The reactor is fuelled with dual mixed oxide (MOX) fuel consisting of (^{233}U-Th)O_2 and (Pu-Th)O_2. AHWR is nearly self-sustaining in ^{233}U. The design of an AHWR is fine-tuned towards deriving two-thirds of its power from thorium based fuel, while achieving negative void coefficient of reactivity. Another version of an AHWR, known as the AHWR-low enriched uranium (LEU), fuelled with (LEU-Th)O_2 is also being designed.

The fuel assembly is suspended from the top in the coolant channel of the reactor. The assembly consists of a single long fuel cluster and two shield sub-assemblies. The cluster has 54 fuel pins arranged in three concentric rings, 12 pins in the inner ring, 18 pins in the intermediate ring and 24 pins in the outer ring, around a central structural tube made of zircaloy. The 24 fuel pins in the outer ring have (Th-Pu)O_2 fuel and the 30 fuel pins in the inner and intermediate rings have (Th-^{233}U)O_2 fuel. Figure 1(b) shows AHWR fuel cluster assembly.

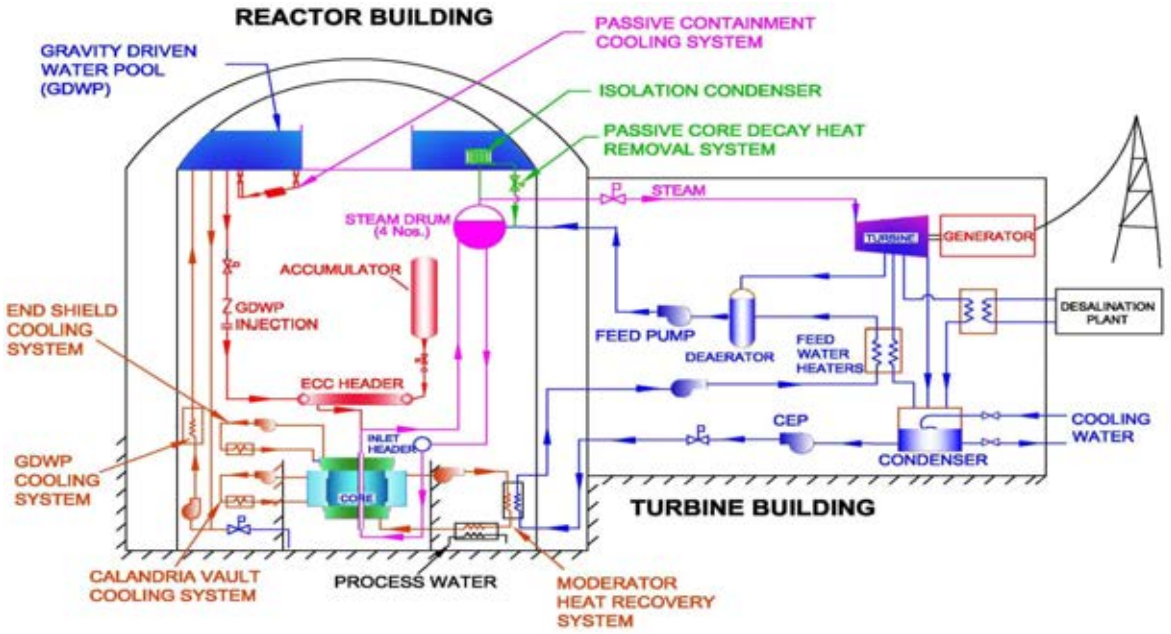

FIG. 2. General arrangement of AHWR.

Heat is removed from the core by natural circulation of coolant. The general arrangement of the AHWR is shown in Fig. 2. The core comprises vertical fuel channels housed inside calandria tubes which, in turn, are installed in a calandria vessel containing the moderator. The calandria vessel is located in a water filled reactor cavity. The core is connected to four steam drums through a large number of riser pipes. A large gravity driven water pool (GDWP) is located near the top of the containment. The GDWP acts as heat sink for a number of systems. Moderator heat is used for feed water heating. As shown in Fig. 2, a double containment system is adopted as part of the defence-in-depth philosophy to prevent any release of radioactivity to environment.

The AHWR incorporates several advanced passive features to increase its safety, reliability, and economics, namely:

- natural circulation heat removal under normal operation and shutdown conditions;
- low core power density and slightly negative void coefficient of reactivity;
- direct injection of emergency core cooling system (ECCS) water into fuel pins during loss of coolant accident (LOCA);
- high pressure accumulator for ECCS;
- gravity driven cooling system ensuring core cooling for three days following a LOCA, without operator intervention;
- passive containment cooling and isolation;
- use of moderator heat;
- and use of low grade heat for desalination.

2.2. ADVANCED POWER REACTOR PLUS (APR+)

Korea Hydro & Nuclear Power Co. Ltd (KHNP) has launched its long-term R&D programme, aiming to develop innovative cutting-edge nuclear power technologies. One of the targets is to develop advanced technologies related to the APR+. APR+ [3] is the third-generation plus (GENIII+) reactor based on the proven design on advanced power reactor 1400 (APR1400). APR+ is a more advanced commercial reactor compared to the APR1400 in terms of economics, safety, and reliability. The standard design of APR+ was finished at the end of 2011. The standard design approval by the Korean regulatory authority is expected to be issued at end of 2012. The first commercial APR+ nuclear power plant will be started by 2016 and its commercial operation is expected to be started by 2022.

The APR+ is a two-loop PWR which has one reactor vessel, two vertical U-tube steam generators, four vertical shaft sealed reactor coolant pumps, one pressurizer attached to four pilot operated safety and relief valves, as shown in Fig. 3.

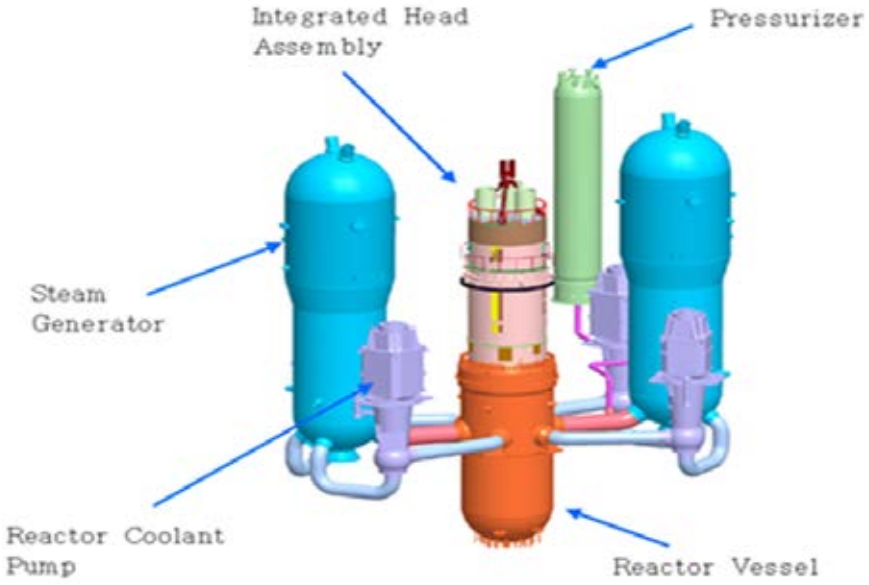

FIG. 3. General arrangement of APR+.

The major design objectives are:

- net electrical power: 1500 MW;
- core damage frequency: less than 1.0E-6/RY;
- containment failure frequency: less than 1.0E-7/RY;
- construction period (from first concrete to fuel loading): 36 months;
- economics: 10% lower than APR1400;
- safety systems: hybrid safety systems (active + passive);
- automatic daily load following and frequency control.

The basic approaches to enhance the economics of nuclear power plants are increasing power level and reducing the number of components. The first approach on power level-up has been adopted for most large capacity APWRs such as APR1400 and EPR. The second approach, of simplicity, has been adopted for the AP600 and the AP1000 by using passive safety systems. The passive safety features are expected to enhance both safety and economics. However, one disadvantage of passive system reactors seems to be that there is a limitation to increased

reactor power due to the low efficiency of passive safety features. Taking this into account, the hybrid safety systems combining active and passive systems are being considered in the system design of the APR+. The main safety system feature is that the APR+ is operated by active components and the existing safety systems are selectively substituted by the passive features. The considered criteria for selecting such features are economic benefits, safety enhancement, and proven technology.

Currently, the PAFS is a potential candidate of the passive safety systems in APR+. The existing auxiliary feedwater system (AFWS) in the APR1400, which is the reference plant for APR+, consists of two motor driven pumps, two turbine driven pumps, two water storage tanks, and related pipes and valves. The AFWS feeds emergency water to steam generators to cool down a reactor coolant system when the main feedwater is lost. This AFWS is replaced by a heat exchanger, a condensation water storage tank, and a few valves and pipes. The main driving forces of the PAFS are steam condensation and two-phase natural circulation.

2.3. CENTRAL ARGENTINA DE ELEMENTOS MODULARES (CAREM)

CAREM-25 is an Argentine project aiming to achieve the development, design and construction of an innovative, simple and small nuclear power plant. It was, chronologically, one of the first of the present new generation of reactor designs. The first step of this project is to construct the prototype of about 27 MW(e) (CAREM-25). The design basis is supported by the cumulative experience acquired in research reactor design, construction and operation, and PHWR operation and also the development of advanced design solutions [4]. The CAREM-25 has been currently recognized as an international near-term deployment reactor by the Generation IV International Forum (GIF).

The CAREM-25 is an indirect cycle reactor with some distinctive features that greatly simplify the design and also contribute to a high safety level. Some of the high level design characteristics are:

- integrated primary cooling system;
- self-pressurized;
- safety systems relying on passive features;
- and balanced and optimized design with a cost-effective internalization of safety.

Despite these features, as an innovative reactor, the interactions between the present phenomena need to be analysed in depth in order to guarantee a safe operation in all ranges. This report deals in particular with the basic phenomenology present in the reactor and its susceptibility to instabilities induced by thermohydraulic phenomena.

2.3.1. Primary circuit and its main characteristics

The CAREM-25 nuclear power plant design is based on a light water integrated reactor. The whole high energy primary system, including core, steam generators, primary coolant, and steam dome is contained inside a single pressure vessel.

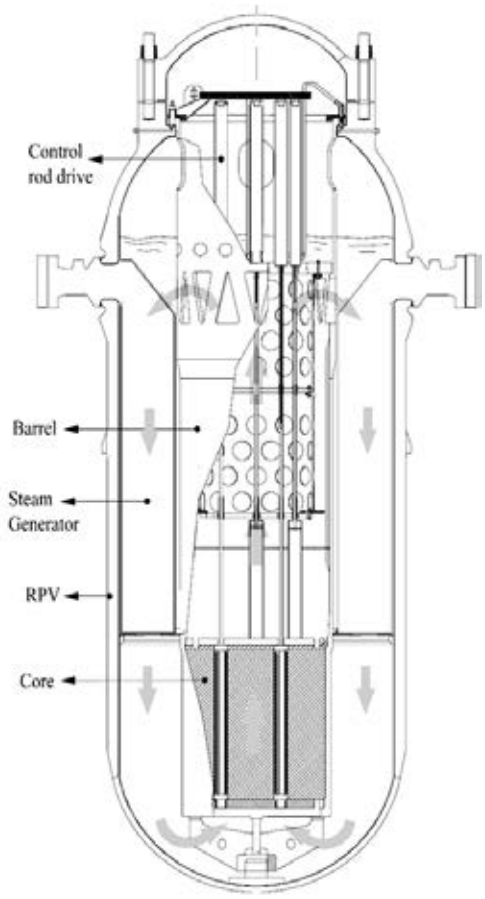

FIG. 4. CAREM-25 reactor — flow circulation.

For low power modules (below 150 MW(e), such as CAREM-25), the flow rate in the reactor primary systems is achieved by natural circulation. Figure 4 shows the natural circulation of the coolant in the primary system. Water enters the core from the lower plenum and, after having been heated, the coolant exits the core and flows up through the chimney to the upper dome. In the upper part, water leaves the chimney through lateral windows to the external region and then flows down through modular steam generators, decreasing its enthalpy. Finally, the coolant exits the steam generators and flows down through the downcomer to the lower plenum, closing the circuit.

The driving forces obtained by the differences in the density along the circuit are balanced by the friction and form losses, producing an adequate flow rate in the core in order to have a sufficient thermal margin to critical phenomena. The coolant's natural circulation is produced by the location of the steam generators above the core. The coolant also acts as neutron moderator.

Self-pressurization of the primary system in the steam dome is the result of the liquid-vapour equilibrium. The large volume of the integral pressurizer also contributes to the dampening of eventual pressure perturbations. Due to self-pressurization, bulk temperature at core outlet corresponds to saturation temperature at primary pressure. In this way, typical heaters present in conventional PWRs are eliminated.

2.3.2. Reactor core and fuel design

The reactor core has fuel assemblies of hexagonal cross section. Each fuel assembly contains 108 fuel rods with 9 mm outer diameter, 18 guide thimbles and one instrumentation thimble (see Fig. 5). Its components are typical of PWR fuel assemblies. The fuel is enriched UO_2. Core reactivity is controlled by the use of Gd_2O_3 as burnable poison in specific fuel rods and movable absorbing elements belonging to the adjustment and control system. Chemical compounds are not used for reactivity control during normal operation. The fuel cycle can be tailored to customer requirements, with a reference design for the prototype of 330 full-power days and 50% of core replacement. Each absorbing element consists of a cluster of rods linked to a structural element ('spider'), so the whole cluster moves as a single unit. Absorber rods fit into the guide tubes. The absorbent material is the commonly used Ag-In-Cd alloy. Absorbing elements are used for reactivity control during normal operation, and to produce a sudden interruption of the nuclear chain reaction when required.

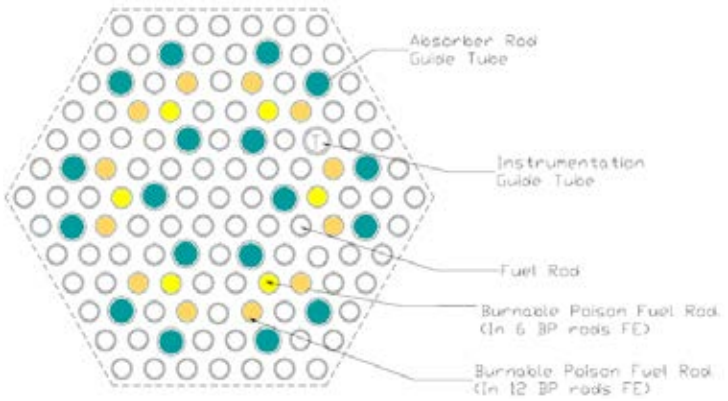

FIG. 5. Fuel assembly.

2.3.3. Primary components

Twelve identical 'mini-helical' vertical steam generators, of the 'once-through' type, are placed equally distant from each other along the inner surface of the reactor pressure vessel (RPV) (Fig. 6). They are used to transfer heat from the primary to the secondary circuit, producing superheated dry steam at 47 bar. The secondary system circulates upwards within the tubes, while the primary coolant goes in counter-current flow. In order to achieve a mostly uniform pressure loss and superheating on the secondary side, the length of all tubes is equalized. For safety reasons, the steam generators are designed to withstand the primary pressure without pressure in the secondary side and the whole live steam system is designed to withstand primary pressure up to isolation valves (including the steam outlet and water inlet headers) in case of steam generator tube breakage. The control rod drive system-hydraulic system circulates water from the RPV to operate and maintain the control rods in position. It has two pumps in operation to enhance system availability, and filters, valves for step-wise control rod motion and for operating safety rods rising, and redundant SCRAM valves.

2.3.4. Operating characteristics

The natural circulation of coolant produces different flow rates in the primary system according to the power generated or removed. Under different power transients, a self-correcting response in the flow rate is obtained [5]. Due to the self-pressurizing of the RPV (steam dome), the system keeps the pressure very close to the saturation pressure. Under all

operating conditions this has proved to be sufficient to guarantee a remarkable stability of the RPV pressure response. The control system is capable of keeping the reactor pressure practically at the operating set point through different transients, even in case of power ramps.

The negative reactivity feedback coefficients and the large water inventory in the primary circuit combined with the self-pressurization features make this behaviour possible with minimum control rod motion. It is concluded that the reactor has excellent behaviour regarding stability under operational transients. In addition, a condensation coil is included in the steam dome in order to tune the reactor operational point (see Figure 7).

FIG. 6. CAREM-25 reactor.

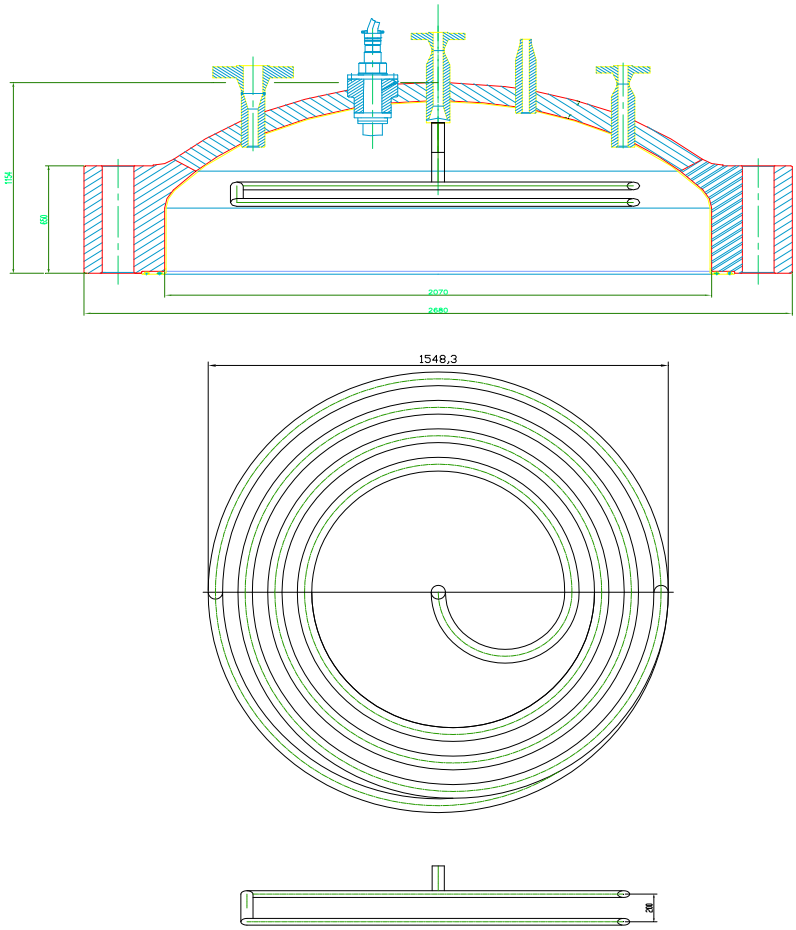

FIG. 7. CAREM-25 reactor — detail of condensation coil of steam dome.

3. PHENOMENA OF COMMON INTEREST

3.1. NATURAL CIRCULATION CONSIDERATIONS FOR SYSTEMS UNDER STUDY

3.1.1. Introduction and relevance of natural circulation to AWCR

In general, natural circulation mode of coolant circulation is caused by buoyancy forces resulting from the density gradients which, in turn, are the result of heat transport from a source to a sink. The phenomenon of natural circulation takes place without the help of fluid-moving machinery and it is expected to continue as long as the heat source and heat sink exist with favorable elevation difference. This natural phenomenon is of great interest to nuclear reactors, which continue to produce heat even after shutdown due to the decay of fission products. This decay heat must be removed to ensure fuel safety and to prevent release of radioactivity to environment in the event of a complete loss of pumping power, as has been demonstrated by the Fukushima event. The current generation of light water reactors (LWRs) is designed to remove decay heat passively in the event of pumping power failure with the help of natural circulation as long as the heat sink is available. Many advanced reactor designs have been proposed with natural circulation as the normal mode of coolant circulation in the primary system. These include both single-phase and two-phase natural circulation based reactors. Examples of single-phase natural circulation based reactors are CAREM and multi-application small light water reactor (MASLWR). Two-phase natural circulation based reactors include AHWR and economic simplified boiling water reactor (ESBWR). Besides, many passive cooling systems have been proposed to remove the decay heat and keep containment cooling following a LOCA.

3.1.2. Advantages and challenges of natural circulation

In a natural circulation system, the driving buoyancy force is provided by the thermally induced density difference. Larger density differences are possible to achieve in two-phase flow systems compared to single-phase flow systems. The main advantage of natural circulation is that the fluid circulation is achieved naturally without any fluid moving machinery. The absence of pumps simplifies the system, reduces operation and maintenance cost and eliminates all postulated initiated events associated with pump failure and operator intervention thereby enhancing safety and reliability.

Steady state flow prevails in a natural circulation loop when the driving buoyancy force is balanced by the retarding frictional forces. Because of this, the natural circulation systems have improved flow characteristics when compared with their forced circulation counterparts. In a natural circulation system, unlike forced circulation two-phase systems, flow increases with increase in power. Hence, in a natural circulation system, flow automatically gets established according to the channel power. This has specific advantages in steam generating power plants. Commercial power plants use a large number of parallel heated channels connected between an inlet and an outlet header/plenum. All analyses are carried out assuming the pressure to be uniform in the headers/plena so that the pressure drop across the parallel channels is constant. However, use of pumps cause maldistribution of pressure in the headers leading to maldistribution of flow in the parallel channels. Operating experience with natural circulation based systems suggests that the problem is eliminated or an order of magnitude less.

The driving force in a natural circulation system is much lower compared to a forced circulation system. With low driving force, measures are to be taken to reduce the frictional

losses. To reduce frictional losses, mechanical separators in the steam drum are eliminated and large diameter pipes are used. The use of large diameter piping results in a larger inventory of primary system fluid which enhances system inertia to cope with transients. Large size components lower the power density and make transients quite sluggish.

Despite the above advantages, natural circulation systems have their own set of challenges. One of the drawbacks of natural circulation systems is that their driving force is low. The most straightforward way to increase the driving force is to increase the loop height, which may be uneconomic. In addition, use of tall risers can make natural circulation systems slender in structure and may raise seismic concerns. Low driving force and the consequent use of large diameter components result in low mass flux in natural circulation systems compared to the forced circulation systems. With low mass flux, the allowable maximum channel power is lower leading to a larger core volume compared to a forced circulation system of the same rating.

While instability is common to both forced and natural circulation systems, the latter is inherently less stable than forced circulation systems. This is attributable to the regenerative feedback inherent in the natural circulation phenomenon, where any change in the driving force affects the flow which, in turn, affects the driving force that may lead to sustained oscillatory behaviour for certain operating conditions.

Natural circulation systems need to be started up from rest at low pressure. Hence, thermohydraulic relationships applicable to low pressure and low flow conditions are of interest to natural circulation systems. Besides, the presence of instability at low pressure conditions requires special startup procedures to be prescribed for natural circulation systems.

Due to low driving forces, the phenomena involved may have considerable three dimensional effects. The problem becomes more compounded due to presence of, for example, elbows or flow area changes. in natural circulation systems. Under these conditions, the conventional 1-D models used for the thermohydraulic design and safety analysis may not be adequate for natural circulation systems. Hence, the tools used for the analysis of such systems need to be separately validated.

3.1.3. Major issues of interest for natural circulation for AWCR

The important phenomena related to natural circulation that can have a bearing on the performance of the main heat transport (MHT) and decay heat removal systems are:

- steady state operation of natural circulation systems;
- instability of natural circulation systems;
- startup of natural circulation systems;
- design and validation of tools for natural circulation systems;
- thermal stratification in large pools.

3.2.THERMAL STRATIFICATION IN POLLS WITH IMMERSED HEAR EXCHANGERS

3.2.1. Brief description of the phenomenon

Advanced reactor designs use several passive systems to improve safety and reliability by reducing the dependence on external sources of energy and human intervention. One of the most prominent safety functions is the passive removal of decay heat. It assumes greater

significance when decay heat is to be removed to maintain core cooling in the event of simultaneous failure of all AC power supplies, i.e. station black out (SBO), for prolonged duration, as may be required if natural external events render the restoration of power supplies virtually impossible. Advanced reactor designs incorporate this capability by using immersed heat exchangers in a large pool of water at high elevation. Heat exchangers immersed in large pools can be used either on the primary side or on the steam generator side. Examples of advanced reactor design using large pools with immersed heat exchangers on the primary side (Fig. 8(a)) are SWR-1000, AHWR and AP1000. Examples of advanced reactor design using immersed heat exchangers in large pools on the secondary side (Fig. 8(b)) are APR+ and PHWR-700. In general, the pool capacity is decided on the basis of mission time which varies from reactor to reactor — from eight hours for an APR+ to three days for an AHWR. The capacities of the pool are relatively large ranging from 1200 m^3 to 8000 m^3. During the operation of such systems, thermal stratification in the pool is an important phenomenon. The immersed heat exchangers can be horizontal or vertical.

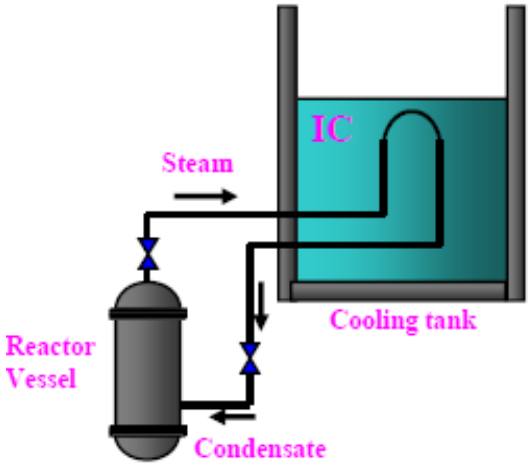

FIG. 8.(a) Isolation condenser in BWR.

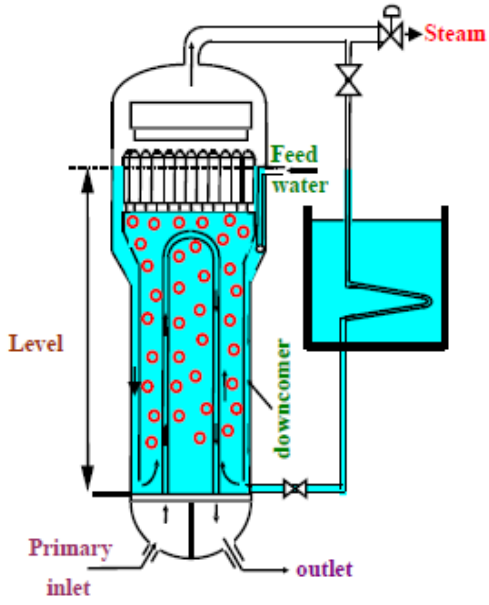

FIG. 8.(b) PHWR-700 PDHRS.

3.2.2. Issues of thermal stratification

In a large pool with submerged heat exchangers, CFD calculations reveal that only water close to heat exchangers participates in the heat transfer process. The hot plume of water rising near the heat exchanger tubes reaches the top surface of pool and spreads horizontally forming a hot layer at the top. Accumulation of hot water further at top reduces the heat transfer and effectiveness of the heat exchanger. Over time, it may lead to the formation of a stratified pool. This process deprives the external surface of the heat exchanger of relatively cold water and, thus, degrades the heat transfer process. Not only does this degrade the heat transfer from the heat exchangers to the pool, but the prolonged contact of hot water with the concrete structure of the pool may also cause the concrete to exceed its allowable temperature. At the same time, thermal stratification may lead to the boiling of pool water near the immersed heat exchanger with subcooled water away from it. This may lead to gradual pressurization of the containment. Also, the thermally stratified pool could adversely affect the decay heat removal from core.

4. NATURAL CIRCULATION STUDIES FOR AWR

4.1. DESCRIPTION OF SPECIFIC SYSTEMS CONSIDERED

4.1.1. Main heat transport system for AHWR

Natural circulation is the coolant circulation mode used to remove heat from the reactor core under normal and also shutdown conditions. Figure 9(a) shows the main heat transport system (MHTS) of an AHWR. The MTHS consists of a vertical core having 452 parallel coolant channels arranged inside the calandria vessel. The fission heat produced in the channels is absorbed by the coolant to produce a two-phase mixture. The two-phase mixture from the coolant channels rises to the steam drums (4 Nos.) through 452 tailpipes (risers). The steam drum is a horizontal cylindrical vessel with appropriate internals, where gravity separation of two-phase mixture is achieved. Nearly dry saturated steam leaves the steam drum through steam lines to feed the turbines. Recirculation water is mixed with feed water in the steam drum and it flows through the downcomer (4 Nos. per steam drum) connected to a header which, in turn, is connected to coolant channels through corresponding feeders.

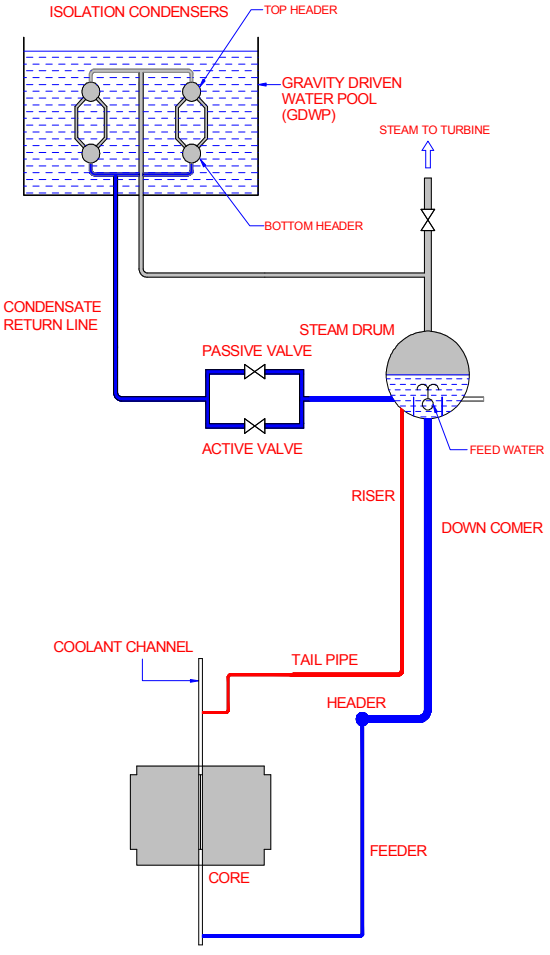

FIG. 9.(a) MHT and ICS of AHWR.

4.1.2. Main heat transport system for CAREM

CAREM-25 is a natural circulation integrated reactor in which the main heat transport system consists of the core, the chimney and the downcomer sections as shown at Fig. 9(b). The downcomer also contains the steam generators in its upper part. Water from the primary system is heated up in the reactor core. Hot water travels through the chimney section placed on top of the core. The steam generators located in the upper part of the downcomer section cool down the water flowing from the chimney. The cold water then travels through the lower part of the downcomer before it enters in the core, completing the cycle.

The density difference between the coolant in the core plus chimney sections and the downcomer section creates the necessary flow rate without the use of active components (e.g. pumps). It is, therefore, obvious that the mass flow rate value cannot be adjusted directly but is a result of the system geometry and operational conditions.

Due to the fact the primary cooling system is self-pressurized, some vapour needs to be generated in the core/chimney sections. The vapour present in the system is condensed in the steam dome and in the cold structures from the control rod driving mechanism. A direct consequence of self-pressurization is that, at a constant pressure value, the coolant enthalpy at the core exit location is very close to saturation. As will be shown in further sections, self-pressurization with natural circulation implies different behaviour of the system to that of more conventional reactors.

The two-phase flow in the primary cooling system allows the formation of density waves, which in turn may lead to thermohydraulic instabilities. The neutronic feedback also plays an important role in determining the dynamics of the system and thus in stability performance. As a result of the aforementioned coupled phenomena, CAREM-25's reactor thermohydraulics need to be investigated in depth in order to guarantee reactor cooling under all circumstances.

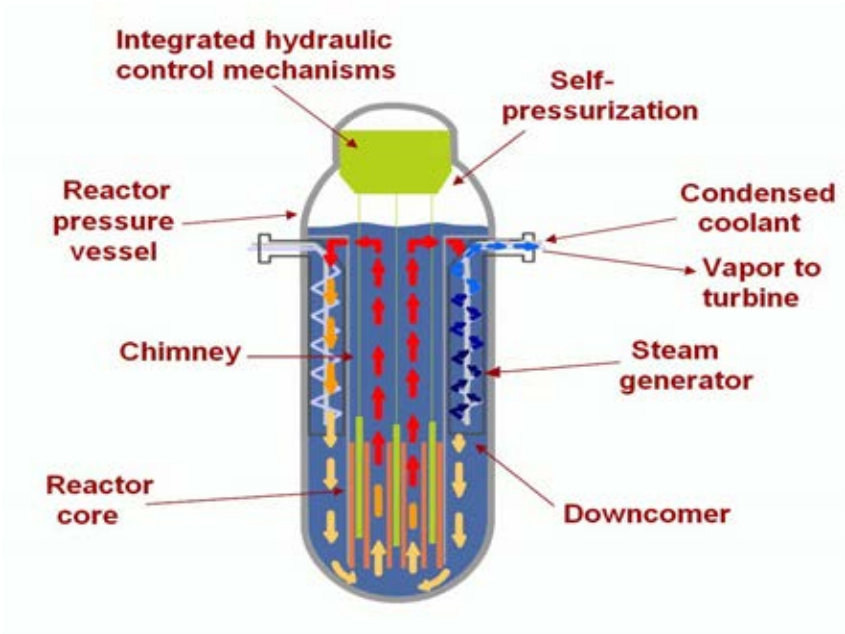

FIG. 9.(b) MHT condenser system of AHWR.

4.2. CASE STUDIES FOR AHWR

As discussed earlier, one of the main challenges involved in the design of natural circulation systems is the lack of adequate data on many associated phenomena and the very low driving force compared to active systems. To address the above issues, a number of separate effect and integral test facilities have been designed and operated. While the separate effect test facilities are being used to study the phenomena of interest and for model validation, it is the integral test facility which is of direct relevance to design and development of natural circulation systems of AHWR. An ITL simulating main heat transport system and the passive safety systems of AHWR has been set up (Fig. 9(c)).

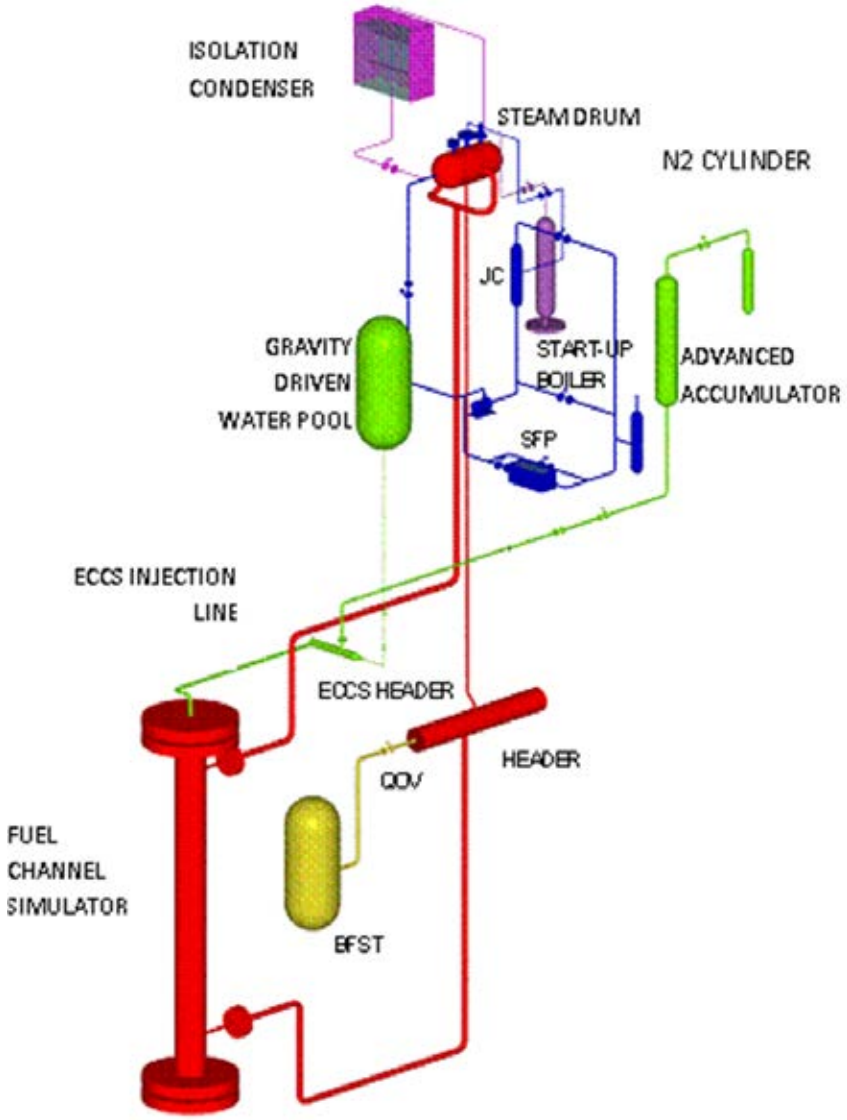

FIG. 9.(c) Isometric view of ITL.

4.2.1. Natural circulation studies in ITL

An ITL simulates main heat transport system and safety systems of AHWR. The test facility is designed using power-to-volume scaling philosophy [6]. Volume scaling of the loop is 1:452 and the elevation scaling is 1:1. The design temperature and pressure of the loop are 304^{o}C and 100 bar respectively. A database for performance evaluation of the natural

circulation MHT loop, plant transients and accident scenarios have been generated in this test facility. Figure 10(a) shows a comparison of the steady state loop mass flow rates obtained experimentally with that predicted using the computer code RELAP5/Mod3.2, an in-house developed code TINFLO-A, and analytical solutions [7] obtained using generalized two-phase flow correlations. Figure 10(b) shows distribution of stable and unstable experimental data across a stability threshold surface generated using the in-house developed computer code TINFLO-S [8].

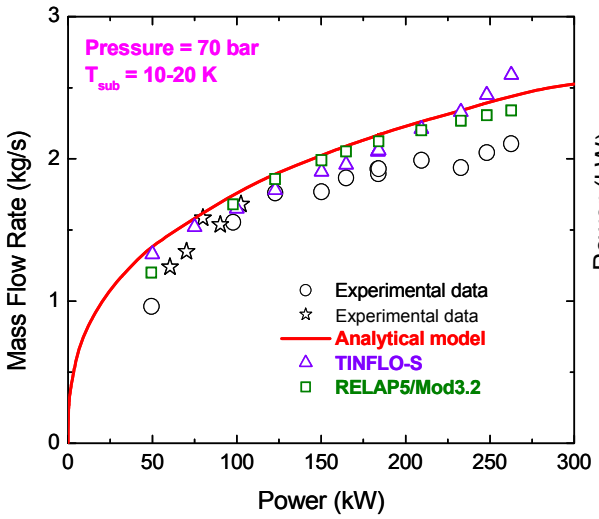

FIG. 10.(a) Comparison measured and predicted steady state mass flow rates.

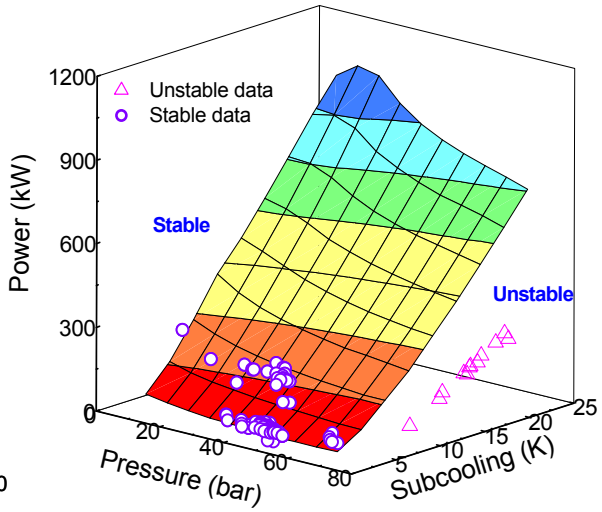

FIG. 10.(b) Comparison of measured and predicted zones of instability.

4.2.2. Stability

Natural circulation is susceptible to flow instabilities depending on the operating conditions of pressure, power and core inlet subcooling. Stability analyses of the AHWR have shown the presence of Type-I and Type-II instabilities. Type-II occurs at power higher than maximum reactor power and Type-I instabilities occur just at the time of boiling inception. Type-I instabilities, which include flashing and geysering, occur only at low pressures and can be avoided by external pressurization of the system. The reactor experiences low pressures and boiling inception during startup transient. A rational startup procedure that avoids all possible instabilities has to be devised. A startup procedure for the AHWR with stage-wise external pressurization up to nominal operating pressure has been proposed [9].

The proposed startup procedure for AHWR consists of:

- heatup of MHTS by single-phase natural circulation at reactor power of 2% full power (FP) to maintain the structural heating rate below 2°C/min. Heatup is carried out without any heat sink except for heat loss from the piping and system components;
- external pressurization in accordance with the system temperatures to avoid cold pressurization;
- stage-wise pressurization of MHTS by admitting steam from external boiler having rating of nominal operating pressure (7 MPa);
- boiling inception at 7 MPa and 2% FP;

- and after achieving steady state two-phase natural circulation at 2% FP (steam removal from steam drum and addition of feed water at controlled temperature) at 7 MPa, further raising power beyond 2% FP.

Figure 11 shows RELAP5/Mod 3.2 simulation of AHWR startup procedure with stage-wise external pressurization [10].

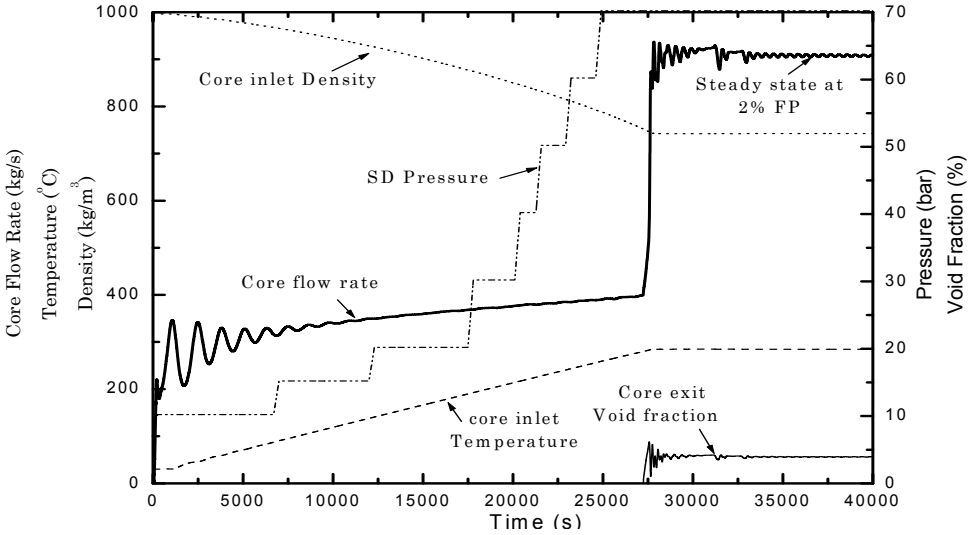

FIG. 11. Predicted startup transient for AHWR (with external stage-wise pressurization) using computer code RELAP5/MOD 3.2.

4.2.3. Studies on startup in ITL

The proposed startup procedure for the AHWR has been validated in ITL [11], where two different startup procedures were studied — startup with self pressurization and startup with external pressurization.

(a) Startup with self pressurization

Figures 12–14 show the loop transient behavior when started at room temperature and steam drum pressure at 1 atmosphere. It can be seen from this figure that flow instabilities are observed at low pressure. Flashing induced instability has been observed in the experiments at low pressure. One of the characteristic features of flashing instability is that its frequency is less and the amplitude of oscillations decreases as the pressure builds up. At the end of flashing instability, high frequency density wave instability is also observed.

It is seen that with higher channel power, flow stability is achieved at lower pressures. With fuel channel simulator (FCS) power, 52 kW flow is unstable up to 35 bar while with FCS power 150 kW flow is stable above 21 bar. However, there is limit on the initial reactor power level during startup. This rate is limited by the maximum permissible temperature rise rate. For ITL, this limit on heatup rate is 75 kW.

(b) Startup with external pressurization

Startup with external pressurization was also simulated in this test facility. For this purpose, startup tests were performed in ITL with initial external pressurization at 10, 20, 30, 40 and 45 bar and subsequent self-pressurization up to 70 bar. Power was kept constant at 2% FP during all these simulations.

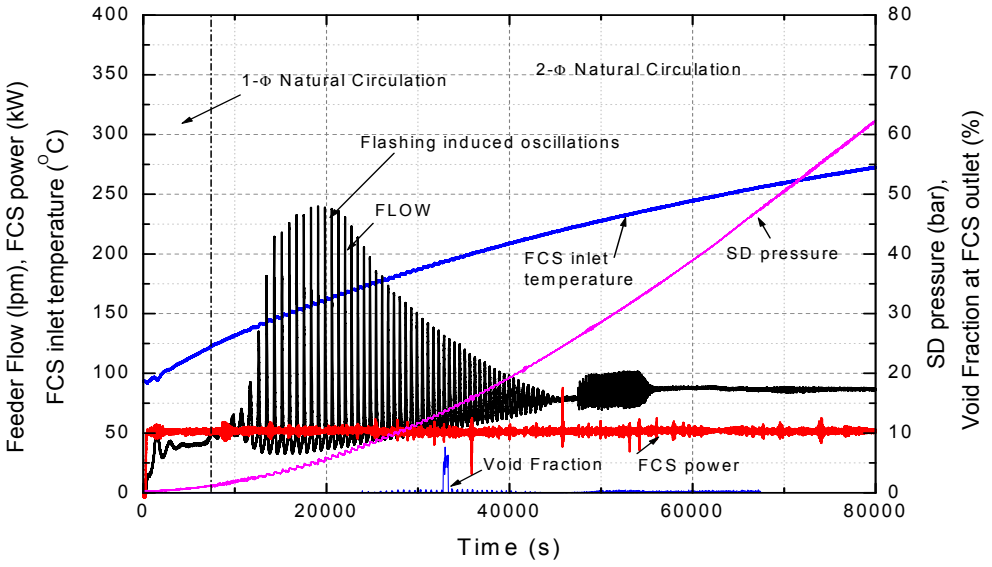

FIG. 12. ITL startup experiment with self-pressurization at 52 kW.

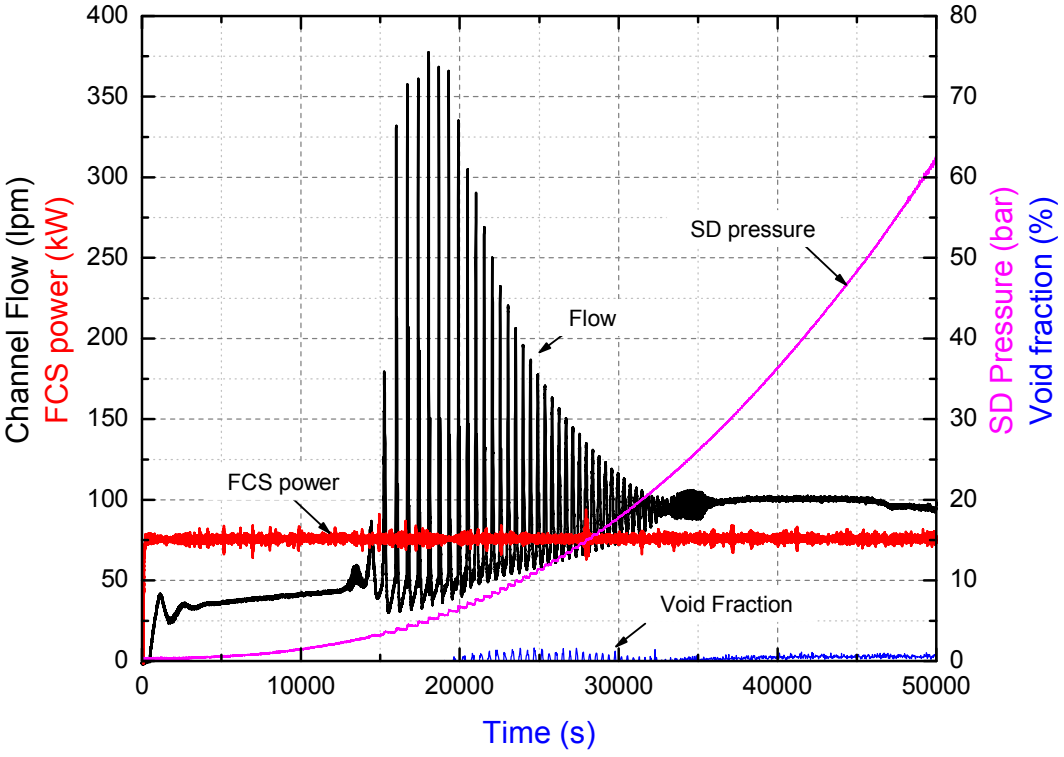

FIG. 13. ITL startup experiment with self-pressurization at 75 kW.

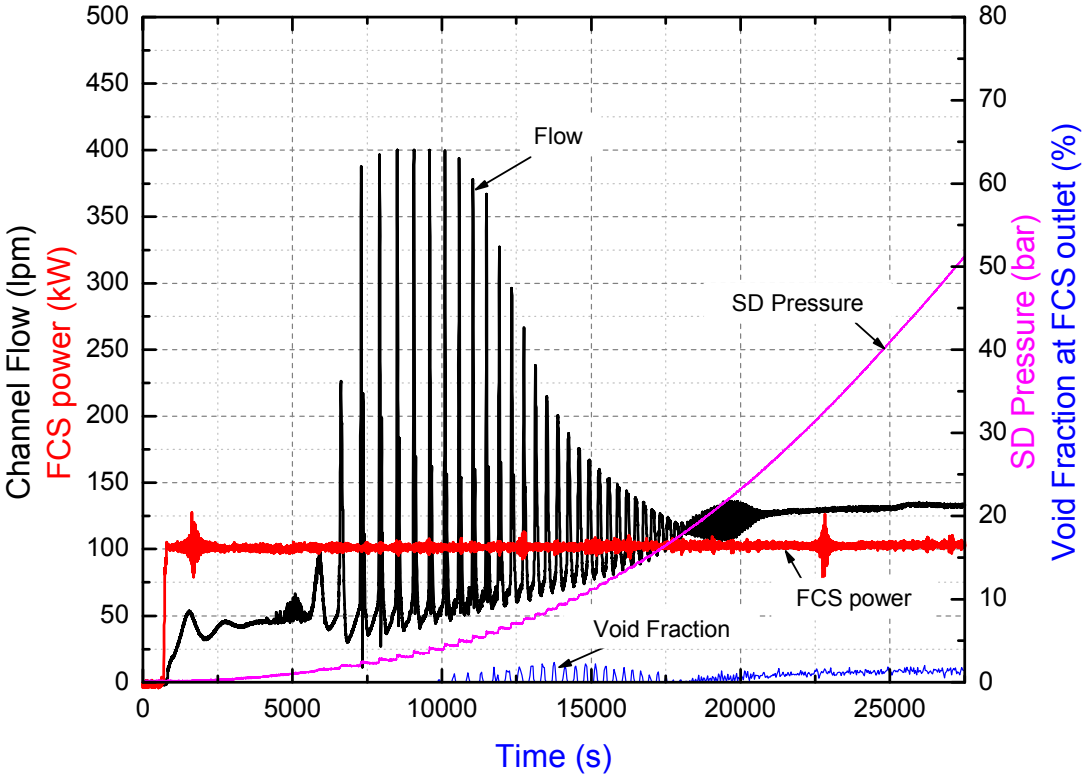

FIG. 14. ITL startup experiment with self-pressurization at 100 kW.

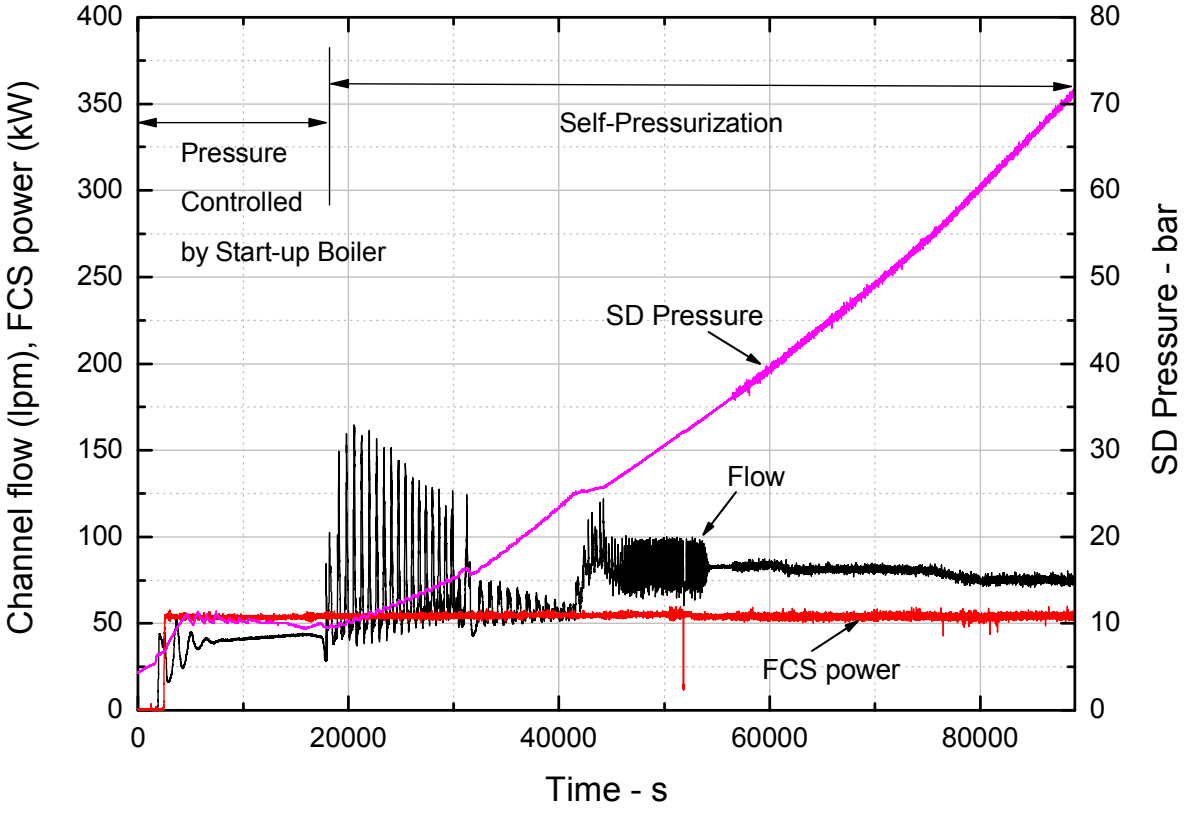

FIG. 15. ITL startup experiment with external pressurization of 10 bar at 52 kW.

Figures 15–17 show ITL transient behaviour at same heater power with different initial pressure values achieved with the help of a startup boiler which pumps in steam to the steam drum. The objective of the experiments was to establish the lowest pressure at which all low pressure instabilities disappear.

During ITL startup experiments with external pressurization, the two-phase natural circulation was observed to be unstable up to 35 bar system pressure (Fig. 17). Flow undergoes oscillations induced due to Type-I density wave oscillation (DWO). For external pressurization of 20 bar and above the flashing induced oscillations are suppressed; however, Type-I density wave oscillations have been found to persist up to 35 bar pressure. All ITL startup transients with external pressurization of 35 bar and above are observed to be stable in single-phase as well as two-phase natural circulation.

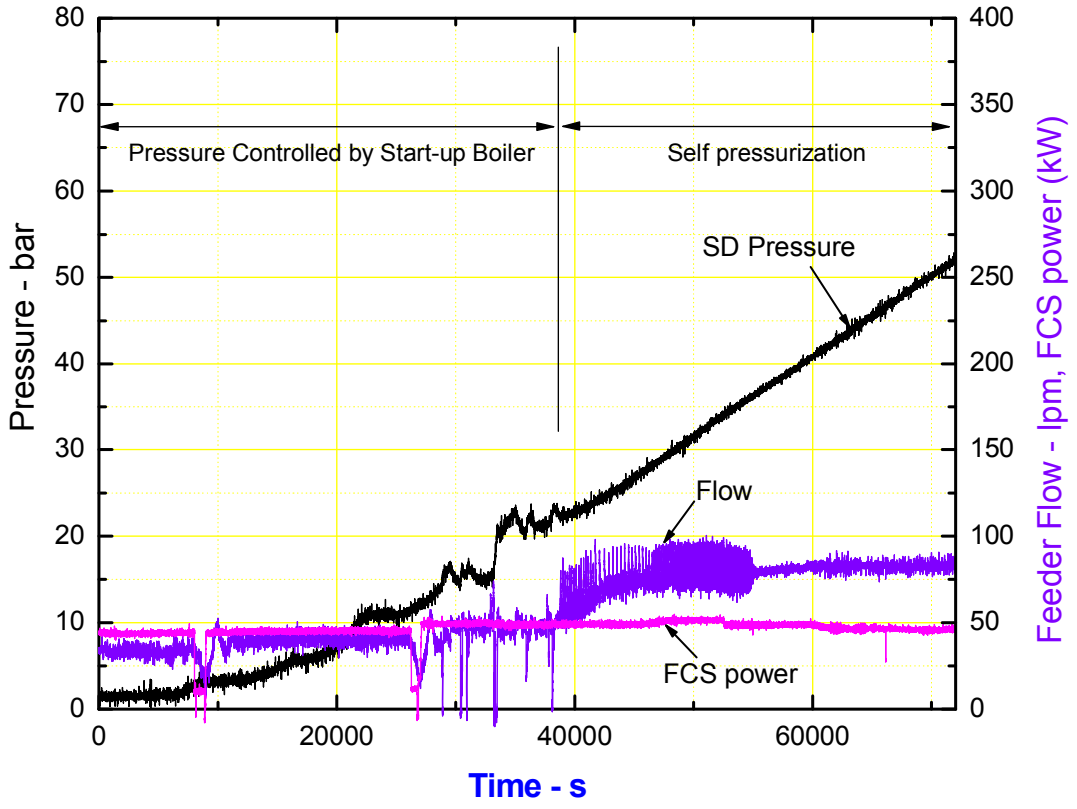

FIG. 16. ITL startup experiment with external pressurization of 20 bar at 52 kW.

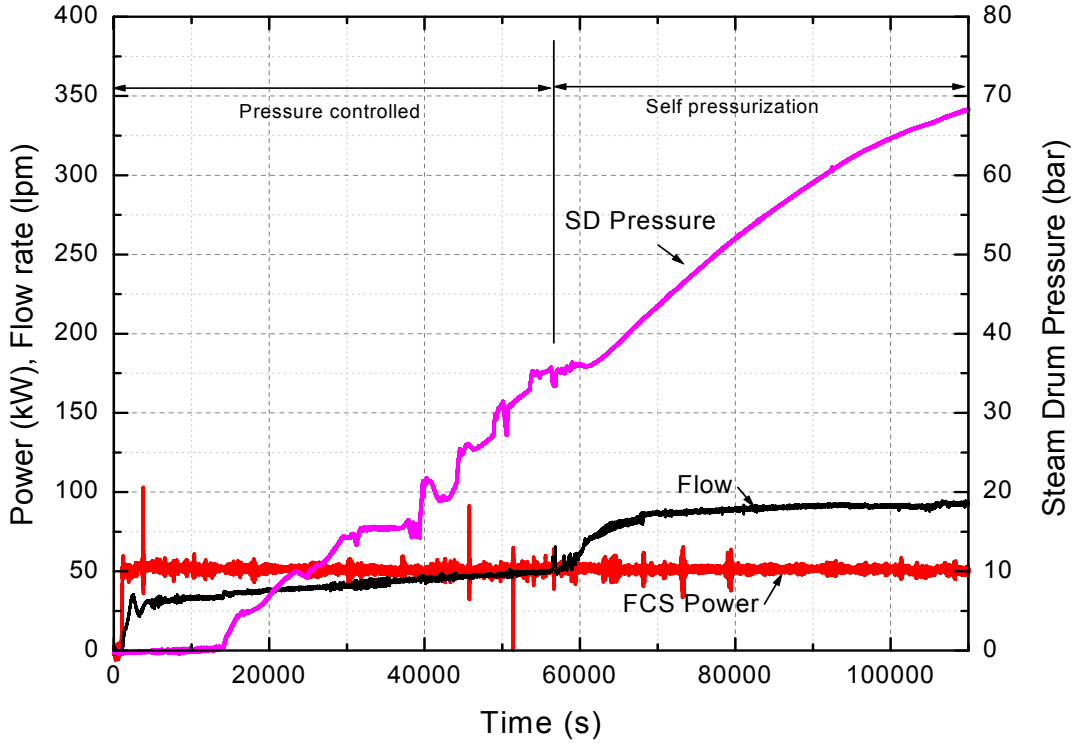

FIG. 17. ITL startup experiment with external pressurization of 35 bar at 52 kW.

4.2.4. Simulation of startup experiments using computer code RELAP5/Mod3.2

(a) Nodalization

RELAP5/Mod3.2 has been used to simulate the experimental transients in ITL. The various components of ITL are discretized in finite volume fluid cells and are connected to each other via junctions. Boundary conditions of pressure, temperature and heat exchange are simulated using time dependent volume (infinite source and sink with predefined state of fluid that can be varied with time), time-dependent junctions (junctions with predefined flow conditions) and heat structures (simulates the heater, heat loss through the insulation, and appropriate heat exchange from fluid to wall or wall to fluid). The steam and feed water system is simulated using time-dependent volumes with predefined conditions. The removal of steam is simulated with valve acting on defined trip signals. The feed water injection is simulated using a time-dependent junction that injects an equal amount of water to the amount of steam withdrawn from the steam drum. The heat addition at the FCS is simulated with a heat structure describing the geometry of flow through the heated rod bundle and appropriate bundle heat transfer area. Heat loss from the piping is also considered by modelling heat structures at tail pipe, downcomer, feeder and FCS with geometry and thermal properties of insulation provided. The loss coefficients are modelled at the bends in loop and at the spacers in the FCS. The loss coefficients at locations of flow area change are calculated by the code. Fig. 18 shows the nodalization scheme adopted in RELAP5/Mod3.2 for the test facility shown in Fig. 9(c).

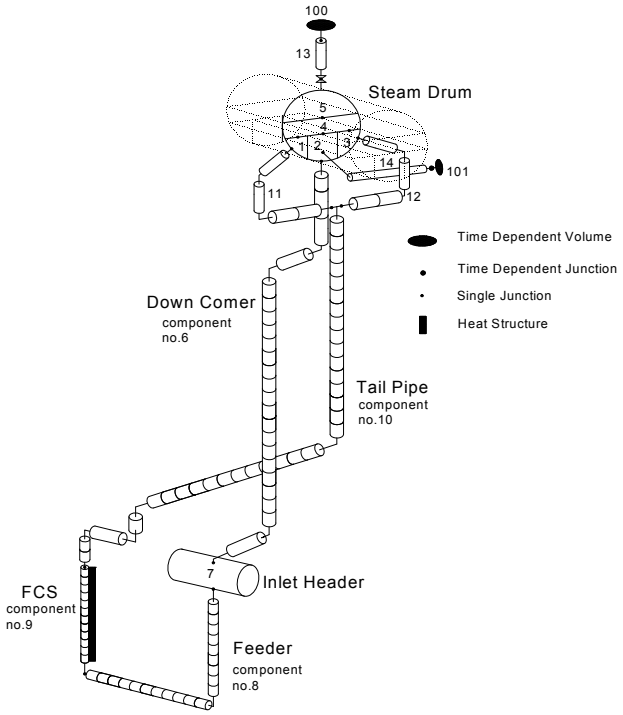

FIG. 18. RELAP5/MOD3.2 nodalization for ITL simulation.

(b) Simulation of startup with self-pressurization

Figures 19–20 show a comparison of test results with RELAP5/Mod3.2 predictions. RELAP5/Mod3.2 simulations are in good agreement with the experimental trends. Both the low frequency flashing and the high frequency instabilities are reproduced. However, the threshold pressure at which density wave instability disappears has been found to be lower than that predicted by RELAP5/Mod3.2. A comparison of measured and predicted values of threshold of instability are given in Table 1.

(c) Simulation of startup with external pressurization

Figures 21–23 show a comparison of test results with RELAP5/Mod3.2 predictions for the startup with external pressurization. Again trends are well predicted. Flashing instability is not predicted for pressures greater than 20 bar.

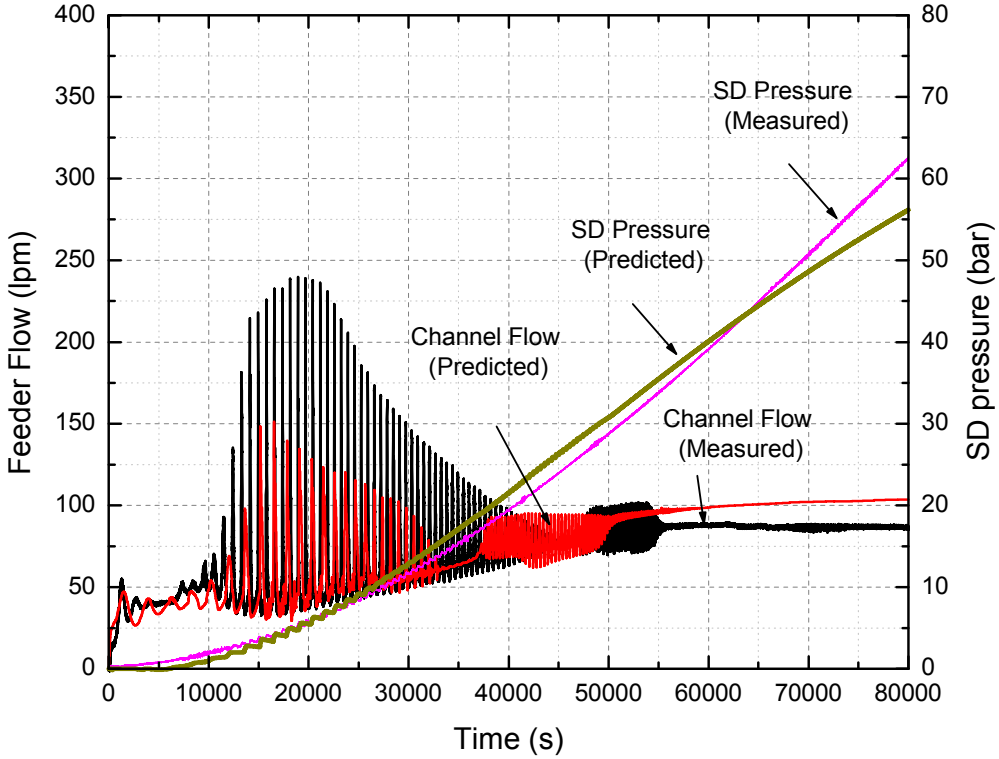

FIG. 19. Comparison of simulation results with experimental data for startup with self-pressurization at 52 kW.

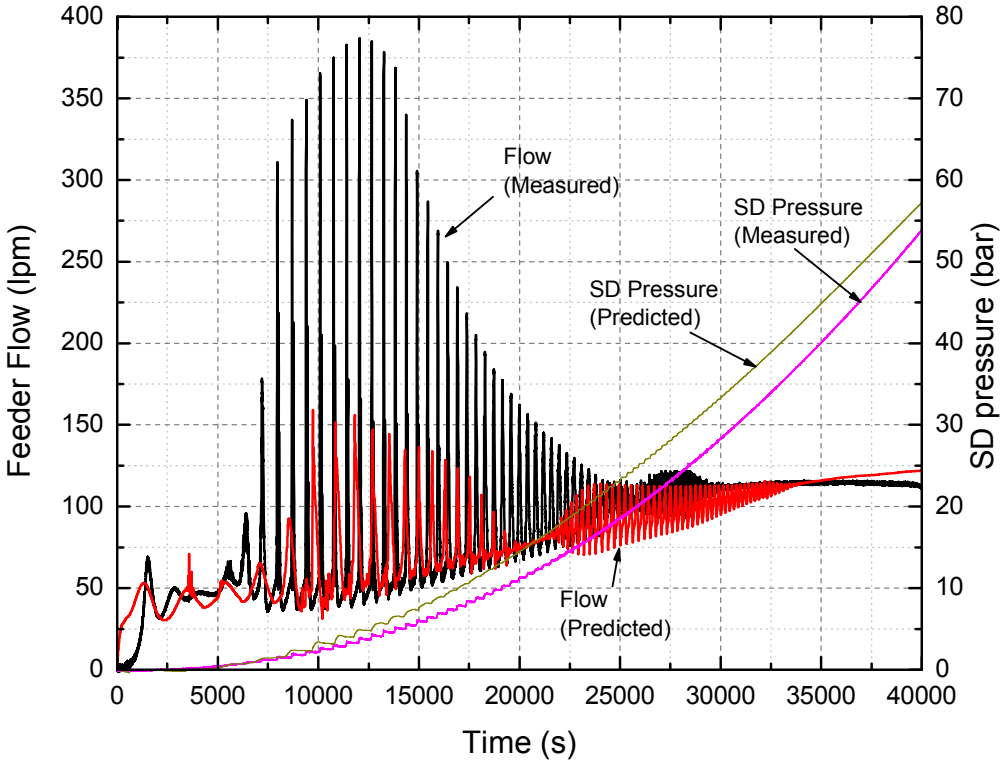

FIG. 20. Comparison of simulation results with experimental data for startup with self-pressurization at 75 kW.

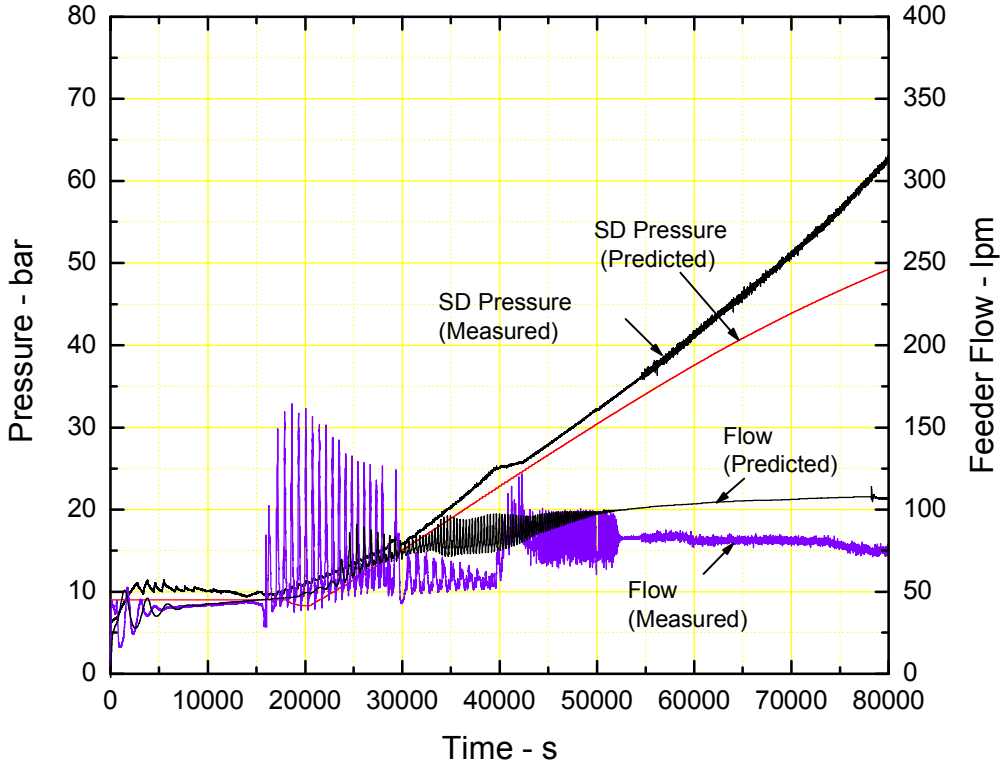

FIG. 21. Comparison of simulation results with experimental data for startup with external pressurization of 10 bar.

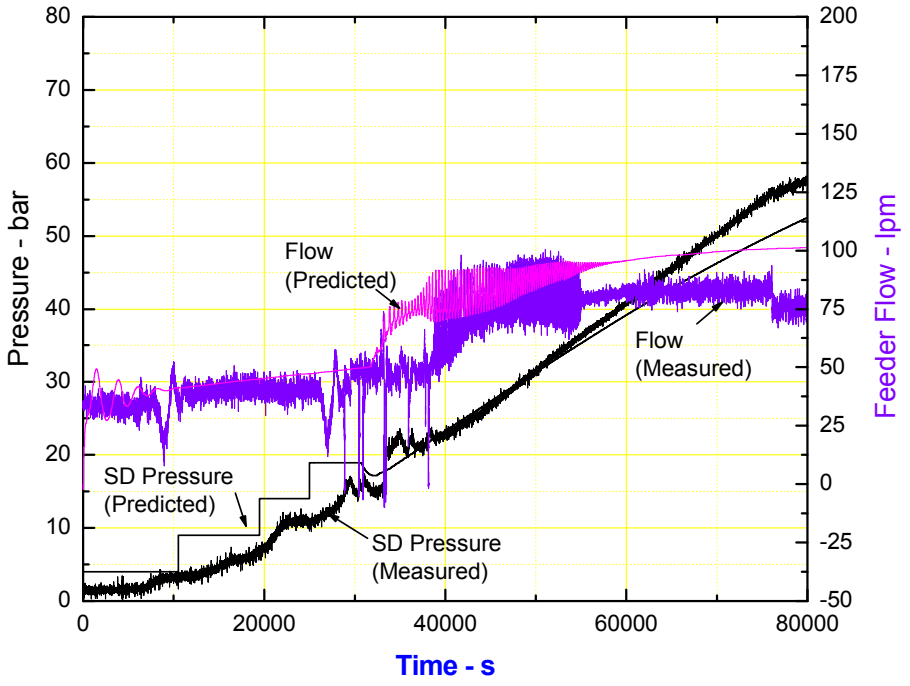

FIG. 22. Comparison of simulation results with experimental data for startup with external pressurization of 20 bar.

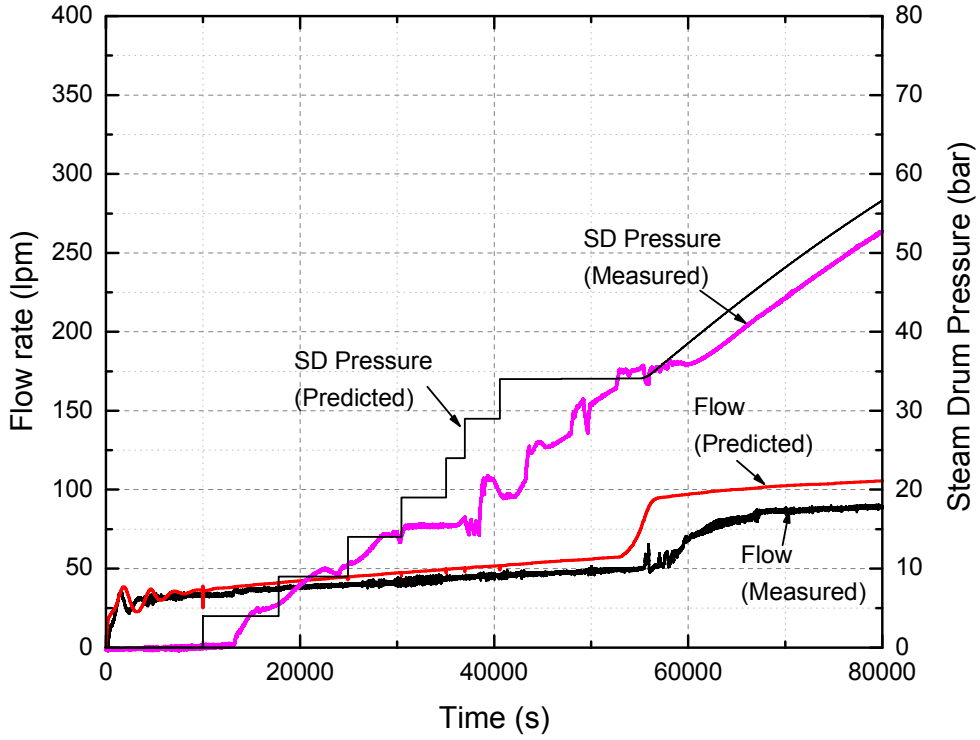

FIG. 23. Comparison of simulation results with experimental data for startup with external pressurization of 35 bar.

TABLE 1. MEASURED AND PREDICTED THRESHOLD PRESSURE BEYOND WHICH INSTABILITIES DISAPPEAR FOR SELF-PRESSURIZATION

Sr. No.	FCS power (kW)	Pressure (bar) as per experiment	Pressure (bar) as per RELAP5/M3.2 code simulations
1	52	35.0	31.1
2	75	28.5	40.8
3	100	26.7	36.9
4	125	21.2	33.1
5	150	21.19	31.4

4.2.5. Studies on flow stabilization

Natural circulation is susceptible to flow instabilities. These instabilities are undesirable for various reasons, such as flow induced vibration of components or problem in control of the system. The literature suggests the use of orifices at the inlet to suppress instability. However, orificing introduces pressure drop, which significantly reduces the flow rate and hence the heat carrying capability of the natural circulation system. Owing to small driving forces in the natural circulation system, orifice as an instability control technique has limited utility in these systems. Therefore, it is desirable to have techniques which help in controlling instability but, at the same time, do not introduce high pressure drop. In the present study, the use of mechanical gadgets and nanofluids on flow instability has been studied.

4.2.5.1. Flow stabilization using mechanical gadgets

Several mechanical gadgets were considered and extensive experiments were carried out in a single-phase rectangular natural circulation loop, called an instability demonstration facility, to study the effect of these mechanical gadgets on instability [12].

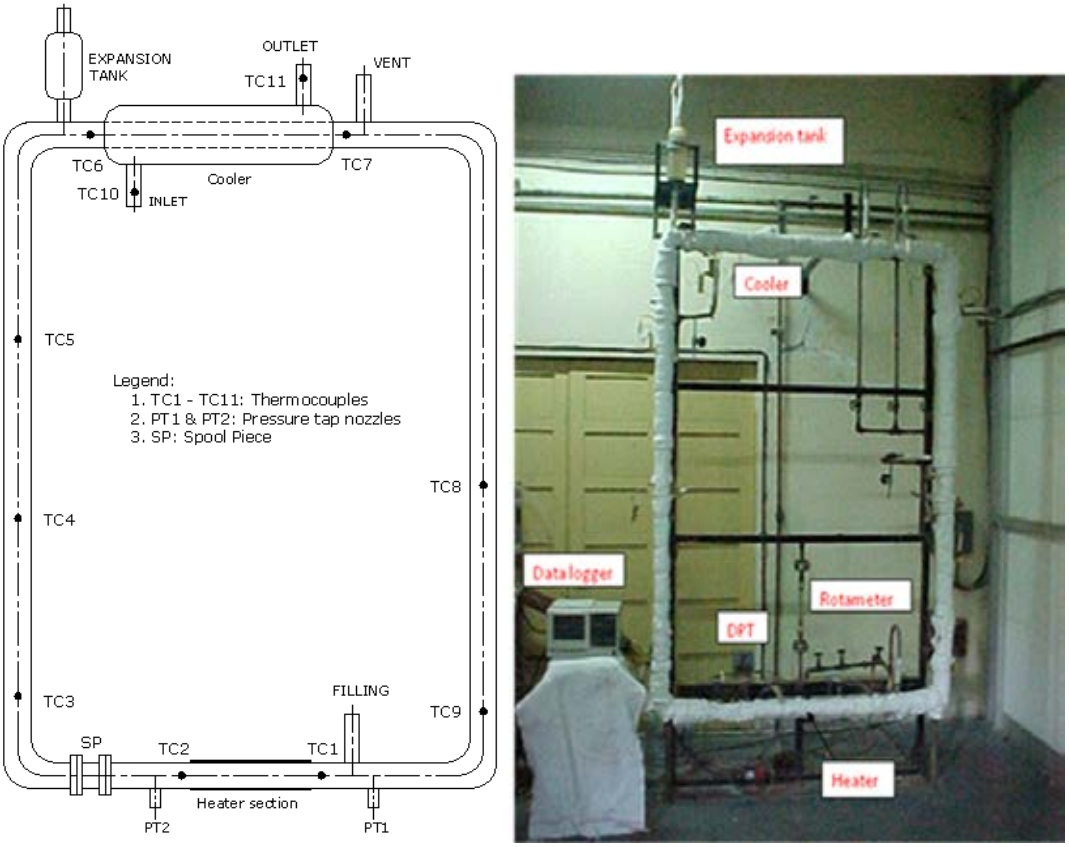

(a) Diagram. *(b) Photograph.*

FIG. 24. Instability demonstration facility.

A diagram and a photograph of the experimental facility are shown in Fig. 24. The instability demonstration facility is a uniform diameter loop made of borosilicate glass tube having 26.9 mm inside diameter and 1.65 mm thickness. The loop consists of a heater, a cooler, a hot leg and a cold leg interconnected by spool pieces with the help of flanged joints. The heater consists of an electrically heated coil wrapped around the outside surface of the glass tube. The heater was mounted in the lower horizontal portion whereas a coaxial pipe-in-pipe heat exchanger was used at the top as a cooler to extract the heat from the working fluid. An expansion tank made of borosilicate glass was also provided in the loop at the highest elevation to take care of thermal expansion of water. Apart from this, a vent connection was also provided. To take care of heat loss to the atmosphere, the loop was insulated with ceramic wool. The facility was adequately instrumented to measure the pressure drop across the heater section, temperatures at different locations and coolant flow rate.

Apart from a smooth spool piece to generate baseline data, the following four different types of mechanical gadgets were used: (1) spool piece with internal threads of 3 mm pitch; (2) spool piece with internal threads of 7 mm pitch; (3) bellows; and (4) spool piece with helical coil.

The effect of mechanical gadgets was investigated by replacing smooth spool piece installed at location 'SP', shown in Fig. 24. Figure 25 shows the mechanical gadgets. Spool pieces were made of stainless steel whereas the bellows were made of teflon.

FIG. 25. Mechanical gadgets. (In clockwise direction from left bottom: bellows, spool piece with helical coil, threaded spool piece with 3 mm pitch, and threaded spool piece with 7 mm pitch).

Figure 26 compares the flow behavior of the natural circulation loop with different mechanical gadgets with the smooth spool piece. Experimental observations showed unstable flow for smooth spool pieces. All mechanical gadgets were able to suppress the instability in the loop. Further, the helical coil was found to be most effective in suppressing instability. The reduction in flow rate caused by different gadgets is shown in Table 2, where it can be observed that the spool piece with helical coil causes the least reduction in mass flow rate and highest increase in the instability threshold among all the gadgets.

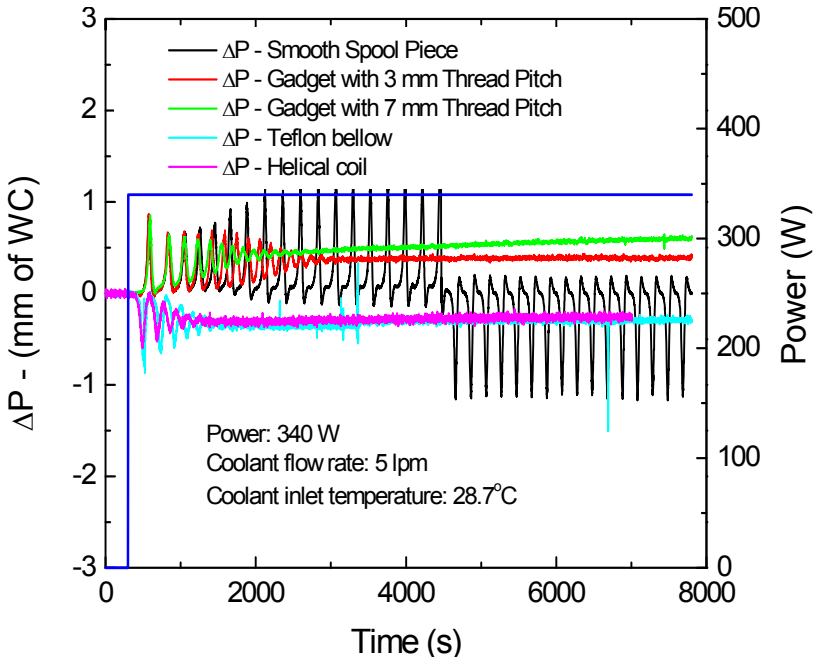

FIG. 26. Effect of mechanical gadgets on stability threshold.

TABLE 2. EFFECT OF DIFFERENT GADGETS ON LOOP MASS FLOW RATE

Mechanical gadgets	Reduction in flow rate (%)	Increase in instability threshold (%)
Spool piece with internal threads of 3mm pitch	4.5	2.9
Spool piece with internal threads of 7mm pitch	14.5	8.8
Bellows	16.8	10.9
Spool piece with helical coil	4.4	11.8

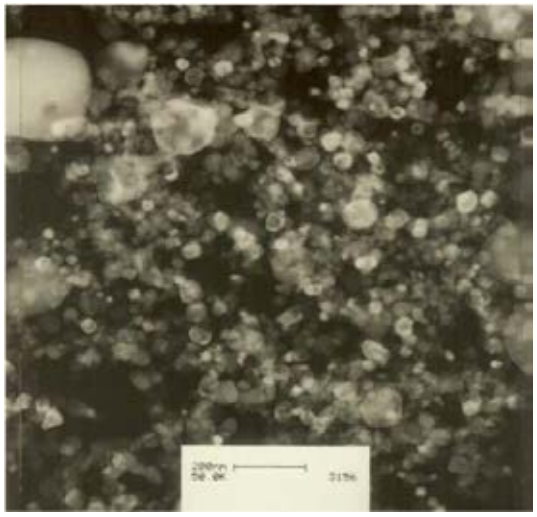

FIG. 27. TEM image of alumina nanoparticles.

4.2.5.2. Flow stabilization using nanofluids

Studies on nanofluids (nanoparticles in water) are gaining in importance owing to their promising heat transfer characteristics vis-à-vis water for applications in future nuclear and process industries. In view of this, experimental investigations were carried out to study the effect of metal oxide nanofluids on single-phase and two-phase flow instability.

(a) Effect of nanofluid on single-phase flow instability

Experiments were carried out in the instability demonstration facility (Fig. 24) to study the effect of nanofluids on single-phase flow instability [13]. The baseline data was obtained with water as the fluid. To study the effect of nanoparticle concentration on flow instability, a small concentration of nanofluids was prepared by adding different concentrations of Al_2O_3 nanoparticles (40–80nm size) in water and sonicating the mixture for four hours. A transmission electron microscope (TEM) image of one representative sample is shown in Fig. 27.

Experiments were conducted with Al_2O_3 nanoparticles having different concentration by weight. Secondary side flow rate was maintained at 1lpm for all tests. Instability was observed with pure water. However, instability was not found in the single-phase region even with 0.5 % concentration. A comparison of the loop behaviour with different nanoparticle fluid concentrations is shown in Fig. 28.

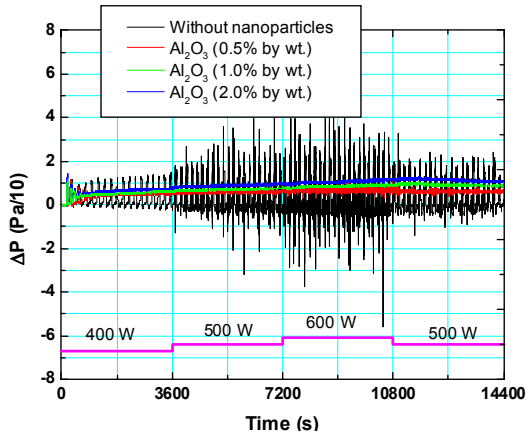

FIG. 28. Suppression of instabilities by adding alumina nanofluids with different concentrations.

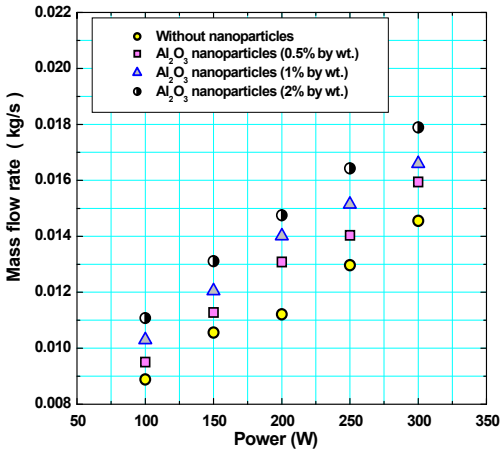

FIG. 29. Enhancement of natural circulation mass flow rates by addition of nanofluid.

It is observed that with addition of nanoparticles, the single-phase instabilities were suppressed. In Fig. 29, a significant increase in loop mass flow rate with nanoparticle fluid concentration is also observed. The increase in flow rate is proportional to the concentration of nanoparticles. The percentage increase in loop mass flow rate for different nanoparticle fluid concentrations is given in Table 3.

TABLE 3. EFFECT OF DIFFERENT CONCENTRATIONS OF Al_2O_3ON LOOP MASS FLOW RATE

Concentration of nanoparticle (% weight of Al_2O_3)	Increase in flow rate (%) over water without nanoparticles
0.5	9.7
1.0	17.2
2.0	26.0

A similar effect was observed when different nanofluids were used. Experiments were performed with Al_2O_3, CuO, TiO_2 and SiO_2, keeping the concentration constant at 1% by weight. Again, instability was observed only with pure water. It is seen from Fig. 30 that all the nanofluids suppress single-phase flow instability. Increased flow rate was also observed with all nanofluids. Highest flow rate was observed with CuO nanoparticles followed by TiO_2, Al_2O_3 and SiO_2 in that order. A comparison of increase in loop flow rate with different nanofluids is given in Table 4. The increase in loop mass flow rate can be either because of increase in thermal coefficient of expansion caused by addition of nanoparticles or because of reduction in friction factor. Experimental investigations on thermal coefficient of expansion show a significant increase with addition of nanoparticles to water as shown in Table 5.

TABLE 4. EFFECT OF DIFFERENT NANOFLUIDS ON LOOP MASS FLOW RATE

Nanoparticle used (% weight of Al_2O_3)	Enhancement in flow rate (%) over water without nanofluid
SiO_2	5.8
Al_2O_3	15.1
TiO_2	20.6
CuO	21.1

TABLE 5. COEFFICIENT OF THERMAL EXPANSION FOR NANOFLUIDS AT 35°C

Fluid	β x 1E-4
Water	3.45
Al_2O_3	4.01
CuO	4.49
SiO_2	4.38
TiO_2	3.96

(b) Effect of nanofluid on two-phase flow instability

Experiments were carried out in two-phase natural circulation loop as shown in Fig. 31. The experimental loop consisted of a vertical tubular heater directly heated by electric current up to a maximum power of 80 kW.

Experiments were carried out for water alone and 1% Al_2O_3 nanofluid for different steam drum pressure and levels [14]. The experimental results are as shown in Figures 32–33. It was observed that in natural circulation with nanofluids: (1) boiling occurs earlier when compared to pure water; (2) the amplitude of type-I instabilities is substantially lower with nanofluids; and (3) the mean ΔP is higher, indicating a higher flow rate with nanofluids.

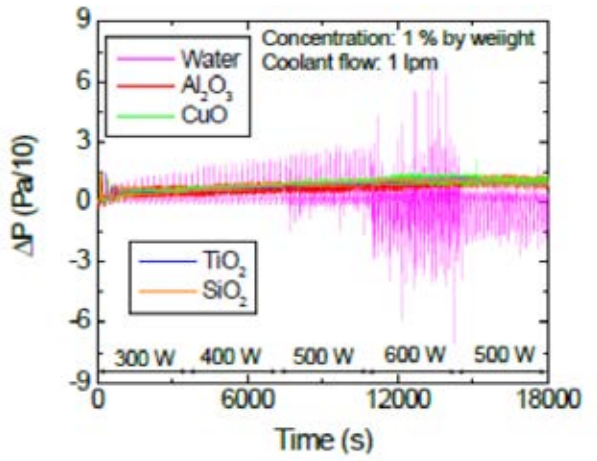

FIG. 30. Stabilization with different nanofluids.

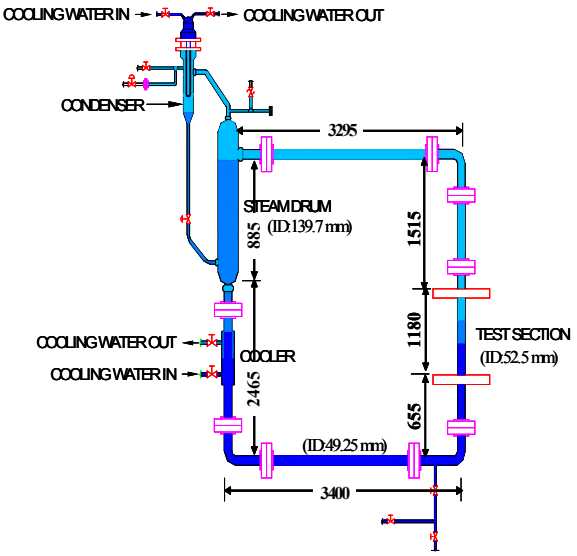

FIG. 31. Two-phase natural circulation loop.

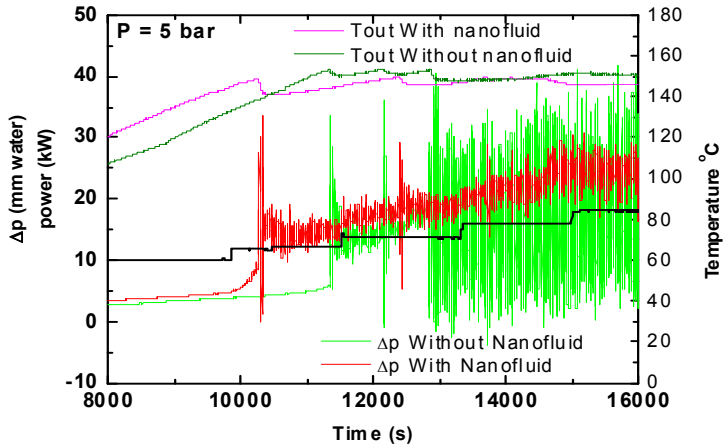

FIG. 32. Stability with and without nanofluids at 5 bar pressure.

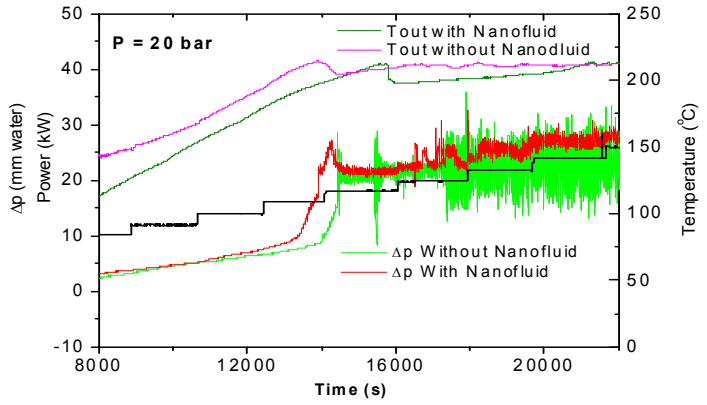

FIG. 33. Stability with and without nanofluids at 20 bar pressure.

4.3. CASE STUDIES FOR CAREM

4.3.1. Phenomenology involved in reactor thermohydraulics

4.3.1.1. Relevant phenomena in CAREM-25 thermohydraulics

The physics involved in the CAREM-25 reactor include different well known phenomena such us self-pressurization, flashing, natural circulation, condensation, density wave instabilities and neutronic coupling. The combination of these, however, creates abundant feedback, influencing the reactor dynamics and creating novel situations which are potentially destabilizing and therefore need to be investigated in depth.

In the following subsections, different aspects of the aforementioned phenomenon are described which will contribute to the understanding of the CAREM-25 reactor behaviour.

4.3.1.2. Single-phase natural circulation

In the CAREM-25 reactor, the steam quality is very low and therefore the largest driving factor contributing to the momentum balance is due to single-phase buoyancy forces. For this reason, in the following simplified analysis only single-phase natural circulation is considered.

The coolant flow in a natural circulation loop is driven by a difference in the density profile between the upwards and downwards branches of the circuit. Formally, the buoyancy force can be defined in terms of the following integral along the circuit:

$$F_{buoy} = -\oint A\rho_{(s)} g \cos\theta \, ds \tag{1}$$

The integration variable s is a curvilinear coordinate along the circuit and θ is the angle formed by the versors $\check{s}$ and $\check{z}$, which correspond to flow direction and gravity respectively.

In the CAREM-25 reactor, since the void fraction is very low, the acceleration component of the pressure drop is negligible. The same approximation is valid when considering the inertial pressure drop, since the flow velocity and its derivative are very small under any condition. Therefore, the pressure drop component which compensates the buoyancy force in the system is due to friction losses. The stationary condition is therefore reached when buoyancy forces are balanced with friction forces.

In order to estimate the flow rate, it is necessary to estimate these two forces in terms of the relevant physical and geometrical magnitudes. To simplify such a calculation, let us assume a closed loop in which only one phase is present, with a uniformly heated section placed at the bottom of the upwards branch and a uniformly cooled section located at the top of the downwards branch, with all other sections isolated (see Fig. 34).

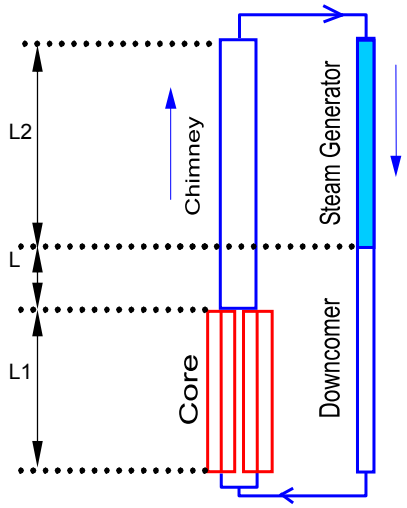

FIG. 34. Considered closed circuit representing CAREM-25.

The length of the heated and cooled sections is *L1* and *L2* respectively while *L* is the vertical distance existing between these two sections. *A* is the reference cross sectional area of the circuit. The buoyancy force for the steady state condition in this circuit is found by solving the integral in Equation (1).

$$F_{buoy} = A\left[-\rho_l g L_1 - \frac{\Delta\rho}{2} g L_1 - \rho_l g\left(L - L_1\right) + \rho_l g L + \Delta\rho g\left(L - L_2\right) + \frac{\Delta\rho}{2} g L_2\right] \tag{2}$$

where ρ_l is the fluid density at the exit of the heated part of the circuit and $\Delta\rho$ is the density change regarding the density at the exit of the cooled section of the circuit. Equation (2) can be rewritten as:

$$F_{buoy} = A\Delta\rho g\left(L - \frac{L_1 + L_2}{2}\right) \tag{3}$$

The total power Q_{Nuc} entering the system must equal the coolant enthalpy change in the core Δh times the mass flow rate $\dot{m}$, mathematically:

$$Q_{Nuc} = \dot{m}\left(h_{Nuc,e} - h_{Nuc,i}\right) = \dot{m}\Delta h = \dot{m}c_p\Delta T_{Nuc} \tag{4}$$

where the fluid temperature changes are related to density changes through the thermal expansion coefficient β: $\Delta\rho = \rho_l\beta\Delta T_{Nuc}$

For simplicity, the Boussinesq approximation is assumed. By replacing and operating it is easy to find the buoyancy force term.

$$\Delta\rho = Q_{Nuc}\frac{\beta}{\dot{m}c_p} \quad \Rightarrow \quad F_{buoy} = A\frac{Q_{Nuc}}{\dot{m}}\frac{g\beta\rho_l}{c_p}\left[L - \frac{L_1 + L_2}{2}\right] \tag{5}$$

The friction losses can be estimated as:

$$F_{fric} = A\left[\underbrace{\sum f\frac{L}{2D}\rho v^2}_{Distributed} + \underbrace{\sum\frac{1}{2}k\rho v^2}_{Concentrated}\right] \equiv K\frac{\dot{m}^2}{2\rho_l A} \tag{6}$$

where v is the local velocity and f and k are distributed and concentrated friction factors respectively. To simplify the analysis, a single friction coefficient K is defined which condenses the two aforementioned effects and relates F_{frict} with $\dot{m}^2$.

The steady state condition is reached when:

$$A\frac{Q_{Nuc}}{\dot{m}}\frac{g\rho_l\beta}{c_p}\left[L - \frac{L1 + L2}{2}\right] = K\frac{\dot{m}^2}{2\rho_l A} \Rightarrow \dot{m}^3 = Q_{Nuc}\frac{2A^2 g\rho_l^2\beta}{Kc_p}\left[L - \frac{L1 + L2}{2}\right] \tag{7}$$

Finally it is possible to obtain the desired relation as:

$$\dot{m} = \sqrt[3]{\frac{2A^2 Q_{Nuc} g\rho_l^2\beta}{Kc_p}\left[L - \frac{L1 + L2}{2}\right]} \tag{8}$$

From Equation (8), it is clear that the relation between the power and the mass flow rate is not linear. By using Equations (8) and (4), the enthalpy increase in the core section can be obtained.

$$h_{Nuc,e} - h_{Nuc,i} = \Delta h = \frac{Q_{Nuc}}{\dot{m}} = \sqrt[3]{\frac{Kc_p Q_{Nuc}^2}{2A^2 g\rho_l^2\beta}\left[L - \frac{L1 + L2}{2}\right]^{-1}} \tag{9}$$

4.3.1.3. Self-pressurization mechanism

In order to have a constant pressure during CAREM-25 normal operation, some vapour needs to be created inside the RPV. Let us assume that, for a while, the vapour generation rate is larger than the condensation rate. Under such a condition, the saturation enthalpy of the liquid increases, decreasing the vapour generation rate, which in turn decreases the system pressure. Such feedback, therefore, tends to maintain the pressure constant.

Assuming that no carry-under is present, the vapour generated in the hot leg of the circuit is condensed before entering the cooling devices.

The energy balance for the entire circuit at steady state yields:

$$Q_{Nuc} = Q_{SG} + Q_{Cond} \tag{10}$$

where Q_{SG} is the power extracted by the cooling devices (i.e. the steam generators) and Q_{cond} is the power related with vapour condensation.

The heat balances in the heated and cooled sections yield:

$$Q_{Nuc} = \dot{m}(h_{Nuc,e} - h_{Nuc,i}) \tag{11a}$$

$$Q_{SG} = \dot{m}(h_{sat} - h_{SG,e}) = \dot{m}(h_{sat} - h_{Nuc,i}) \tag{11b}$$

By replacing Equation (10) with Equation (11), we finally obtain an expression for the condensation power Q_{cond}:

$$Q_{Cond} = \dot{m}(h_{Nuc,e} - h_{sat}) \tag{12}$$

Such a condensation takes place in the upper part of the reactor and is a direct consequence of the heat losses and the interaction of the vapour with cold structures present in the steam dome such as those from the reactivity control mechanism.

Equation (9) combined with Equation (12) and (8) can be used to find an expression for the core inlet enthalpy $h_{Nuc,i}$,

$$h_{Nuc,i} = h_{sat} - \left(Q_{Nuc} - Q_{Cond} \right) \sqrt[3]{\frac{Kc_p}{2A^2 Q_{Nuc}\, g\rho_l^{\,2}\, \beta \left[L - \frac{L1+L2}{2} \right]^{-1}}} \tag{13}$$

From this result, it can be observed that in a self-pressurized, natural circulation such as CAREM-25, the core inlet enthalpy cannot be controlled directly but it is a result of the combination of the produced and condensed power in the system.

Equation (9) can be used to calculate the mean enthalpy in the reactor core, $\overline{h}_{Nuc}$, thus:

$$\overline{h}_{Nuc} = \frac{h_{Nuc,e} + h_{Nuc,i}}{2} = \frac{1}{2} \sqrt[3]{\frac{Kc_p Q_{Nuc}^{\,2}}{2A^2\, g\rho_l^{\,2}\, \beta \left[L - \frac{L1+L2}{2} \right]^{-1}}} + h_{Nuc,i} \tag{14}$$

Replacing Equation (14) with Equation (13), the mean core enthalpy is obtained in terms of the produced and condensed powers.

$$\overline{h}_{Nuc} = h_{sat} - \left(\frac{Q_{Nuc}}{2} - Q_{Cond} \right) \sqrt[3]{\frac{Kc_p}{2A^2 Q_{Nuc}\, g\rho_l^{\,2}\, \beta \left[L - \frac{L1 + L2}{2} \right]^{-1}}} \qquad (15)$$

Equation (15) clearly shows that when decreasing the power level while maintaining all other parameters constant, the mean enthalpy in the core approaches to the saturation value, which indicates that the core is hotter at low power levels than at nominal condition. This result is quite anti-intuitive and reveals different behaviour of CAREM-25 reactor compared to conventional nuclear PWRs. In such reactors, a lower power level is associated with a lower value of the core enthalpy exit while the core inlet enthalpy is roughly constant. In the CAREM-25 reactor, the core exit enthalpy is very close to the saturation enthalpy under all conditions and a lower power level is associated with a higher core inlet enthalpy.

4.3.1.4. Limitations in coolant mass flow rate

In a self-pressurized, natural circulation reactor such as CAREM-25, the uncertainties related to the prediction of the resulting coolant mass flow rate need to be carefully studied. In particular, two extreme cases might occur:

(a) the total friction in the system is overestimated beyond the calculated uncertainty;

(b) the total friction in the system is underestimated beyond the calculated uncertainty.

In case a), if K is overestimated it the friction might actually be much smaller than estimated and thus $\overline{h}_{Nuc}$ could be very close to the saturation enthalpy (See Equation (15)). This might result in degradation of the thermal margin. In case b), on the contrary, if the friction is actually much larger than the estimated one, the resulting mass flow rate will be much smaller than expected. This implies the steam generators need to be able to cool with a lower primary-secondary temperature difference (see Equation (11b)). It may, therefore, occur that the steam generators are not able to evacuate the prescribed power.

From this simple analysis, it is clear that for a given power the mass flow rate must remain in a certain range in order to avoid any undesired consequences in the system. In order to eliminate deviations of the obtained mass flow rate regarding the design value, special pressure drop devices located at the core inlet location will be adjusted during commissioning of the reactor.

4.3.1.5. Density wave instabilities

The highly complex phenomena occurring in nuclear reactors cooled by two-phase flows have motivated extensive research programmes in the past with a strong emphasis on stability studies. As a result of these, important knowledge has been generated which has helped us to understand the main instability mechanisms. For instance, it is known that the most important instabilities in currently operating boiling water reactors (BWRs) are purely thermohydraulic and coupled neutronic-thermohydraulic instabilities [15–16]. These instability types are basically induced by the 'density-wave' character of the two-phase flow in the coolant channels.

It is usual to divide the density wave oscillations (DWOs) into two main instability types: low-frequency Type-I instabilities induced by the gravitational pressure drop term, and high-frequency Type-II instabilities due to frictional pressure losses.

The Type-I instability mechanism usually becomes dominant in natural circulation reactors operating at low quality flows, e.g. during BWR startup and in novel reactors such as CAREM-25. Under these conditions, the mass percentage of steam, i.e. the flow quality, at the core exit becomes very small. For small flow qualities (and particularly at low pressures) the volumetric amount of steam (the void fraction) increases very rapidly as a function of the flow quality. A small decrease in the core inlet flow then leads to a large increase of the volume of steam produced at the core exit. In a natural circulation reactor, this causes a low-density wave travelling through the chimney. This enhances the driving head, and the inlet flow therefore increases. Then the opposite process occurs, and the void fraction in the chimney decreases. Consequently, the driving head becomes smaller and the flow rate therefore decreases. This completes one cycle of a Type-I oscillation. The main time constant governing this type of DWO is the transit time of the voids through the chimney section (~5–15 s) [17–18].

4.3.1.6. Flashing phenomenon

In CAREM-25, besides some vapour created in the core (the vapour quality at the exit of such a section is practically zero), this amount of vapour is created by the 'flashing phenomenon' occurring in the chimney. The natural circulation CAREM-25 reactor can be represented as a loop, (see Fig. 34), with a cold section (the downcomer), a heated section (the core), an adiabatic section (the chimney) and a heat exchanger. As shown before, density differences between the cold and hot legs cause the water to flow without using pumps. Natural circulation is thus enhanced in this type of reactor by using a tall chimney.

As the heated coolant flows upwards, the hydrostatic pressure will decrease. Hence, the saturation temperature will also decrease. If the saturation enthalpy becomes equal to the (constant) fluid enthalpy in the chimney, vapour created by flashing occurs — i.e. boiling out of the heated reactor core (see Fig. 35). This ex-core boiling is enhanced as the reactor pressure decreases because at low pressure the saturation enthalpy is more dependent on the axial position. In the particular case of the CAREM-25 reactor, the flashing phenomenon is crucial for the stability analysis in both the reactor startup, i.e. at low pressure, and under nominal conditions.

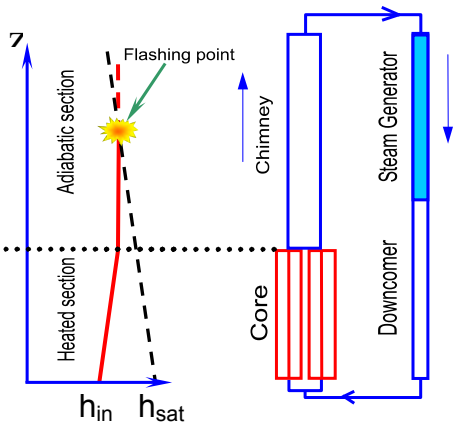

FIG. 35. CAREM-25 reactor and the occurrence of flashing.

Let us add the flashing mechanism to the closed loop model described previously.

The fluid entering the cooling section (representing the steam generators) is assumed to be saturated. In addition, the coolant leaves the section (i.e. it enters the heated section) with an enthalpy $h_{Nuc,i}$. The enthalpy of the fluid leaving the reactor core is $h_{Nuc,\,e}$.

Pressure in the system will vary along the vertical direction due to the hydrostatic pressure decrease and friction losses (the acceleration and inertial contributions are small and thus not considered). Let us call P_{sys} the pressure at the highest part of the circuit which coincides with the pressure at the entrance of the cooled section. Neglecting the friction contribution, the pressure as a function of the axial location is given by:

$$P(z) = P_{sys} + \rho g z \tag{16}$$

where z is the distance from the top of the heated section. The density is assumed constant along the hot leg above the heated section. This axial pressure variation causes a variation of the saturation enthalpy along z. This can be expressed as:

$$h_{sat}(z) = h_{sat}(P(z)) = h_{sat}(P_{sys} + \rho g z) \tag{17}$$

Taking a first order approximation in the enthalpy variation:

$$h_{sat}(z) = h_{sat}(P_{sys}) + \left.\frac{\partial h_{sat}}{\partial P}\right|_{P=P_{sys}} \rho g z \tag{18}$$

the onset of flashing will take place at the value of $z = \lambda$ in the hot leg that satisfies the following equality:

$$h_{sat}(\lambda) = h_{Nuc,e} \tag{19}$$

with λ being the flashing boundary measured from the chimney top. The condition that the fluid is at saturation point at the entrance of the cooled section has certain implications. Since no carry-under of bubbles is present, all vapour needs to be condensed before entering the cooled section. This phenomenon occurs in CAREM-25 in the upper dome zone. In other words, the excess of enthalpy over the saturation value (at the chimney exit) is evacuated through condensation of the vapour originated by flashing (and boiling, if present) in the steam dome walls or other structures. It is assumed that the mass of condensed fluid flows back into the liquid stream at saturation enthalpy. The fluid that remains liquid during flashing is also assumed to be at saturation condition at local pressure.

The energy balance for the entire circuit at steady state, as presented before is thus modified accordingly:

$$Q_{Nuc} = Q_{SG} + Q_{Cond} \tag{20}$$

The heat balances in the heated and cooled sections are now:

$$Q_{Nuc} = \dot{m}(h_{Nuc,e} - h_{Nuc,i}) \tag{21a}$$

$$Q_{SG} = \dot{m}(h_{sat}(P_{sys}) - h_{SG,e}) = \dot{m}(h_{sat}(P_{sys}) - h_{Nuc,i}) \tag{21b}$$

By replacing Equation (20) with (21), we obtain an expression for the condensation power Q_{cond} in the case the flashing effect is considered.

$$Q_{Cond} = \dot{m}(h_{Nuc,e} - h_{sat}(P_{sys})) \tag{22}$$

We can now use Equations (18), (19) and (21) to evaluate the point at which flashing starts:

$$\lambda = \frac{Q_{Cond}}{\dot{m}} \frac{1}{\rho g \left.\frac{\partial h_{sat}}{\partial P}\right|_{P=P_{sys}}} \tag{23}$$

By using Equation (8) to describe the mass flow rate, Equation (23) is transformed into:

$$\lambda = \frac{Q_{cond}}{\left.\frac{\partial h_{sat}}{\partial P}\right|_{P=P_{sys}}} \sqrt[3]{\frac{Kc_p}{2A^2 Q_{Nuc} g^4 \rho_0^{\,5} \beta \left[L - \frac{L1+L2}{2}\right]}} \tag{24}$$

As can be observed, the flashing boundary λ has a proportional relation with the condensation power Q_{cond} and the inverse of the cubic root of the core power Q_{Nuc}.

Equation (24) has important implications. It is well known that the location of the boiling-flashing boundary has a strong effect on the void transport delay which is the basis of density wave instabilities mechanism. The importance of the boiling-flashing boundary location is therefore obvious (note that when vapour is produced only in the chimney we refer to *the flashing boundary*; however, in general we use the term *boiling-flashing boundary*). From the aforementioned equation, it can be seen that a possible way of *varying* the stability performance of the system (for a large range of core powers) is by changing the condensation power in the steam dome. In other words, the condensation power seems to be a very efficient means for varying the phase lag of the density waves travelling through the system and, therefore, can be used for stabilizing purposes.

To give an idea of the importance of this effect in the CAREM-25 case, a simple calculation is presented with which the amount of power involved in the flashing phenomena is estimated. Let us assume the reactor is working under nominal conditions and the core exit quality is zero.

TABLE 6. CAREM-25 REFERENCE VALUES AT NOMINAL CONDITIONS

	Symbol, unit	Chimney inlet	Chimney outlet
Position	z, [m]	0	4.6
Hydrostatic pressure	P, [MPa]	12.25	12.22
Liquid density	ρ, [kg/m^3]	651.0	651.5
Saturation temperature	T_{sat}, [°C]	326.26	326.07
Liquid enthalpy	h_{liq} ,[kJ/kg]	1501.5	1500.3
Mass flow rate	$\dot{m}$,[kg/s]	410	410

By using data from Table 6, the amount of power converted into vapour by means of the flashing phenomenon Q_{cond} can be estimated as:

$$Q_{Cond} = \dot{m}\left(h_{Sat,Ch,i} - h_{Sat,Ch,i}\right) = 0.5 \text{ MW} \tag{25}$$

Thus, since the coolant is saturated at the core exit, i.e. the chimney inlet, the flashing phenomenon provides vapour in the steam dome carrying a power equal to 0.5 MW. As mentioned before, the vapour is separated in the free region located above the chimney and condensed in the dome and in the surface of the control mechanisms. Due to the large area for the void separation and the low coolant velocities, no or little carry-under of bubbles is expected.

The presence of this vapour generated by flashing enhances self-pressurization of the system. However, if the vapour generation rate is greater than the condensation rate, the system pressure will increase and the vapour creation by means of flashing will diminish. This feedback also contributes to maintain the pressure constant.

Vapour production in the chimney directly affects the gravitational pressure drop over this section. Hence, it can be expected that the Type-I feedback mechanism is amplified by the occurrence of void flashing, especially in a natural circulation reactor with a tall chimney section such as CAREM-25.

4.3.1.7. Natural variables of the system

As can be noted from the previous calculations (see e.g. Equations (8), (9) and (24)), the thermohydraulic behaviour of CAREM-25 can be described by using three independent parameters, 'natural variables'. These are the:

- system pressure, P_{sys} (defined at the steam dome), which influences the fluid properties and the saturation enthalpy variation with the pressure, see Equation (24);
- nuclear core power, Q_{Nuc};
- power which is condensed in the steam dome, Q_{Cond}.

Although this selection is not unique, it has proven to be very useful in practice since it immediately refers to controllable parameters of the system. In addition, for the CAREM-25 reactor (at constant pressure), the use of the Q_{Cond} vs. Q_{Nuc} plane for constructing the stability maps enlarged the region of interest which is, on the contrary, a very narrow region in the more conventional N_{sub} vs. N_{PCH} dimensionless plane. From the definition of these two dimensionless numbers, a direct relation to the natural variables of the system can be obtained. For simplicity, in the following analysis the flashing effect is not considered. In this way:

$$N_{PCH} \equiv \frac{Q_{Nuc}}{\dot{m}\, h_{fg}} \frac{\rho_l - \rho_v}{\rho_v} \tag{26}$$

where both liquid and vapour densities correspond to saturation condition. By using Equation (8) for expressing the mass flow rate we obtain

$$N_{PCH} = \frac{1}{h_{fg}} \frac{\rho_l - \rho_v}{\rho_v} \sqrt[3]{\frac{{Q_{Nuc}}^2 Kc_p}{2A^2\, g{\rho_l}^2\, \beta}\left[L - \frac{L1 + L2}{2}\right]^{-1}} \tag{27}$$

Which states the following relation exists between the phase change number and the core power:

$$N_{PCH} \propto {Q_{Nuc}}^{2/3} \tag{28a}$$

And then:

$$Q_{Nuc} \propto {N_{PCH}}^{3/2} \tag{28b}$$

The same can be done for the subcooling number, which is defined as:

$$N_{sub} \equiv \frac{h_{l,sat} - h_{Nuc,i}}{h_{fg}} \frac{\rho_l - \rho_v}{\rho_v} \tag{29}$$

where $h_{l,sat}$ refers to the liquid saturation enthalpy.

Equation (29) can be easily transformed into:

$$N_{sub} = \left(\frac{h_{l,sat} - h_{Nuc,e}}{h_{fg}} + \frac{h_{Nuc,e} - h_{Nuc,i}}{h_{fg}} \right) \frac{\rho_l - \rho_v}{\rho_v} \tag{30}$$

Recalling Equation (9), we immediately see that the enthalpy increase in the heated section can be expressed as:

$$h_{Nuc,e} - h_{Nuc,i} = \frac{Q_{Nuc}}{\dot{m}} = \sqrt[3]{\frac{K c_p {Q_{Nuc}}^2}{2A^2 g {\rho_l}^2 \beta \left[L - \frac{L1 + L2}{2} \right]^{-1}}} \tag{31}$$

By using this result, Equation (30) cab be rewritten as:

$$N_{sub} = \left(\frac{h_{l,sat} - h_{Nuc,e}}{h_{fg}} + \frac{Q_{Nuc}}{\dot{m} h_{fg}} \right) \frac{\rho_l - \rho_v}{\rho_v} \tag{32}$$

from which the phase change number can be easily identified.

$$N_{sub} = \left(\frac{h_{l,sat} - h_{Nuc,e}}{h_{fg}} \right) \frac{\rho_l - \rho_v}{\rho_v} + N_{PCH} \tag{33}$$

The saturation enthalpy and the core exit enthalpy are related with the condensation power as:

$$h_{l,sat} - h_{Nuc,e} = -\frac{Q_{Cond}}{\dot{m}} \tag{34}$$

By replacing Equation (33) with Equation (34), and manipulating the expression we can write:

$$Q_{Cond} = \left(N_{PCH} - N_{sub}\right)\frac{\rho_v \dot{m} h_{fg}}{\rho_l - \rho_v} \tag{35}$$

By identifying the last term of Equation (35) with Equation (26) we can see that:

$$Q_{Cond} = \left(N_{PCH} - N_{sub}\right)\frac{Q_{Nuc}}{N_{PCH}} \tag{36}$$

By manipulating Equation (27) we get:

$$Q_{Nuc} = N_{PCH} N_{PCH}^{1/2} \sqrt{\left(h_{fg}\frac{\rho_v}{\rho_l - \rho_v}\right)^3 \frac{2A^2 g\rho_l^2 \beta}{Kc_p}\left[L - \frac{L1+L2}{2}\right]} \tag{37}$$

Finally, by replacing Equation (36) with Equation (37), we can obtain the desired relation:

$$Q_{Cond} = N_{PCH}^{1/2}\left(N_{PCH} - N_{sub}\right)\sqrt{\left(h_{fg}\frac{\rho_v}{\rho_l - \rho_v}\right)^3 \frac{2A^2 g\rho_l^2 \beta}{Kc_p}\left[L - \frac{L1+L2}{2}\right]} \tag{38}$$

and thus:

$$Q_{Cond} \propto N_{PCH}^{1/2}\left(N_{PCH} - N_{sub}\right) \tag{39}$$

From this result, it is clear that the condensation power has a certain relation to the core exit quality.

As a corollary, we immediately see that the power extracted by the steam generators is associated with:

$$Q_{SG} \propto N_{PCH}^{1/2} N_{sub} \tag{40}$$

In order to stress the mapping obtained with the transformation of the N_{PCH} vs. N_{Sub} plane into the Q_{Nuc} vs. Q_{Cond} plane, the following approximate calculation is performed. Equations (10) and (11) can be combined to show that:

$$h_{sat} - h_{Nuc,i} = \frac{Q_{Nuc} - Q_{Cond}}{\dot{m}} = \frac{Q_{Nuc} - Q_{Cond}}{Q_{Nuc}^{1/3}}\sqrt[3]{\frac{Kc_p}{2A^2 g\rho_l^2 \beta}\left[L - \frac{L1+L2}{2}\right]^{-1}} \tag{41}$$

Replacing Equation (29) with Equation (41) yields:

$$N_{sub} = \frac{Q_{Nuc} - Q_{Cond}}{Q_{Nuc}^{1/3}}\frac{\rho_l - \rho_v}{h_{fg}\rho_v}\sqrt[3]{\frac{Kc_p}{2A^2 g\rho_l^2 \beta}\left[L - \frac{L1+L2}{2}\right]^{-1}} \tag{42}$$

For most cases, it can be stated that $Q_{Nuc} \gg Q_{Cond}$ By neglecting the condensation power in Equation (42) we can write:

$$N_{sub} \approx Q_{Nuc}^{2/3} \frac{\rho_l - \rho_v}{h_{fg}\rho_v} \sqrt[3]{\frac{Kc_p}{2A^2 g\rho_l^2 \beta}\left[L - \frac{L1+L2}{2}\right]^{-1}} \tag{43}$$

and finally, the core power can be related to the subcooling number as:

$$Q_{Nuc} \propto N_{sub}^{3/2} \tag{44}$$

The similarity between Equations (44) and (28) is obvious and is explained by the fact CAREM-25's operational range is very close to the quality line equal to zero.

To visualize the mapping defined by Equations (27), (38) and (43), the following stability maps are constructed which correspond to typical situations observed in CAREM-25 (for which the pressure is assumed to be constant). In this report, the stability maps are presented as contour plots with the amplification factor *a* as the vertical axis. Such a factor will be formally defined in the following sections; however, the larger this factor, the more unstable the system is. Moreover, the colour in the plots represents the level of the vertical coordinate.

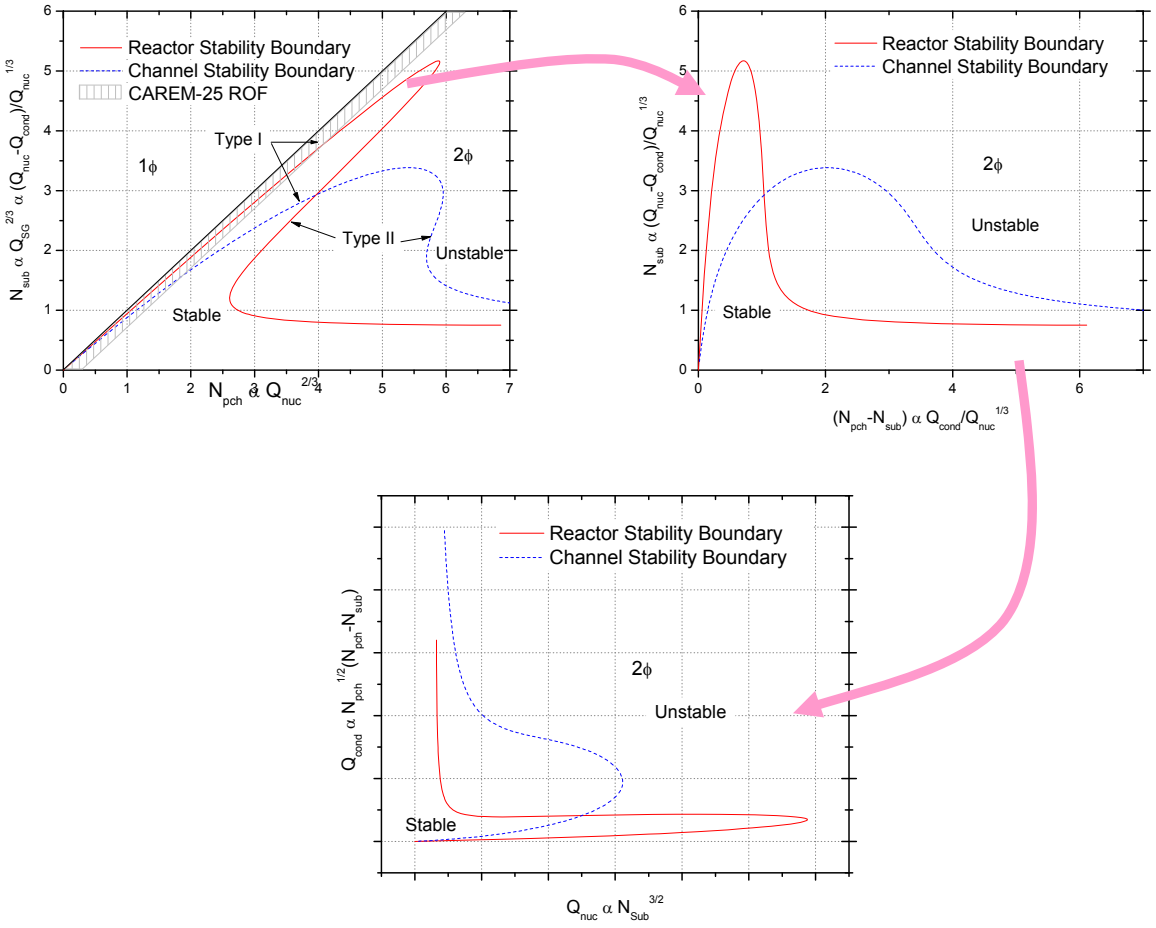

FIG. 36. Transformation of N_{PCH} vs.N_{Sub} plane into Q_{Nuc} vs. Q_{Cond} plane.

As can be observed from Fig. 36, the region of interest for the CAREM-25 reactor is considerably enlarged by using the proposed selection of variables. This result confirms the practical use of the Q_{Nuc} vs. Q_{Cond} plane instead of the common N_{PCH} vs. N_{Sub} plane for the case of self-pressurized natural circulation reactors such as CAREM-25.

It needs to be emphasized that when considering a steady state condition, all thermohydraulic parameters of the system can be expressed in terms of the aforementioned natural variables.

4.3.1.8. Conclusions

From the results shown in this section, it is clear that the thermohydraulics governing self-pressurized, natural circulation reactors such as CAREM-25 can be expected to be different from conventional BWRs, NC-BWRs and PWRs and, thus, cannot be extrapolated from these.

The natural variables of the system are Q_{Nuc}, Q_{Cond} and P_{sys}. For this reason, most of the results presented in this report, including the stability maps, are based in the Q_{Nuc} vs. P and Q_{Nuc} vs. Q_{cond} planes instead of the more common N_{sub} vs. N_{PCH} dimensionless plane.

In a steady state self-pressurized system in which no carry-under takes place, all the vapour produced in the hot leg needs to be condensed in the steam dome. When such a system works with very low quality natural circulation, the two-phase contribution in the buoyancy force can be neglected. In this case, the lower the location of the flashing limit (λ) is, the larger the condensation power. In other words, a more or less direct relation between the condensation power and λ exists (the effect of Q_{Nuc} is attenuated for the cubic root), as explicitly shown in Equation (24).

The condensation power in the steam dome has been identified as a potential effective means of choosing the operational point and its stability performance. This is due to the fact that, by condensing more or less vapour in the steam dome, the location of the boiling boundary can be varied. As can be imagined, such a location has great importance in determining the dynamics of the density waves and, thus, in the reactor stability. For this reason, a condensation coil has been included in the first CAREM-25 prototype in order to enhance the condensation power in the steam dome of the reactor.

It is also shown that the mass flow rate needs to be very close to the designed value. For this reason, special devices located at the reactor core inlet are installed in order to adjust the friction of the system accordingly.

4.3.2. Numerical code

4.3.2.1. Introduction

In this section, the code used for the study of the reactor stability is described. The HUARPE code was developed by Zanocco [19] to study the dynamics and stability of a reactor similar to CAREM-25, focusing on the behaviour of self-pressurization and the influence of diverse physical phenomena on the reactor stability. HUARPE includes modelling options in the time domain and in the frequency domain. With this code, it is possible to create stability maps and to carry out parametric studies in different variables, making it possible to assess the effect that those variables have on the system stability. In addition, it is possible to simulate transitory states and assess the system response to perturbations, thus enabling study, for example, of oscillation maximum amplitudes and limit cycles.

The code also includes an 'adaptive nodalization' scheme which allows the minimizing of diffusive effects from numerical origin. This scheme has an iterative routine that nodalizes the system on the basis of the perturbation transport speed, thus reducing numerical diffusion effects.

It is interesting to study the influence of certain parameters on system stability. In particular, it is a goal to investigate the influence that the implementation of a heat removal device at the dome should have, with the purpose of incrementing the steam condensation during the startup.

In this report, the stability during startup of a reactor with the aforementioned characteristics is studied, identifying the conditions that make it unstable.

4.3.2.2. Modelled hypothesis

The hypotheses considered in the HUARPE code are listed below:

- One-dimensional flux is assumed, by modelling a special coordinate in the direction of flow circulation. This is applied in all circuit nodes, excepting the node that represents the dome, since there is not a preferential direction of the flow circulation here. Such assumption is considered to be conservative since in a 3D flow geometry the enthalpy fronts tend to dissipate more efficiently any perturbation which may lead to instabilities.
- The model of drift-flux is considered valid for the two-phase dynamics. It is assumed that both phases behave as a mixture, with appropriately averaged properties and, therefore, assuming the phases is in thermodynamic equilibrium. Neglecting subcooled boiling is conservative because of two different effects which will be detailed later: the neutronic feedback and the underestimation of the condensation power.
- For the saturated flow properties calculation, the pressure change due to friction is neglected and such properties are dependent only on time and on hydrostatic position. In general, this is valid for circuits with natural circulation at low qualities. In the case of CAREM-25, the pressure change due to friction is an order of magnitude lower than the change caused by height and in the case of the chimney, it can be of two orders of magnitude lower.
- 'Carry-under' is not considered from the dome to the inner part of the steam generators. Due to the large size of the passing through area at the steam generator's inlet, it is expected that the flow speed will be low enough to avoid the carry-under effect.
- Stratified flow is considered at the dome while thermal non-equilibrium is also assumed: the steam will be naturally accumulated at the upper part of the dome. At this place there is not a circulation preferential direction, due to the boiling and condensation processes that are expected to occur. It is also expected that these processes, together with the re-circulation caused by the volume control system, will favour mixing in the two-phase region. That is why averaged properties are considered.
- This model results in four Equations: mass and energy for the mixing zone and for the steam zone.
- The axial heat conduction is neglected in the fuel, and the temperature is averaged in a radial way. It is considered that the fuel is homogeneous (mixed cladding and pellet) and the thermal conductivity is independent from temperature.
- It is supposed that the core power has a cosinoidal-type distribution with the maximum moved to the lower part. In this work, different phenomena which affect the power distribution are considered, such as control rod positions, the void fraction at the core outlet, and the effects related to neutron leakage at the core ends.

- A point-kinetics model with six delayed neutron groups for the core power is used. Reactivity feedbacks caused by coolant density and fuel temperature are contemplated with constant feedback coefficients.
- The dome structures are modelling with a part in contact with steam and another part in contact with a two-phase mixture, considering a mobile boundary. In addition, the heat exchange between these parts when moving the boundary is taken into consideration.
- Heat transference through the RPV structures and the power extracted by the liquid circulation in the control rod movement systems are contemplated in the condensation power.
- It is expected that in the lower plenum there are mixing processes which enhance enthalpy front diffusion coming from the steam generators. This process is ruled by a strongly three-dimensional geometry, fact which makes its modelling difficult. However, when this enthalpy front diffusion is not considered, a conservative approximation from the stability point of view is carried out. Therefore, the lower plenum is not included in the circuit.
- It is considered that the power extracted by the steam generators is constant and uniform in its length.

4.3.3. Steady state results

4.3.3.1. CAREM-25 behaviour at steady state nominal conditions

The following aspects are relevant for describing the CAREM-25's behaviour under steady state nominal conditions.

4.3.3.2. Coolant flow vs. power curve

In order to assess the behaviour of the natural circulation in the CAREM-25 reactor, the HUARPE code is used to calculate the coolant mass flow rate obtained for different nuclear core power levels when operating the reactor at nominal pressure and at a condensation power value equal to 0.5 MW. The resulting relation is presented in Fig. 37. For completeness, the relation between these two parameters predicted by Equation (8) is also included.

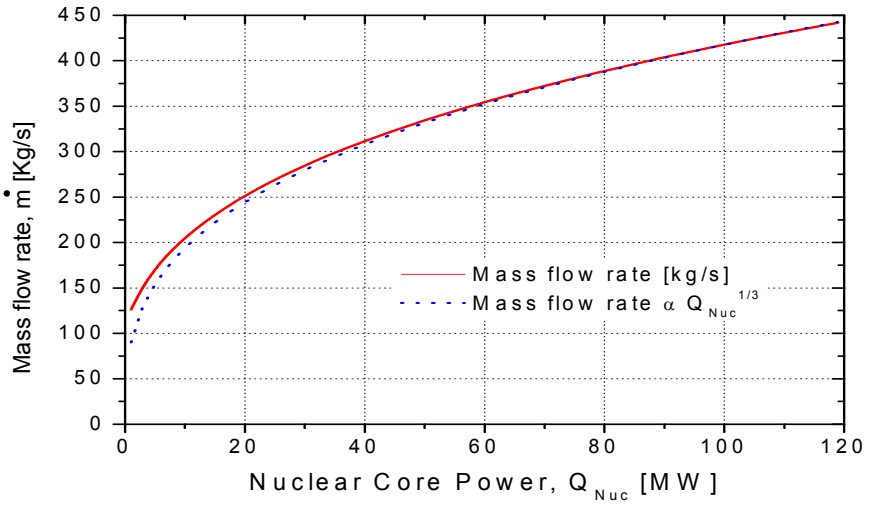

FIG. 37. The relation between the mass flow rate and the core power obeys a relation given by Equation (8) which is of the form $\dot{m} \propto Q_{Nuc}^{1/3}$.

As can be observed in the figure, the mass flow rate as estimated with the numerical code shows a good agreement with the relation given by Equation (8). It can be noted, however, that the result from the HUARPE code predicts a higher mass flow rate than the explicit relation at low nuclear core power levels. This difference is explained by the fact that the condensation power (which is kept constant in this analysis) is relatively higher in this case. A relatively high condensation power causes the flashing boundary position to move downwards, which enhances the two-phase contribution in the momentum balance (see Equation (24)). This is not considered in the simplified model from which Equation (8) is derived.

(a) Density profile along reactor

In this subsection, the coolant density profile along the reactor circulation coolant path is shown as Fig. 38. Different correlations are used in order to estimate the heat transfer in the steam generators according to the corresponding mechanism in the steam generators' secondary side: single-phase (overheated steam), nucleation or single-phase (subcooled) mechanism.

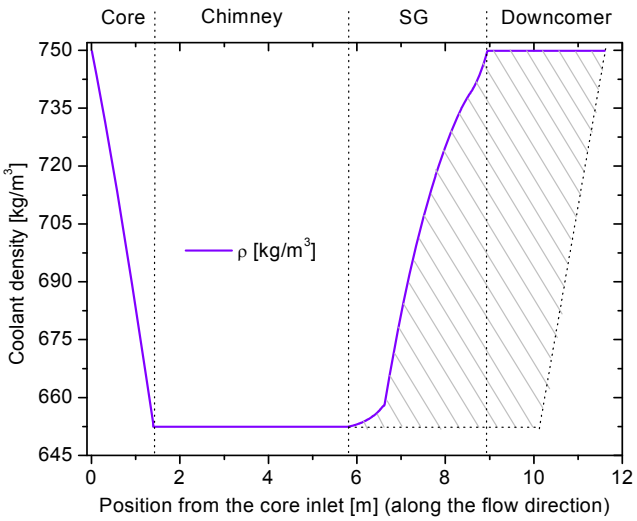

FIG.38. Coolant density profile along CAREM-25's primary circuit.

From the figure it can be seen the density decreases linearly in the reactor core and remains at a low value in the chimney. As the coolant enters the steam generators, it is cooled showing a density increase which is more or less linear. The density remains at a high value until it enters the core section, closing the cycle. The dashed area in Fig. 38 is proportional to the buoyancy force driving the coolant.

(b) The primary circuit pressure drop distribution

Another interesting aspect which is important for stability issues is the pressure drop distribution along the reactor primary circuit. Such a distribution corresponding to nominal conditions is presented in Fig. 39.

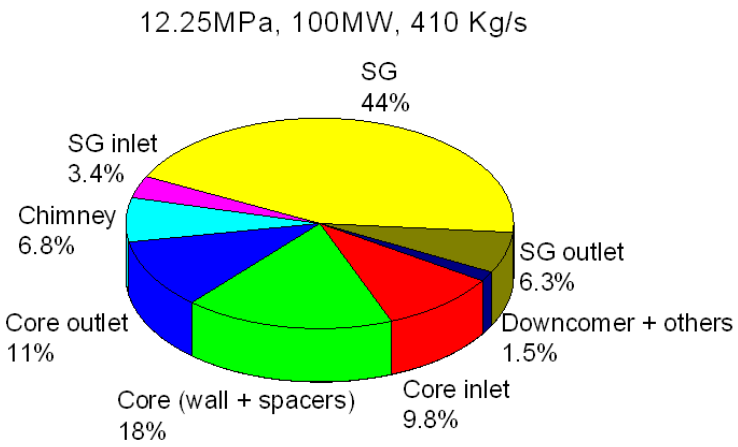

FIG. 39. CAREM-25's primary circuit pressure drop distribution at nominal conditions.

Since the void fraction is very low in the system, the acceleration component of the pressure drop is negligible. The same approximation is valid when considering the inertial pressure loss, since the flow velocity and its derivative is very small at any condition. Due to these, the pressure drop component which compensates the buoyancy force is due to friction losses in the system.

From the results, the large contribution of the steam generators to the total pressure drop (~54%) is noticeable.

(c) Core enthalpy increase

In this section, the HUARPE code is used to investigate the evolution of the core inlet enthalpy and also the enthalpy increase in the core when the system core power is varied. As in previous cases, the reactor is operated at nominal pressure and at a condensation power level equal to 0.5 MW. The result of this numerical experiment is shown in Fig. 40.

As can be seen from Fig. 40, the core inlet enthalpy increases when the core power decreases. In addition, the enthalpy increase in the core reduces when the power level decreases. This is explained by the fact the core outlet enthalpy is, at any condition, very close to the saturation value, which implies that the enthalpy at the core inlet has to increase when the power level decreases in order to satisfy Equation (31).

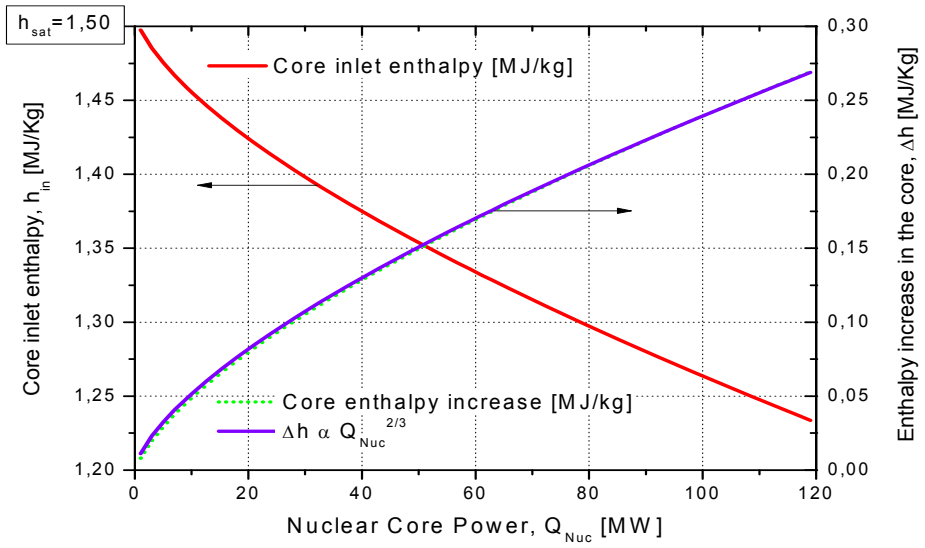

FIG. 40. Evolution of enthalpy increase in core section (relation between Δh and core power obeys relation given by Equation (9), which is $\Delta h \propto Q_{Nuc}^{2/3}$).

This result is directly related to the self-pressurization mechanism which *fixes* the value of the core outlet enthalpy since vapour needs to be produced in order to maintain the system pressure. This behaviour is different from other nuclear reactors for which the enthalpy at the core inlet is more or less fixed and the core exit enthalpy follows the power variations.

(d) Boiling boundary location

As mentioned before, a very important parameter for stability analysis regarding density wave oscillations is the location of the boiling-flashing boundary in the system. Accordingly, Fig. 41 corresponds to the CAREM-25 reactor operated at nominal pressure, at a condensation power level equal to 0.5 MW and at different core power levels.

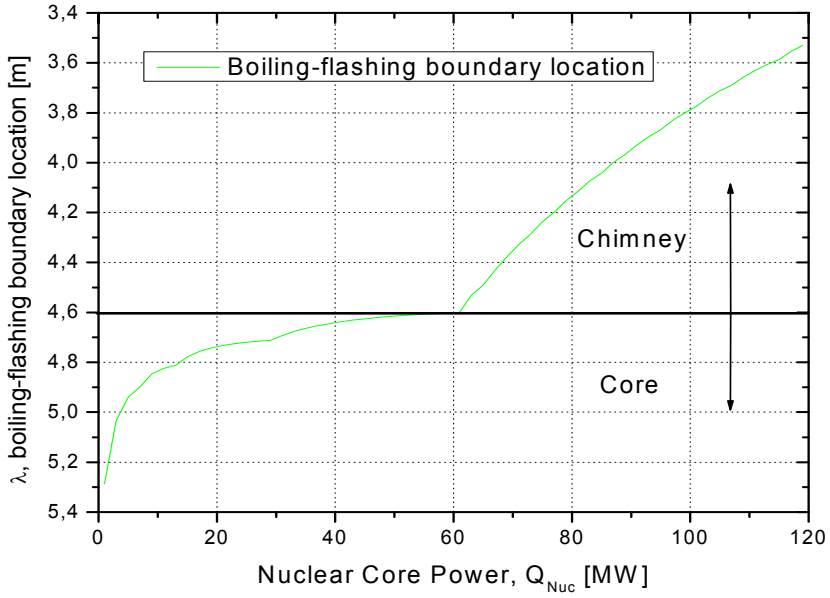

FIG. 41. Evolution of boiling-flashing boundary location according to different reactor power levels.

From Fig. 41, it is seen that the boiling-flashing boundary location moves downwards according to decreasing core power levels. In particular, when there is no vapour production by means of boiling, the result is in agreement with the relation given by Equation (24).

4.3.3.3. Conclusions

The CAREM-25 reactor's thermohydraulic behaviour is different from that of PWRs and also of natural circulation BWRs. Thus, it is clear that the combination of different effects makes CAREM-25's behaviour impossible to be extrapolated from existing knowledge and accumulated experience. Therefore, an exhaustive analysis regarding the thermohydraulic performance (including stability analysis) needs to be performed. Summarizing, the following conclusions can be drawn from the CAREM-25's steady state results.

- Single-phase natural circulation is the most important driving mechanism in the reactor, which follows a relation of the form $\dot{m} \propto Q_{Nuc}^{1/3}$.
- The friction pressure loss corresponding to the steam generators represents around half of the total pressure losses in the system.
- When CAREM-25 operates with a prescribed condensation power and pressure levels, the boiling-flashing boundary location moves downwards as the core power level is decreased.
- Unlike most nuclear reactors, in CAREM-25 the core inlet enthalpy increases when decreasing the core power.
- Unlike NC-BWRs, the self-pressurization phenomenon does not allow direct control of the coolant enthalpy at the CAREM-25 core inlet.
- The condensation power seems to be a very sensitive parameter in determining the boiling-flashing boundary location and, thus, the stability of CAREM-25. For this reason, this variable is highly suitable to optimize the stability performance of the reactor.
- The mass flow rate needs to be as close as possible to the designed value.

4.3.4. Linear stability results

The analysis referring to the CAREM-25 reactor's stability is presented building the stability maps. The preparation of such stability maps is carried out by using the power generated at the core (Q_{nuc}) as abscises variable, and the power extracted by condensation in the region of the steam dome (Q_{cond}) as ordinates variable. As already mentioned in a previous section, such a selection is preferred instead of the dimensionless sub-cooling number N_{Sub} and phase change number N_{PCH} since CAREM-25 operational region is a very narrow region close to the steam quality line equal to zero, which makes its perception difficult (see Fig. 15). Besides, the natural variables of the system are Q_{nuc} and Q_{cond}, which make the stability maps comprehension easy and enable an optimal visualization of the area of interest: wide range in Q_{nuc} with low values of Q_{cond}.

Perturbing a linear system may progress in several ways: it may oscillate (or not) or it may present growing or decaying amplitude behaviour. The evolving of a dynamic response should be adjusted using an exponential function of e^{at} kind. From this, amplification factor a can be defined, which is used in this report to define system stability: positive values are equivalent to unstable conditions, and negative values to stable cases.

In this report, stability maps are presented as contour plots with the amplification factor a as the vertical axis. Moreover, the colour in the plots represents the level of the vertical coordinate.

In this report oscillations lower than $1.4 \cdot 10^{-4}$ Hz are not considered (periods of about two hours) since the nature of these oscillations is quite different from density wave instabilities.

4.3.4.1. Stability at nominal conditions (P=12.25 MPa) – parametric study

In this section, the CAREM-25 linear stability performance at nominal pressure is investigated. In order to clarify the effects derived from the different feedback mechanisms, three different cases are considered. These are: 1) purely thermohydraulic stability; 2) neutronic-thermohydraulic stability (thermohydraulic stability with the neutronic feedback); and 3) reactor stability (thermohydraulic stability with the neutronic and pressure feedback).

(a) Purely thermohydraulic stability

In previous research, it has been shown that under a certain condensation power, for which the boiling limit λ is outside the core, the system shows a significant increment in the amplification factor [20]. This happens when, without core boiling, enthalpy outside the core is higher than the saturation enthalpy at the chimney outlet, producing vapour by means of flashing. The presence of void fraction in the hot leg generates an increment in the buoyancy force: the higher the void fraction is, the lower the average density in the hot leg and thus the higher the buoyancy force. If the boiling limit λ is located in the chimney, the sensitivity of the buoyancy force to changes in the coolant enthalpy, therefore, increases. This is due to a slight perturbation in the core outlet enthalpy causing a great movement of λ, which in turn produces a great variation of the buoyancy force. This effect tends to destabilize the system, incrementing the amplification factor, which shows a maximum value when λ is located in the central region of the chimney and a minimum value when λ is close to the chimney inlet and outlet. For this reason, when the system is unstable, i.e. λ is placed in the central region of the chimney, it can be stabilized both by increasing or decreasing Q_{cond}. This effect is shown in Figures 42–43, which show the case in which neither the neutron nor the pressure feedback pressure have been considered in the system. As can be observed for any core power, there are two condensation powers for which the stability line is crossed.

In order to point out the two-phase region in the system, in the following plots presented in this report, the points for which the boiling-flashing boundary coincides with the core exit location and also the chimney middle location are included. Such lines are labelled as ´23´ and ´62´ since these points are located at heights which are respectively the 23% and 62% of the total hot leg length measured from the core inlet point.

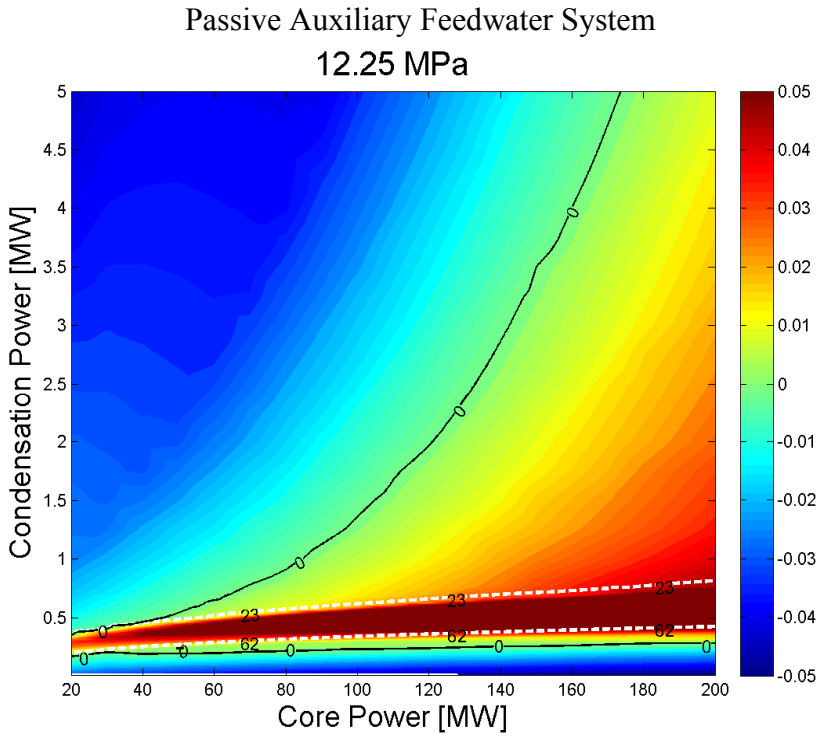

FIG. 42. Thermohydraulic stability map, expressed in terms of amplification factor for when neither neutron nor pressure feedback have been considered.

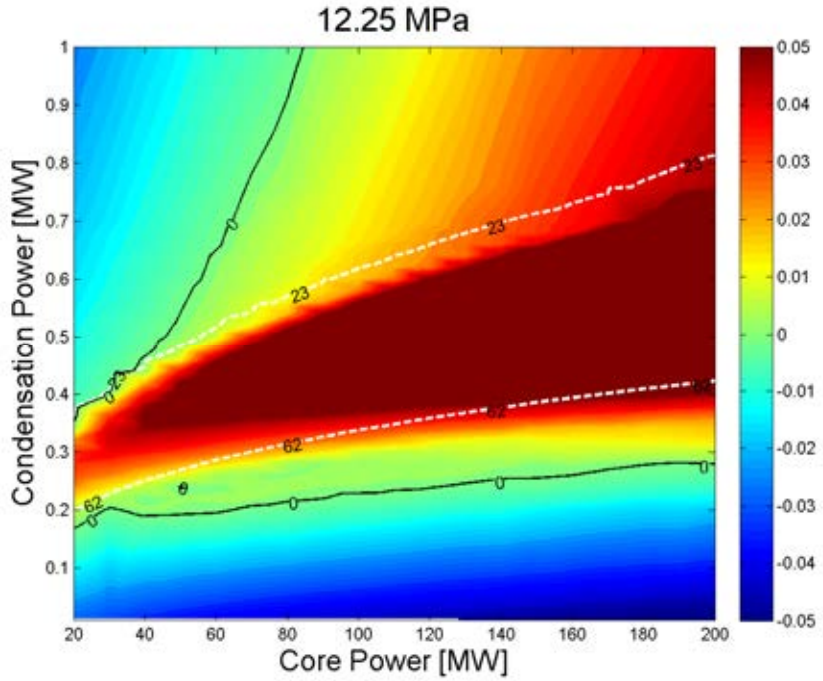

FIG. 43. Detail of thermohydraulic stability map for case when neither neutron nor pressure feedback are considered.

As can be noted, the lower Q_{cond} is, the closer is λ regarding the chimney outlet (see Equation 24). Therefore, by lowering Q_{cond}, the two-phase region becomes smaller, reducing

the void fraction contribution in the buoyant force; as a result, it reduces its relative sensitivity. Then, the oscillations are more efficiently dampened, and a new stability area emerges.

From this analysis, it is clear that the system is unstable when λ is located in a wide range of values, starting from positions which are close to the last quarter of the chimney and extending to cases in which boiling takes place in the core.

Analysing the system dominant frequency in an arbitrary reference point (with an associated period T=13.5 s) it is possible to verify that the mechanism responsible for the aforementioned instabilities corresponds well with density waves travelling mainly through the reactor chimney (corresponding travelling time in such a section: T_t=14.4 s). This result matches published research results where it is found that the period of such instabilities is one to two times the flow transit time in the considered section, this is, $T \in (T_t, 2T_t)$ [15, 21].

(b) Neutronic-thermohydraulic stability

In order to study the core dynamic influence in the system stability, the thermal model of the fuel and the corresponding neutronic feedback is included. The resulting stability map is shown in Figures 44–45.

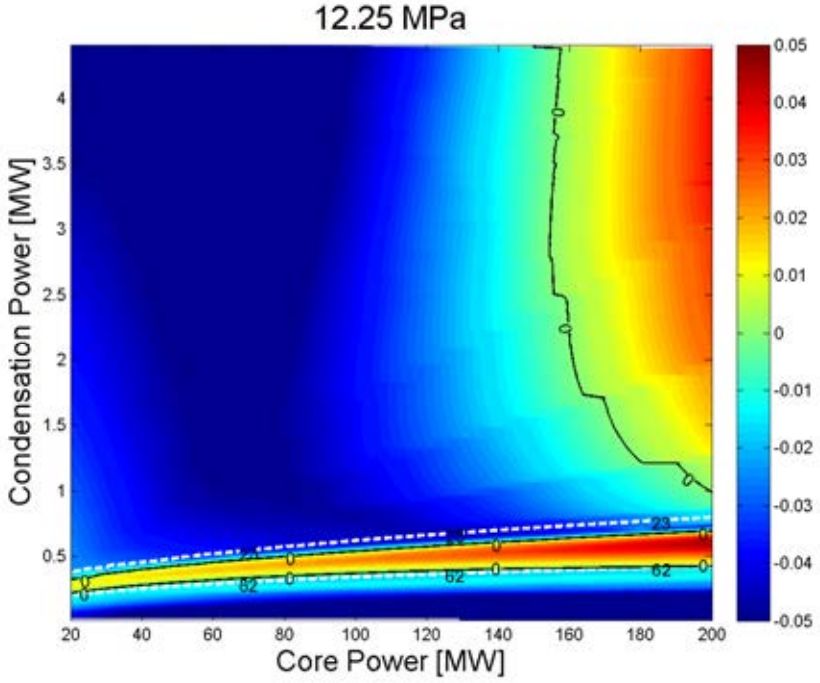

FIG. 44. Neutronic-thermohydraulic stability map, expressed in terms of amplification factor for the case where neutronic feedback but not pressure feedback is considered.

One of the most important effects in this case is that due to the neutronic feedback resulting from coolant density changes: in the case of having a constant heat flux condition, an increment in the core flow is followed by an enthalpy decrease at the channel outlet and, consequently, an increment in the coolant average density there. When the neutronic feedback is included, a reactivity insertion is produced because the reactivity coefficient due to coolant density ($R\rho$) is positive. Then, the power by fission increments and, therefore, increases the enthalpy at the core outlet, which tends to balance the thermohydraulic effect, stabilizing the

system. Besides, the neutronic feedback also presents a faster response compared to the dynamics of the density waves travelling through the chimney. This is due to the fact an average coolant density change affects the nuclear core power before the arrival of the enthalpy front to the chimney outlet. This reduces the associated phase delay. The explained phenomenon provides a stabilizing effect for low frequency oscillations, which occur when Q_{cond} is small.

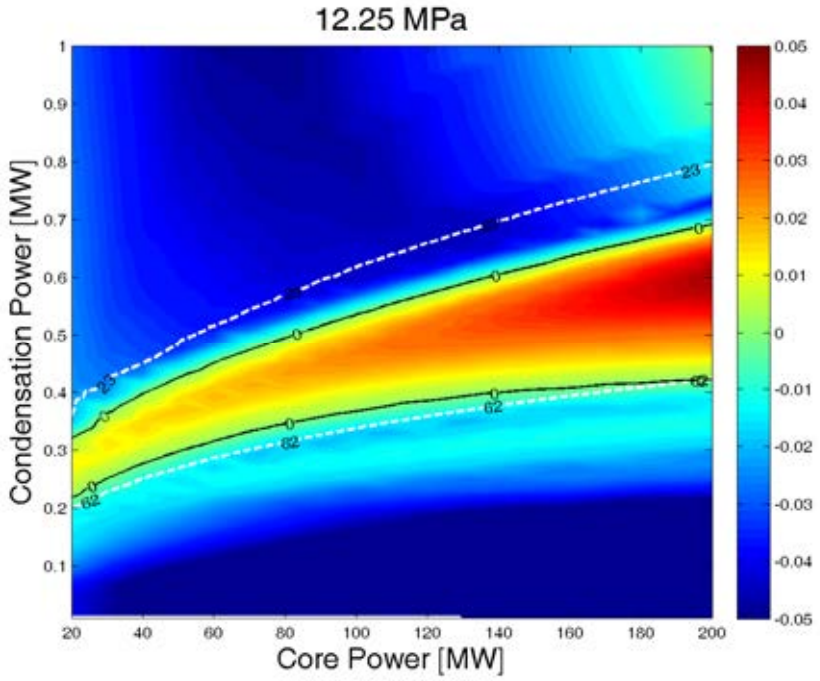

FIG. 45. Stability map detail for the case where neutron feedback but not pressure feedback is considered.

The effect of the core dynamics provides a stabilizing effect in the system regarding the unstable region induced by the flashing phenomenon. In this case, the system dominant frequency in the reference point (associated to an oscillation period T=12.9 s) also corresponds to the phenomenology of density waves travelling through the chimney (with a transit time equal to T_t=14.3 s). This result is remarkable and shows that CAREM-25 operates in a region characterized by competing Type-I and Type-II instability mechanisms. In this way, the CAREM-25 reactor differs from natural circulation BWRs, for which strong coupling between the thermohydraulics with the neutronics causes the typical oscillation frequency corresponding to the time required by density waves to travel along the core. This behaviour corresponds to Type-II instability mechanism [22].

As a result of the aforementioned phenomena, the Type-I unstable region is limited to cases in which the boiling-flashing boundary limit λ is located within a region which extends approximately from the core outlet to the half of the chimney.

(c) Reactor stability

The effect of pressure feedback is expected to cause a stabilizing effect regarding the case of considering constant pressure (which is equivalent to assuming an infinite steam volume). Such an effect responds to the following mechanism: an increment of the void fraction in the chimney expands the entire coolant, pressurizing the system. The system pressure increases

the saturation enthalpy, which tends to reduce the void fraction. Therefore, the pressure feedback natural effect is to balance the density changes of the two-phase region. The feedback in pressure is stronger when the steam volume is lower.

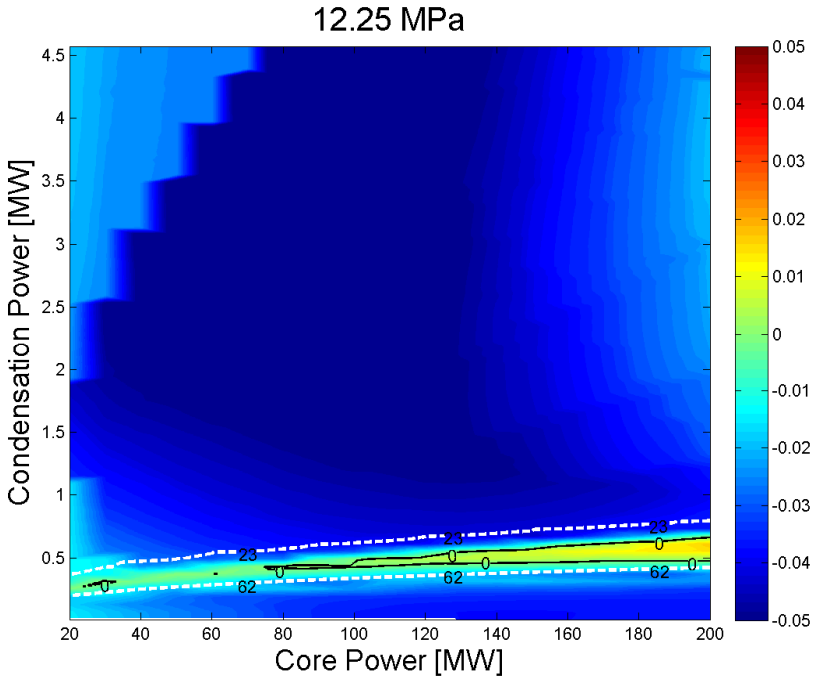

FIG. 46. Reactor stability map for the case where both core dynamics and feedback in pressure are considered.

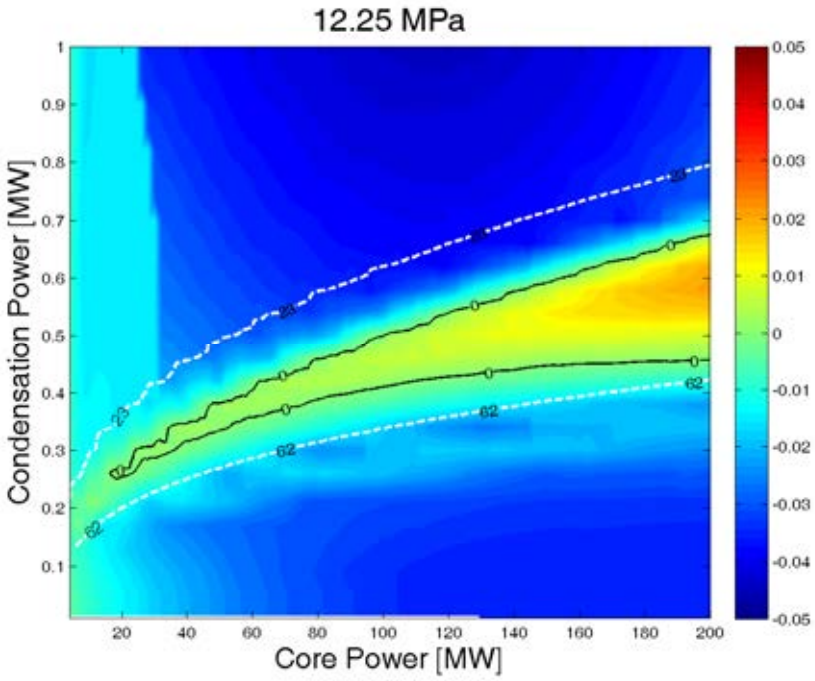

FIG. 47. Stability map for the case where both core dynamics and feedback in pressure are considered.

Figures 46–47 show the CAREM-25 reactor stability map for the case in which both the neutronics and the pressure feedback effect are included in the simulation. In this manner, all relevant mechanisms that determine reactor dynamics behaviour are taken into account.

As can be seen, the feedback pressure effect stabilizes the system. By comparing, for instance, Figures 45–47, it can be noted that the unstable Type-I region is clearly reduced. Such a result is particularly important at low core power levels (Q_{nu}). In addition, the unstable region is still bounded by the region defined by the core outlet and the chimney middle point.

The previously obtained results are promising regarding CAREM-25 reactor stability performance since they show a large region at which the system can be operated with sufficient stability margins. In needs to be remarked that such a margin may be considerably incremented by slightly incrementing the condensation power at the dome. In this way, the reactor operational point may be tuned, thus optimizing its stability performance.

Because of this result, it has been decided to implement a condensation device in the reactor steam dome (i.e. the condensation coil depicted in Fig. 7) in order to ensure a minimum condensation power at any operational point.

4.3.4.2. Stability analysis at low pressure (4.7 MPa – 12.25 MPa)

In this section, besides representing the stability results in the Q_{nuc} vs. Q_{cond} plane, a second type of plot has been constructed. In this second modality, Q_{nuc} and P were taken as variables, keeping Q_{cond} constant, which enables a better characterization of the system during a heating ramp. This is because during the pressurization stage, it is expected that P will vary depending on power misbalances. For this reason, it is useful to visualize a wide range of Q_{nuc} and P at a value of Q_{cond} defined as constant.

In this section, we present the results assuming steady state conditions; however, during the aforementioned pressurization stage; there must be an increase in the unbalanced power between the generated power in the core, and the power removed by the steam generators. This increment produces the necessary increase in the vapour production in order to have a given pressurization rate. As was shown, at steady state conditions, an increase in the condensation power produces a similar effect. So, in order to use steady state stability maps for low pressurization ramps, in which the system can be considered to be in quasi-stationary condition, an effective condensation power greater than the real one should be considered.

(a) Stability maps in Q_{nuc}-Q_{cond} at low pressure

When lowering the pressure, the buoyancy force becomes more sensitive than at higher pressure, both to changes in the enthalpy at the core outlet and to movements of the boiling-flashing limit λ. This effect is more significant at low pressures since lowering the pressure makes the flashing effect more important. Moreover, when the pressure decreases, it increases the liquid/steam density relation, thus incrementing the void fraction and, consequently, the buoyancy force generated by its presence. In this way, the total buoyancy force is more sensitive to changes in the void fraction at the hot leg. These two effects imply the range of Q_{cond} for which the system is unstable extends to higher values. All this leads to an increment in the region where the system shows unstable behaviour on the stability map. This result can be observed by comparing Fig. 46 with Figures 48–50, where stability maps obtained at different pressures are presented.

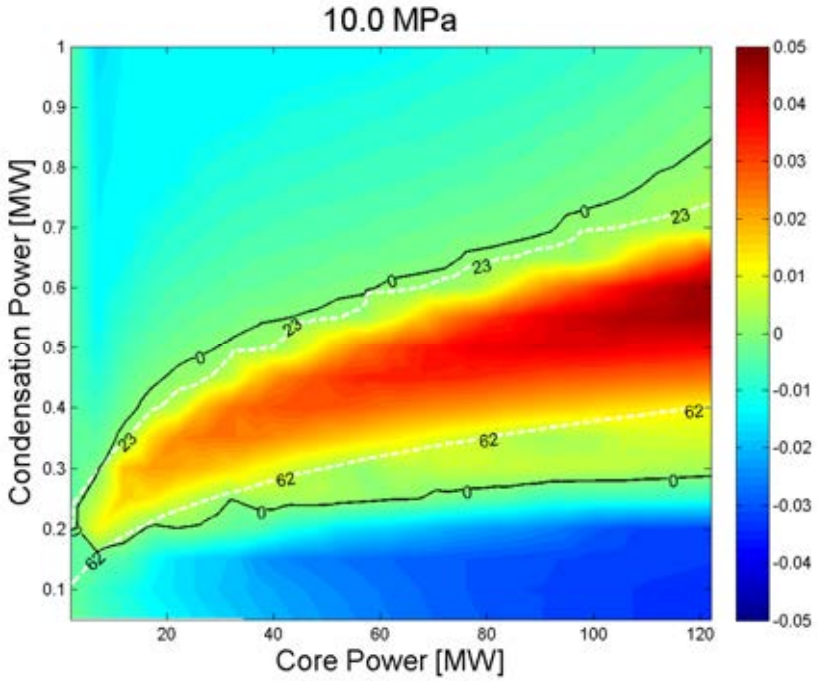

FIG. 48. Stability map for pressure equal to 10.0 MPa.

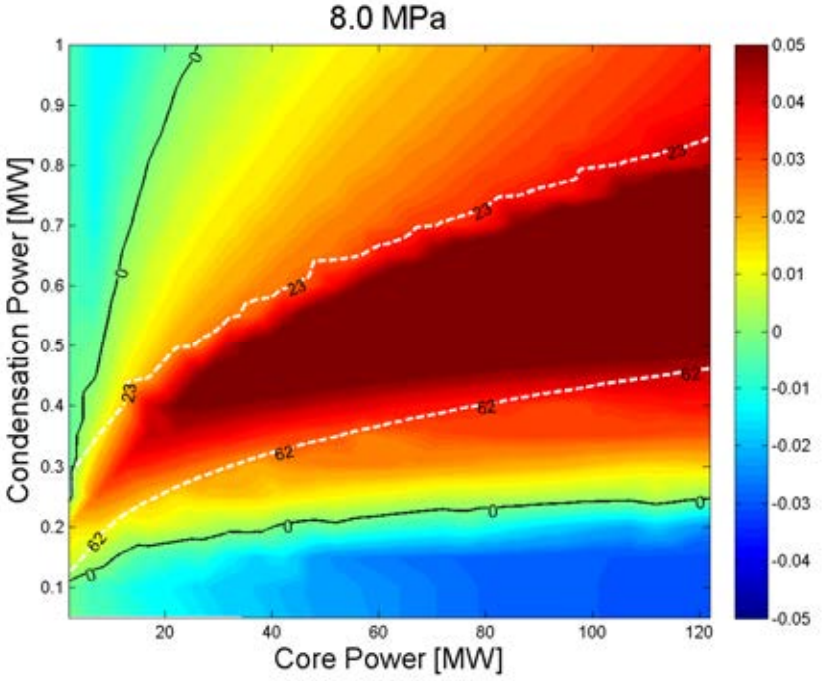

FIG. 49. Stability map for pressure equal to 8.0 Mpa.

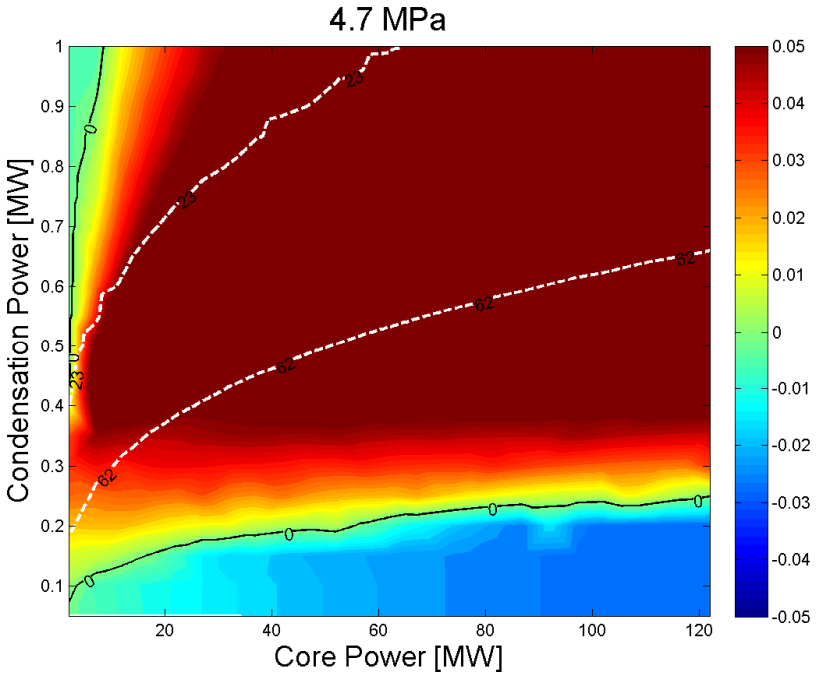

FIG. 50. Stability map for pressure equal to 4.7 Mpa.

As can be observed from the figures, the unstable Type-I region rapidly enlarges when the pressure is reduced. This result is in agreement with both numerical and experimental results found in the iterature [18, 23].

(b) Stability maps in Q_{nuc}-P

As mentioned, a practical way of visualizing the system stability performance during the pressurization stage is by presenting the results in the P vs Q_{nuc} plane thus, assuming Q_{cond} constant. This assumption is supported by the fact that Q_{cond} is a parameter which is supposed to be regulated during startup.

Figures 52–56 show stability maps obtained at different Q_{cond} values. From the maps it is found that for Q_{cond} equal to 0.2 MW, the system is not stabilized when increasing Q_{cond}. The reason for this behaviour is related to the movement of λ in the chimney (due to flashing).

The figures also show the unstable region moves by increasing Q_{cond}. An important result is that when Q_{cond} is higher than about 0.5 MW, a stable region emerges in the low Q_{nuc} and low P region. Moreover, this behaviour is in contrast to that observed for Q_{cond} equal to 0.2 MW. The reason for this change in behaviour is given by the new positioning of λ. Due to the fact that Q_{cond} is now higher than before, λ is located at a lower position in the hot leg. As λ movement responds to the aforementioned mechanism, when Q_{nuc} increases, λ tends to move upwards and, therefore, it is positioned close to the middle of the chimney, which is the λ location most susceptible to cause instabilities due to flashing.

From Figures 51–56, the aforementioned pressure stabilizing effect can be observed. In the investigated range of Q_{cond}, it can be seen that at high P the system is stable, regardless of the value taken by Q_{nuc}.

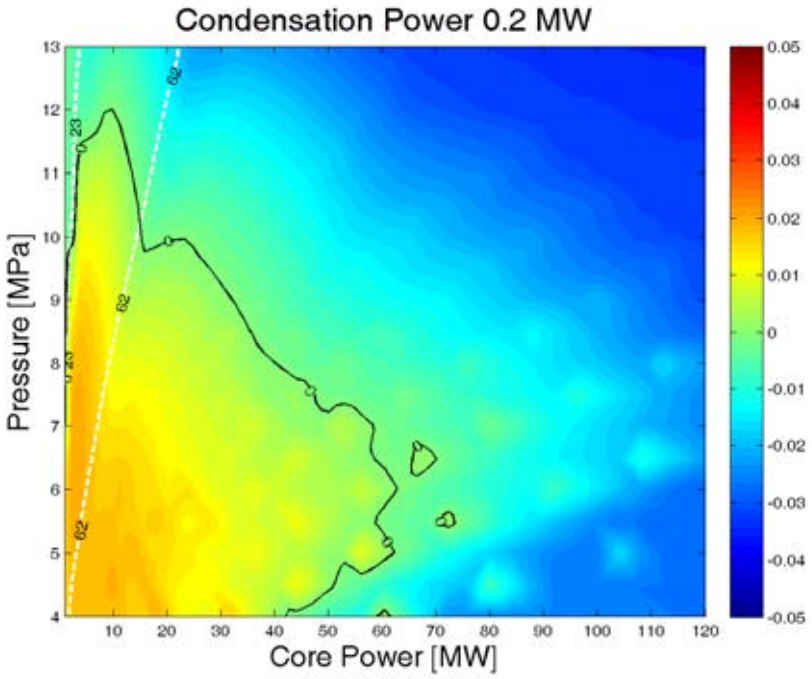

FIG. 51. Stability map at Q_{cond} = 0.2 MW.

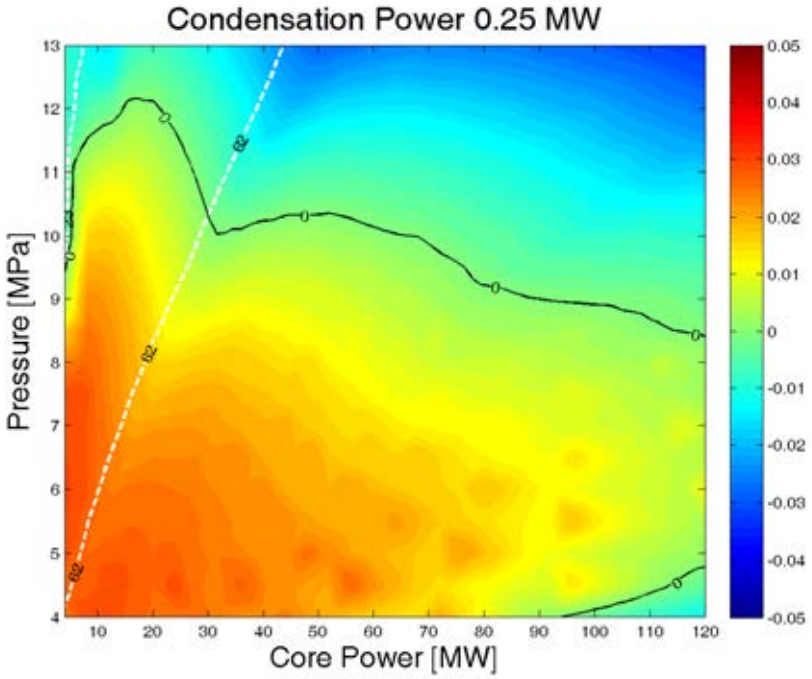

FIG. 52. Stability map at Q_{cond} = 0.25 MW.

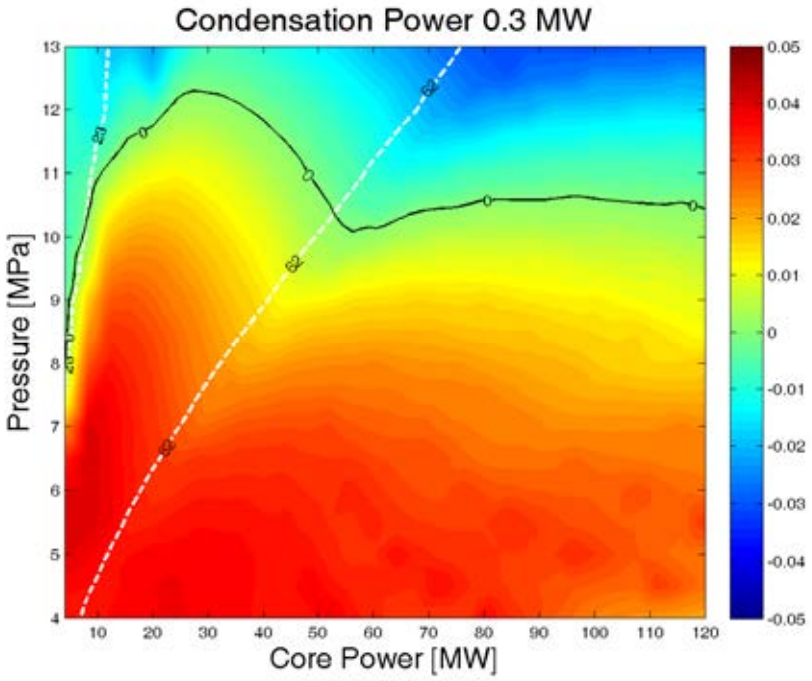

FIG. 53. Stability map at Q_{cond} = 0.3 MW.

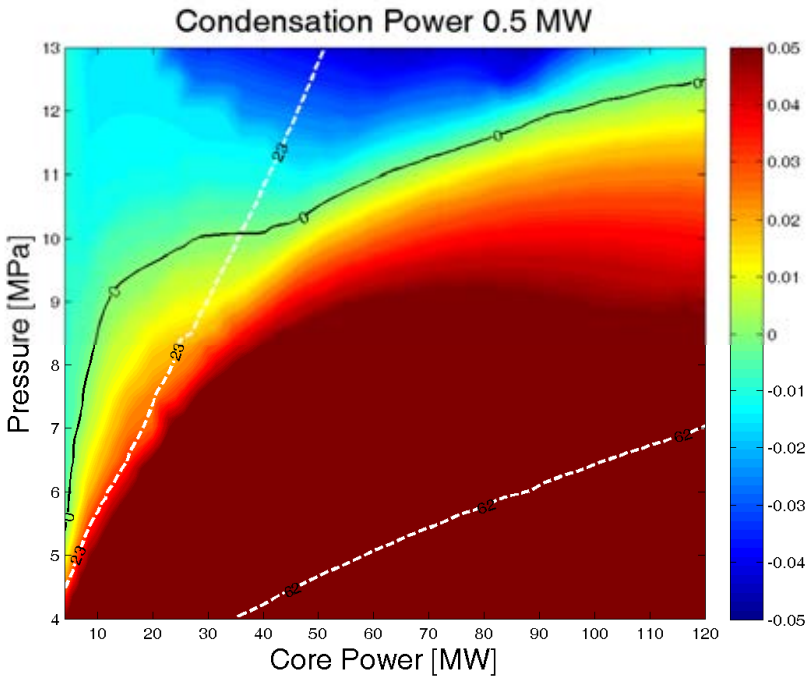

FIG. 54. Stability map at Q_{cond} = 0.5 MW.

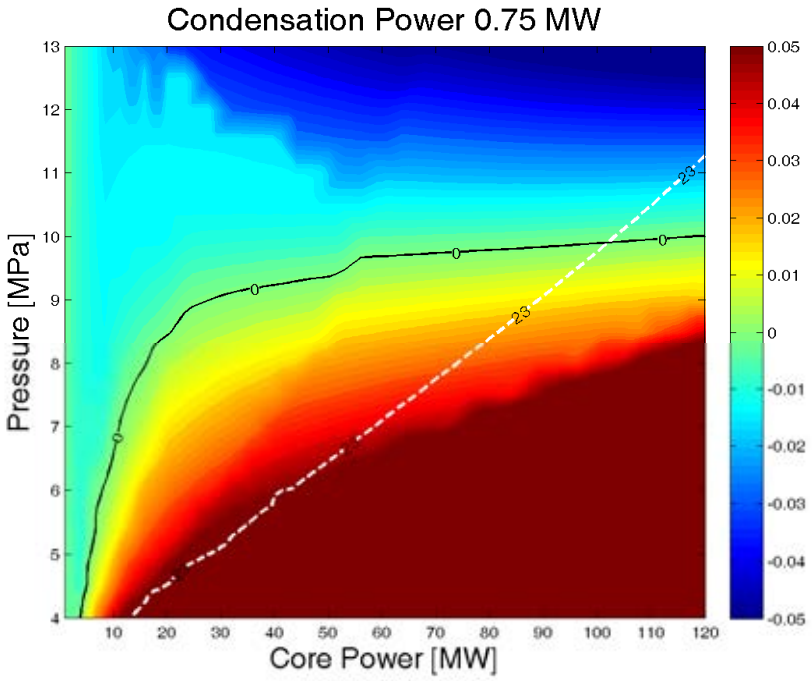

FIG. 55. Stability map at Q_{cond} = 0.75 MW.

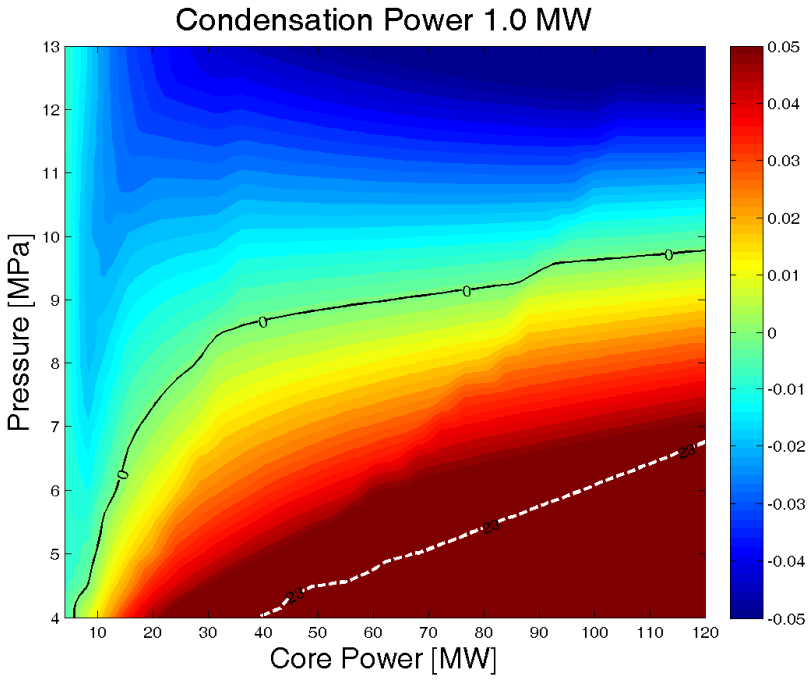

FIG. 56. Stability map at Q_{cond} = 1.0 MW.

In addition, it is observed that for Q_{cond} higher than 0.75 MW it is possible to go from low P and low Q_{nuc} to high P and high Q_{nuc} without encountering instabilities. This result is explained by the fact by increasing the condensation in the steam dome, the boiling-flashing limit moves downwards in the hot leg. In this manner, such a boundary locates at different positions in the hot leg, inducing different feedback mechanisms. As explained before, if λ is located around the middle of the chimney, the phase lag introduced by the transport of the density waves promotes the occurrence of instabilities. Otherwise, the system is stable.

However, if λ is located inside the core region, the system is stabilized by the neutronic feedback. In this way, if a certain minimum condensation power level is guaranteed, for which the boiling-flashing boundary is located in the core region at any pressure, the system is stable regardless of the value of Q_{nuc}. In the case of the CAREM-25 nuclear reactor, such a threshold value of Q_{cond} is found to be close to 0.75 MW.

By comparing Figures 51–56, it can be seen that for low P, both for Q_{cond} = 0.2 MW and 0.75 MW the system may be unstable if λ is located approximately between the core outlet and the middle region of the chimney. This position of boiling boundary seems to be more prone to lead to instabilities due to flashing. The same can be said for the stable region; for Q_{cond} = 0.2 MW it is observed that the location of the stable region approximately coincides with the region for which λ is placed at the upper part of the chimney. On the other hand, for Q_{cond} = 0.75 MW, this region coincides with the one defined by the cases for which λ is placed in the core region.

Another important result obtained from the comparison of these maps is that at high pressure, the stability line does not show significant changes when condensing power exceeds 0.75 MW. This result implies that the sensitivity in case of uncertainties in Q_{cond} is reduced when operation is at nominal pressure. However, at low pressure, the stable region enlarges when increasing the condensation power. So, it is expected that during the startup pressurization stage, more stable behaviour than predicted by the steady state stability maps should be expected due to greater effective condensation power.

The previous insensitive behaviour is not seen in the maps for condensation powers around 0.25 MW. Between Figures 51–52 the condensation power varied only 0.05 MW, but the area of the unstable region in the maps increased to more than double in size. From the maps, it is also observed that the distance between two consecutive contour lines varies with Q_{cond}. For high Q_{cond}, the lines are closer than for low Q_{cond}, which means that the gradient with which the amplification factor varies in the map increases when increasing Q_{cond}. This means that for low Q_{cond}, any operation point is 'closer' to unstable conditions than for high Q_{cond}. Therefore, when the system is operating at low condensing powers, a slight change in the system conditions may lead to unstable conditions.

4.3.4.3. Conclusions

In this section, different stability maps obtained from a linearized model are presented. It is shown that the flashing effect is crucial to correctly investigating the stability performance of the CAREM-25 reactor. In addition, it is verified that the dominant destabilizing mechanism is density waves travelling through the chimney section corresponding to Type-I instabilities.

The results also indicate that the condensation taking place in the steam dome has great impact on defining the stability of the reactor and, thus, can be used to tune the CAREM-25 operational point. It is also observed that the reactor shows a better stability performance when increasing the system pressure. The steady state results indicate that the system could be pressurized without encountering instabilities if a certain minimum condensation power level is guaranteed.

As a result of this investigation, two important decisions have been taken in order to increase the stability margin of the reactor, namely:

- to include the reactor coil depicted in Fig. 7 in order to ensure a minimum condensation value in the steam dome.
- to increase the pressurization capability of the preheating system (which uses non-nuclear means) up to 4.7 MPa. In this way, the condensation value to ensure a stable reactor startup is decreased. As a result, the operative state from which the startup stage is defined corresponds to zero nuclear core power and a system pressure equal to 4.7 Mpa.

4.3.5. Final remarks and engineering features

In this section, a description of the CAREM-25 reactor and its main features is presented.

Under the hypothesis of the HUARPE model, it is possible to show the CAREM-25 reactor's stability performance for a wide range of operational conditions. At nominal conditions, the stabilizing effects that the neutronic feedback and reactor pressure have over such performance have been verified.

The results obtained at nominal pressure indicate an unstable area located at relatively low condensation powers. It is confirmed that such unstable region is induced by instabilities generated by density waves that travel along the reactor chimney.

A wide area in the stability map has been detected at condensation power values close to 0.75 MW in which the stability margins are considerably increased. This region offers excellent conditions to guarantee that the reactor will be stable for a wide range of operation conditions. For this reason, to enhance reactor stability performance, it has been decided to implement a device to enable an increase in the power condensed in the pressure vessel dome. Preliminary estimations show that incrementing the condensed power up to 0.75 MW would be enough to increase the reactor stability margins and thus optimize the plant's safety.

The stability maps presented in terms of Q_{nuc} and P enabled a clear visualization of a possible trajectory for the startup stage. In addition, it allowed observation of a wide range of both variables. It has been corroborated that the flashing phenomenon is of crucial importance for the stability analysis in the studied range of P, Q_{nuc} and Q_{cond}. This result emphasizes the need to use tools which consider the pressure variation by hydrostatic height.

The results show that pressure has a stabilizing effect. In all the stability maps presented in terms of Q_{nuc} and P, it was observed that incrementing P made it possible to reach a stable condition regardless the value of Q_{nuc}. From this result, it can be concluded that it is desirable to maximize tha increase in pressure of the operational point from which the reactor needs to begin the startup phase. For this reason, it has been decided to begin the pressurization stage by nuclear core power at 4.7 MPa. In addition, it is observed that in the studied range of conditions, by reducing P, the system becomes unstable due to two different effects: on the one hand, the relation of densities liquid/steam is incremented, which enhances the feedback due to buoyancy; and on the other hand, the flashing phenomenon is also enhanced, expanding the region where λ perturbations lead to unstable cases.

A remarkable result is the effect that Q_{cond} has on the system when Q_{nuc} is varied. It is observed that when Q_{cond} is equal to 0.2 MW, by increasing Q_{nuc} the system tends to be stabilized and the opposite occurs for Q_{cond} higher than 0.5 MW. This result is related to the positioning of λ in the chimney, which favours the existence of instabilities.

It is found that the maps presented in the Q_{nuc} and P plane do not show significant changes when incrementing Q_{cond} from 0.75 MW to 1.0 MW. In addition, these maps also show that the reactor may be operated from a condition of low P and low Q_{nuc} to a nominal condition of P and Q_{nuc}, without passing through unstable regions. On the one hand, this provides a criterion for condensation power determination required for the reactor startup and, on the other hand, it shows that for a Q_{cond} higher than 0.75 MW the stability is not enhanced any more.

According to the implemented model, it is possible to pressurize the reactor without encountering instabilities if a condensation power of at least 0.75 MW can be guaranteed. This important result indicates that the reactor can be started up without encountering instabilities of thermohydraulic origin.

4.4. SUMMARY OF CASE STUDY RESULTS

4.4.1. AHWR

Experiments on steady state, stability and validation of startup procedure were carried out in a scaled ITL simulating AHWR. The steady state and stability data generated were compared with predictions of in-house developed as well as RELAP5/Mod3.2 codes giving good agreement. Two startup procedures — with self-pressurization and external pressurization — were also simulated in ITL. In both cases, low frequency flashing induced instability followed by high frequency density wave oscillations were observed during low pressure. With external pressurization, both flashing instability and high frequency density wave instability were suppressed if pressure was greater than 35 bar. Even for startup with self-pressurization, the void fraction measurements indicated that there was practically no boiling inside the fuel channel, indicating that power oscillations due to coupling of void reactivity feedback with neutronics could be avoided. Simulation of startup both with self-pressurization and with external pressurization indicated that both the low frequency flashing and high frequency density wave instability could be reproduced with RELAP5/Mod3.2.

Experimental investigations on stabilization were carried out using four different mechanical gadgets including spool pieces with helical coil and bellows. It was found that all gadgets were able to suppress single-phase instability in the loop. The spool piece with helical coil caused the least reduction in mass flow rate and the highest increase in the instability threshold among all the gadgets. Therefore, it can be concluded that helical coil is an effective tool to suppress instability in single-phase natural circulation systems. Experimental investigations with nanoparticles showed that they were able to suppress the instabilities in both single-phase and two-phase natural circulation systems besides enhancing the flow rate. The enhancement in single-phase flow rate was brought out by the enhancement of the thermal expansion coefficient resulting from the addition of nano-particles. The increase in loop flow rate in the presence of nanoparticles was also found to be proportional to the concentration of nanoparticles. Highest flow rate was observed with CuO nanoparticles followed by TiO_2, Al_2O_3 and SiO_2 in that order.

4.4.2. CAREM

The case study of CAREM-25 focused on the analytical investigation of the influence on stability of different phenomena and feedback mechanisms in an integral self-pressurized natural circulation nuclear reactor designed to work at low quality values. In this case study, investigations were carried out on neutronic feedback mechanism using a point kinetic

neutronic model, pressure feedback and self-pressurization effect, flow modelling, flashing effect, and transient simulations. From the results obtained analysing the CAREM-25 case study, the following general conclusions can be drawn for low quality natural circulation, self-pressurized nuclear reactors:

- The corresponding thermohydraulic behaviour cannot be extrapolated from existing knowledge and accumulated experience. Therefore, an exhaustive analysis regarding the thermohydraulic performance (including stability analysis) needs to be performed for this type of reactor.

- The flashing and condensation phenomena need to be considered in models intended to capture the physics involved in CAREM type reactors.

- When operating low quality natural circulation, self-pressurized nuclear reactors with a prescribed condensation power and pressure levels, the core inlet enthalpy increases when decreasing the core power.

- It is observed that in CAREM type reactors, the dominant destabilizing mechanism is due to density waves travelling through the chimney section corresponding to Type-I instabilities.

- The steam dome condensation power seems to be a very sensitive parameter in determining the boiling-flashing boundary location and thus the stability of this type of reactors. It is, thus, clear that by varying the condensation power level, the stability performance could be optimized.

- The neutronic feedback has a stabilizing effect in low quality natural circulation, self-pressurized nuclear reactors.

- The results verify that CAREM type reactors could be started up without observing instabilities of thermohydraulic origin if a minimum condensation power level can be guaranteed.

5. THERMAL STRATIFICATION IN POOLS

5.1. DESCRIPTION OF SPECIFIC SYSTEMS CONSIDERED

5.1.1. Isolation condenser system for AHWR

AHWR uses several passive systems to improve safety and reliability by reducing the dependence on external sources of energy and human intervention. One of the most prominent safety functions is the passive removal of decay heat. It assumes greater significance when decay heat is to be removed to maintain core cooling in the event of simultaneous failure of Class IV and Class III AC power supplies, i.e. station black out (SBO), in particular for prolonged duration as may be required if natural external events render the restoration of power supplies virtually impossible. AHWR design incorporates this capability by means of an isolation condenser system (ICS) with a large pool of water at high elevation, i.e. gravity driven water pool (GDWP), within the containment.

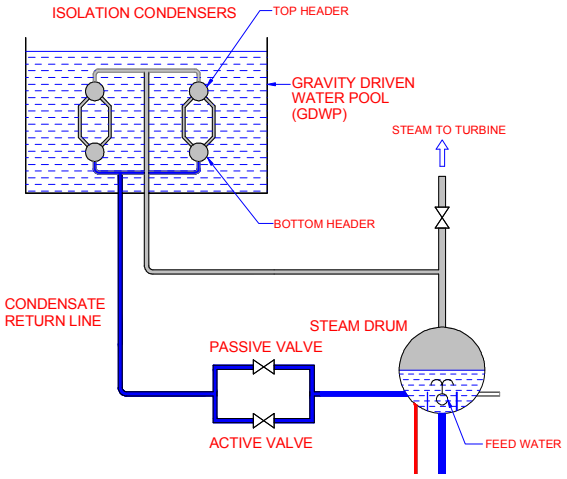

FIG. 57.(a) ICS of AHWR.

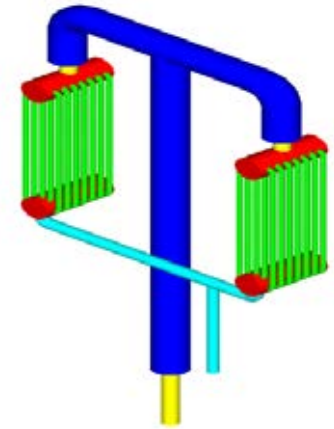

FIG. 57.(b) Isomeric view of IC of AHWR.

The ICS is designed to remove decay heat in a passive manner. During normal operation, the decay heat is removed by dumping steam into the main condenser. However, during the non-availability of the main condenser, the decay heat is removed using isolation condensers. An example of non-availability of the main condenser is an SBO. Steam from the steam drum flows into the isolation condenser, where it gets condensed and the the condensate returns to the steam drum. Both the MHT and ICS flow rates are maintained by natural circulation. The isolation condensers reject heat into a large pool of water in which they are immersed.

Isolation condensers are the submerged heat exchangers connected to the main heat transport system (MHTS) through steam drums and located inside a water pool at high elevation as shown in Fig. 57(a).

The GDWP of the AHWR is a water pool with capacity of 8000 m^3 located at sufficient elevation with regard to the steam drums. A diagram of the ICS and the GDWP is shown in Fig. 57(a). The MHTS of the AHWR comprises four steam drums. A branch of steam line leaving the steam drum to the turbine is connected to isolation condensers through a system of distributor and headers. An isolation condenser is a submerged heat exchanger with a large number (90 tubes) of vertical tubes connected between a top header and a bottom header. The condensate leaving the isolation condenser flows through the condensate line and enters the steam drum back into the subcooled water region. The condensate line is provided with a set

of valves in parallel known as passive and active valves respectively. The passive ones are diaphragm type valves actuating in response to a pressure signal in the steam drum. The passive valves are designed to start opening at 76.5 bar and open fully at 79.5 bar, whereas the active ones are pneumatically operated and open at a pressure of 80 bar. The purpose of the passive valves is to maintain a hot shutdown whereas the active valves are there to bring the reactor to a cold shutdown.

The GDWP comprises eight identical compartments, each having an isolation condenser submerged in it. Thus, the steam leaving one steam drum feeds two isolation condensers. Under the condition of SBO, the reactor gets isolated from the turbine and feedwater supply is cut off. Initially the system pressure rises and the reactor trips at high pressure. At 76.5 bars the passive valve starts to open and tries to maintain the system pressure. However, if pressure reaches 79.5 bar the passive valve gets fully open. In case, pressure continues to rise, the active valve opens at 80 bar and reactor is brought to cold shutdown.

The heat transport from the MHTS to isolation condenser and then to GDWP is affected in a passive manner. A natural circulation loop gets established between isolation condenser s and SDs, whereas the heat is rejected to GDWP by natural convection. The ICS with GDWP is designed to remove the decay heat for a period of three days following a SBO. Figure 57(b) shows the isometric view of a typical isolation condenser of AHWR whereas the arrangement of isolation condensers in GDWP for AHWR is as shown in Fig. 57(c).

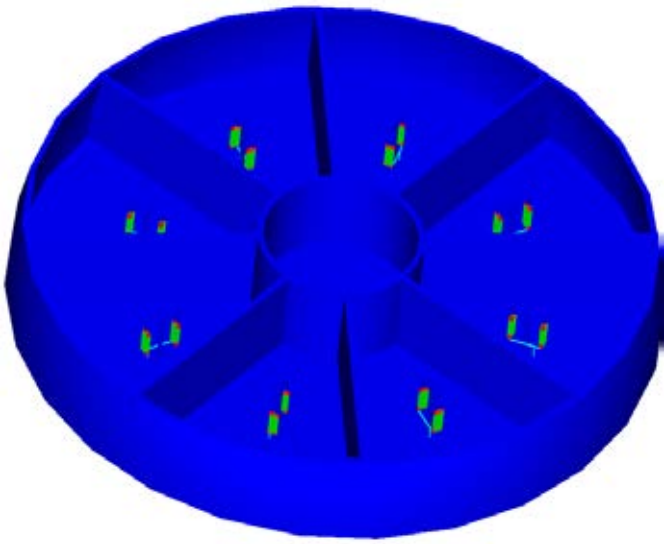

FIG. 57.(c) Isomeric view of arrangement of isolation condenser in GDWP for AHWR.

5.1.2. Passive auxiliary feedwater system for APR+

The PAFS [24] consists of heat exchanger, passive condensation cooling water tank (PCCT), check valves, isolation valves powered by battery (Class 1E DC), piping, instrumentation, and control systems. A PAFS in APR+ is shown in Fig. 58. The PAFS has two independent high-pressure closed loops and each loop has a heat exchanger submerged in the PCCT. The steam supply line branched from the main steam line upstream of the main steam isolation valves (MSIVs) is normally opened, and the condensate return line is connected to the feed water line downstream of main feed water isolation valves (MFIVs) and redundant check valves are

normally closed. The PAFS is in standby condition during power operation, plant startup, plant shutdown, and refuelling operation. The PAFS is actuated by a steam generator low level signal. When the PAFS actuation signal occurs, one or two isolation valves in parallel on the condensate return line are slowly opened by DC power. The supplied steam is condensed on the tube side and condensed water goes into steam generator. The circulation force is driven by condensation in the tubes and gravity force.

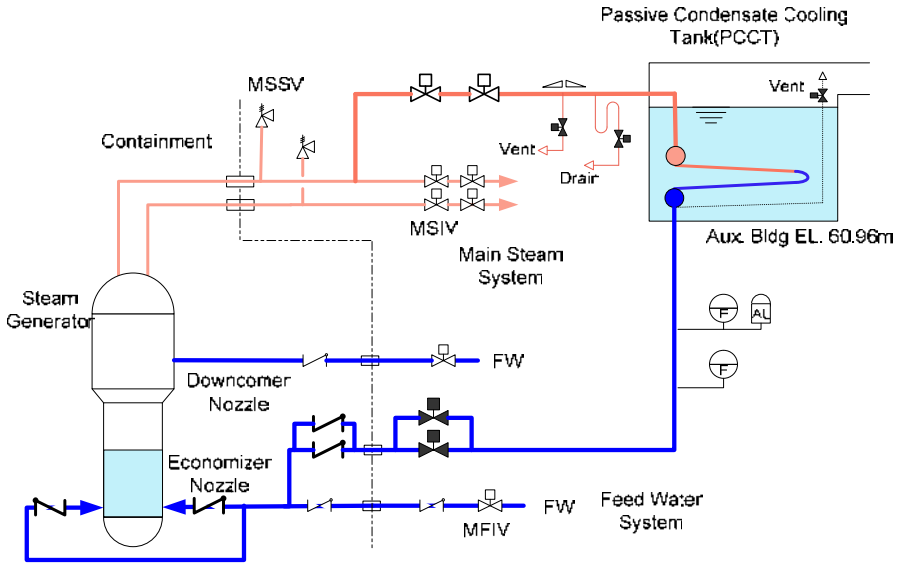

FIG. 58. PAFS in APR+.

The PAFS cools down the secondary system by heat transfer in a slightly inclined U-tube in a PCCT. High pressure steam from the steam generator is condensed in the heat exchanger. The cooling water in PCCT is maintained at an atmospheric pressure, so that boiling heat transfers at the outside wall of heat exchanger and natural convection occurs in the PCCT pool. The location of the heat exchanger and the PCCT are higher than the location of the steam generator, so condensed water can be drained and injected to feed water injection line without any active system.

The PAFS condensate return line isolation and check valves are arranged in parallel so that single valve failure does not prevent PAFS actuation. In a PAFS, we assume the common cause failure for valves. To avoid this problem, there are two distinct types of condensate return line isolation valves; the motor-operated valve and the electrohydraulic valve. To protect reverse flow, check valves are installed at the downstream of actuation valves.

The design target of the PAFS is to replace the function of current AFWS. To meet this target, the following design requirements are selected [25]:

- The residual core heat should be removed in case of design based postulated accidents;
- The capacity of PAFS should be sufficient to maintain hot shutdown condition for at least eight hours without any operator action in the case of an SBO to prevent the core damage;
- All power sources should be eliminated except the Class 1E DC power source;
- The capacity of Class 1E batteries should cover at least a 24-hour duty cycle;
- The required condensate flow for heat removal has to be sufficient to maintain the predetermined steam generator water level;

- Delivering condensate flow to the steam generator should be ensured automatically within 60 seconds;
- All PAFS components and piping have to be designed to withstand the effects of natural phenomena such as earthquakes, tornadoes, hurricanes, floods, and tsunami without loss of capability to perform their safety functions;
- The PAFS should be controllable in a post-accident environment from either the main control room or the remote shutdown room;
- Operation of the PAFS should not result in overfilling the intact steam generator;
- The PAFS should be capable of receiving an actuation signal from the emergency safety facility and the diverse protection system;
- It has to include connection to permit the addition of chemicals while the system is operating;
- The quality of dedicated condensate flow water has to be of the same as or better than that of the secondary makeup water.

The PAFS is composed of two independent trains and each train has a PCCT used as a coolant source for the PAFS. It is a rectangular shape concrete tank, located at elevation 60.96 m from the auxiliary building. A diagram is shown in Fig. 59. The PCCT capacity has to be determined on the basis of the mission time of PAFS, which is defined by the duration time for cooling down the reactor coolant system (RCS) from the initial condition by PAFS actuation to the shut down cooling entry condition for all design basis accidents. PCCT preliminary capacity included dead volume was determined as 1400 m^3. It means that PAFS can operate from 5 minutes after reactor trip occurrence to 8 hours without refill. However, in fact, the PCCT level will be controlled by the makeup water system operated by PCCT level controller during the normal operation condition.

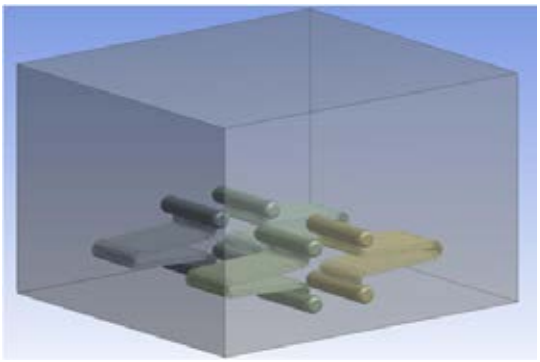

FIG. 59. Design of U-tube bundle.

The heat exchanger consists of slightly inclined stainless steel U-tubes. Figure 60 shows a design of U-tube bundle in heat exchanger. Total 4 heat exchangers are installed in one PCCT. The tube bundles are shaped to minimize thermal stress during their operation. The heat exchanger tubes are filled with condensate water during normal operation and it starts to remove heat from the steam generator after the PAFS actuation signal occurs. The cooling water in the PCCT is heated up through convection heat transfer at the outside of the heat exchanger tubes. Boiling starts after the PCCT pool temperature rises beyond the saturation temperature of the PCCT pressure.

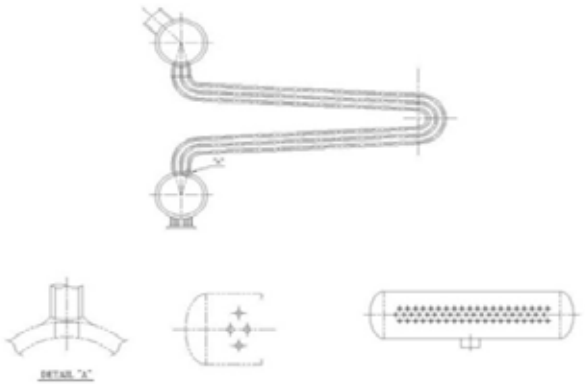

FIG. 60. Design of U-tube bundle.

5.2. CASE STUDIES FOR ICS OF AHWR

For analysing any complicated system in which thermal stratification is expected, it is worthwhile to make a few basic case studies which fundamentally represent the main system. Hence, thermal stratification was first studied in heated rectangular enclosures.

5.2.1. Phenomenological tests in simple facilities

Single-phase natural convection flow pattern in a water pool due to immersed vertical plate heater was studied using particle image velocimetry (PIV) system. The experimental setup consisted of vertical heater plate immersed in a water tank as shown in Fig. 61(a). The heater plate was given electrical power of 313 W. As the plate was heated, boundary layer flow developed adjacent to the plate. PIV measurements were taken 15 sec after switching on the heater. CFD analysis was also carried out to study the natural convection flow pattern.

The flow visualization was done with aluminum particles and, as shown in Fig. 61(c), the flow pattern closely matched the stream line pattern obtained from the PIV system as shown in Fig. 61(b). It can be observed from Figures 61(b) and 61(c) that fluid moves up along the vertical heater to the free surface. At the free surface, the detaching boundary layer is reflected downwards. However, due to its higher temperature (lower density), it rises back to the free surface and flows along horizontally towards the wall of the container. Velocities from PIV and CFD resulting as a function of distance from the vertical heater are compared in Figures 61(d) and 61(e) for 5 mm and 50 mm below free surface respectively.

5.2.2. GDWP behaviour studies in ITL

A scaled ITL was set up in BARC to simulate the overall system behaviour studies for the AHWR. This facility simulates the MHTS, the emergency core cooling system (ECCS) and ICS, feed water system (FWS) and the associated controls as shown in Fig. 9(b). Power to volume scaling philosophy has been adopted for the design of the ITL systems.

The ICS, as simulated in ITL, consists of steam inlet header and condensate outlet header connected by nine vertical heat exchanger tubes immersed in a scaled isolation condenser pool as shown in Fig. 62. To measure thermal stratification in pools, strips with brazed thermocouples at various elevations were inserted from slots cut from the top lid of isolation condenser pool.

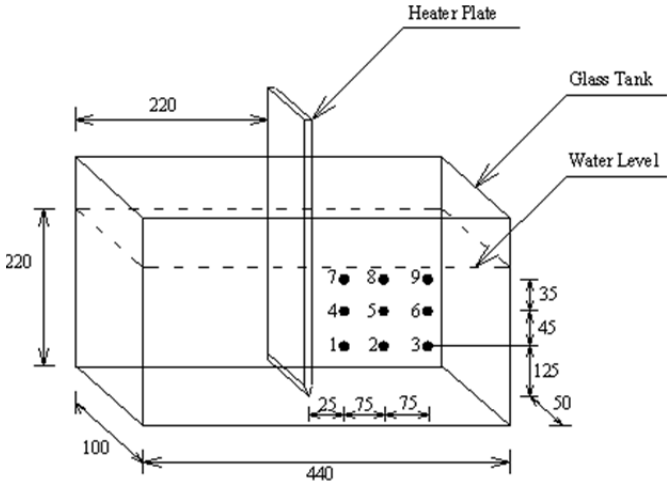

- Thermocouple

FIG. 61.(a) Vertical heater in glass tank.

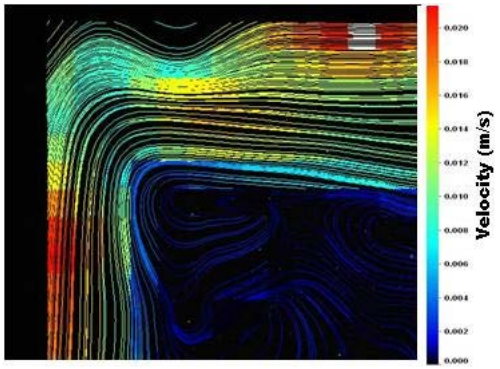

FIG. 61.(b) Velocity stream lines and contours by digital PIV.

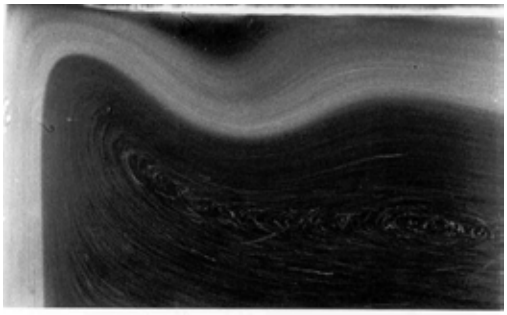

FIG.61.(c)Flow visualization with aluminum particles.

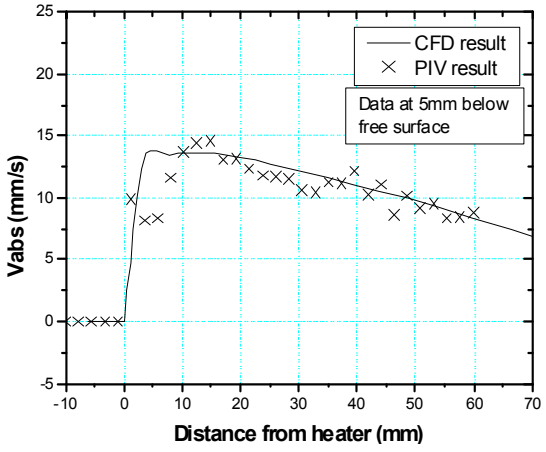

FIG. 61.(d) Comparison of PIV and CFD results at 5 mm below free surface of water.

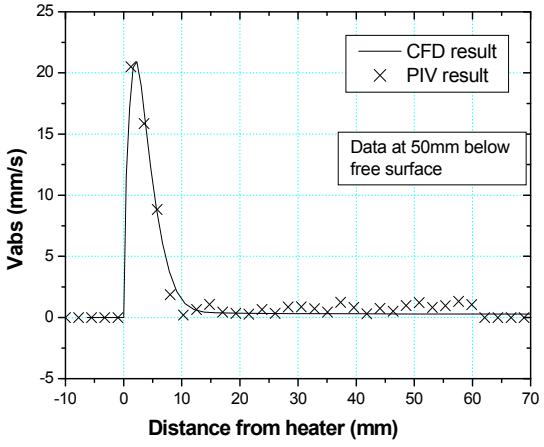

FIG. 61.(e) Comparison of PIV and CFD results at 50 mm below free surface of water.

Tests simulating passive decay heat removal by isolation condenser following SBO were conducted in ITL at different powers (i.e. 3%, 4%, 5% and 6% of full power) to evaluate the performance of isolation condenser and collect data on isolation condenser pool thermal stratification. The power is kept constant throughout the duration of the experiment. Degradation in isolation condenser performance has been investigated, which can be due to: (1) reduction in pool level (due to boil-off on isolation condenser pool side) resulting in exposure of isolation condenser tubes; (2) reduction in MHT pressure resulting in reduction of driving temperature difference for heat transfer from isolation condenser primary to secondary side.

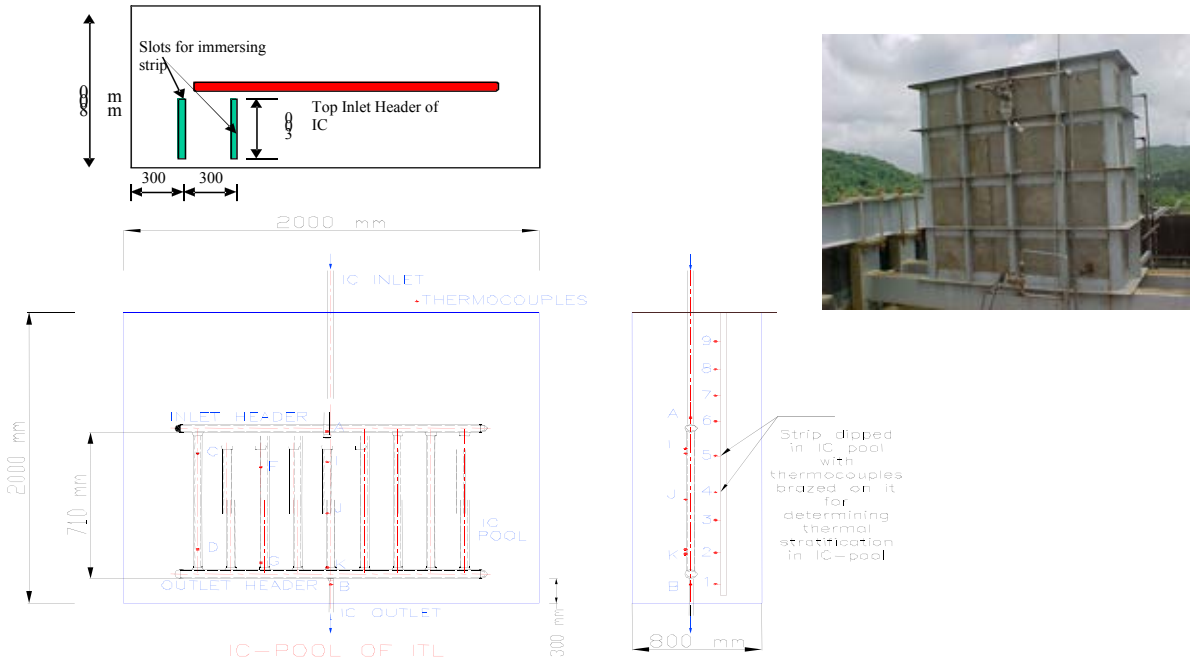

FIG. 62. Isolation condenser and isolation condenser pool along with instrumentation for pool stratification measurement in ITL.

The scenario considered for experimentation is as follows:

- The ITL is operating at steady state at a given constant power.
- The steam outlet valve and feed water inlet valve to SD are closed at t=0, following SBO.
- The system starts bottling up and as the SD pressure reaches 80 bar, the isolation condenser active valve opens fully and SD/ MHT pressure starts reducing.

Typical experimental results for 75 kW (3% FP) and its comparison with predictions made using computer code, RELAP5/MOD3.2, are shown in Figures 63(a) and 63(b). RELAP5 has been found to adequately simulate the performance of isolation condenser in ITL and predicts significant boil-off and decrease in isolation condenser pool level as shown in Fig. 63(a). Figure 63(b) indicates that thermal stratification (indicated by delay in temperature rise at lower elevation) of pool during experimentation could not be adequately simulated by RELAP5/MOD3.2 due to the one dimensional nature of the code as natural convection in a stagnant pool is a three dimensional phenomenon [26].

The experimental results show that thermal stratification in the isolation condenser pool is present only during the initial period of the transient, but after 11 500 s there is hardly any temperature gradient along the elevation of the isolation condenser pool (see Fig. 64).

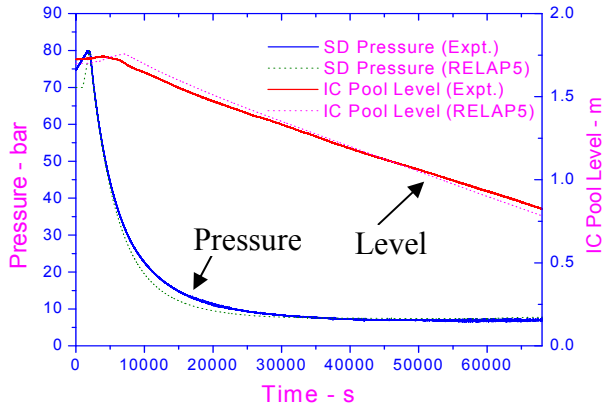

FIG. 63.(a) Simulation of isolation condenser performance at 75 kW and 1.75 m initial pool.

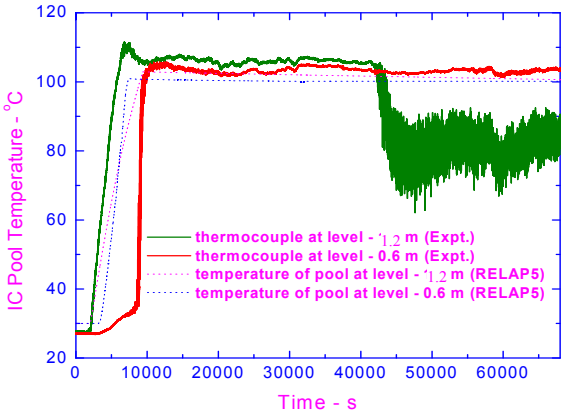

FIG. 63.(b) Simulation of isolation condenser pool temperatures at 75 kW and 1.75 m initial pool level.

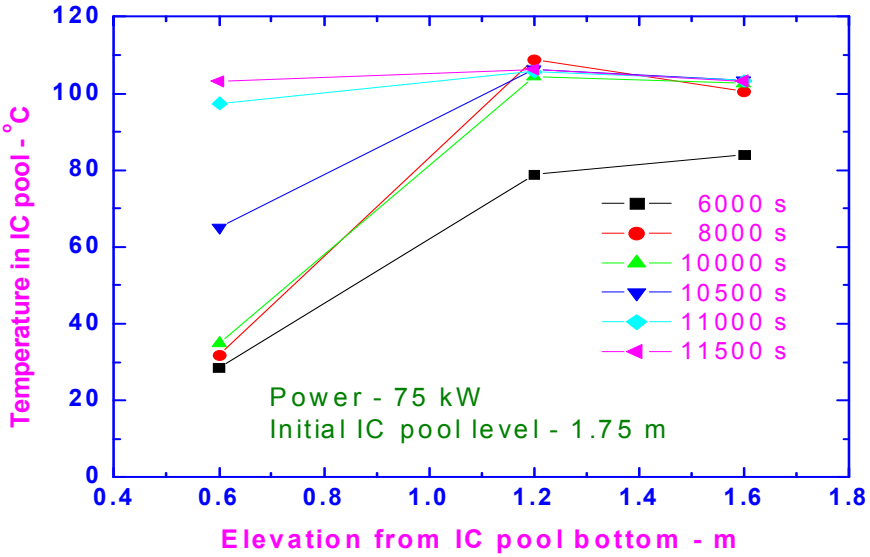

FIG. 64. Experimentally observed thermal stratification in isolation condenser pool at different times of station black out transient.

5.2.3. CFD analysis of ICs in GDWP

CFD analysis of thermal stratification in the GDWP with isolation condensers is carried out in one sector (housing one isolation condenser) of the GDWP using CFD code PHOENICS for finding 3D temperature distribution in the GDWP.

Figure 65 shows the temperature distribution in the water pool after six hours. Due to thermal stratification, the upper layers of water are hotter than the lower layers. Figure 66 shows that the variation of the temperature distribution with height of the water pool near the wall and in the centre are similar. Figure 67 shows the distribution of temperature after three days. The average temperature of the pool has increased from 40°C–62°C, which is much below the boiling temperature of the water. Figure 68 shows the temperature variation in the pool after three days. The temperature distribution becomes uniform with time while thermal stratification becomes less with time.

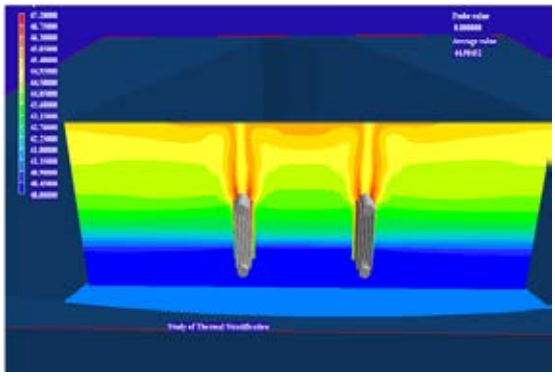

FIG. 65. Temperature distribution in the GDWP sector after 6 hours.

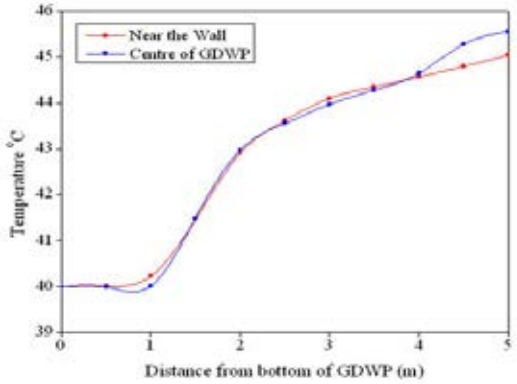

FIG. 66. Temperature distribution near the wall and centre after 6 hours.

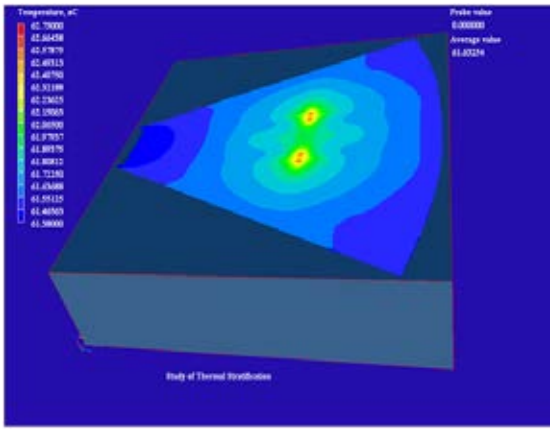

FIG. 67. Temperature distribution in the GDWP sector after 3 days.

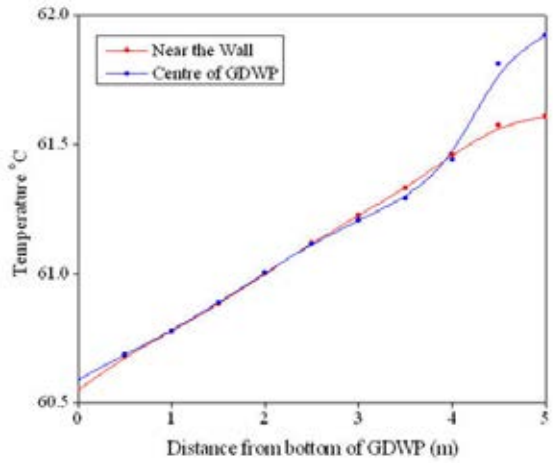

FIG. 68. Temperature distribution near the wall and centre after 3 days.

5.2.4. Effect of shrouds on thermal stratification

(a) Flow pattern with shrouds. *(b) Arrangement of shrouds around IC.*

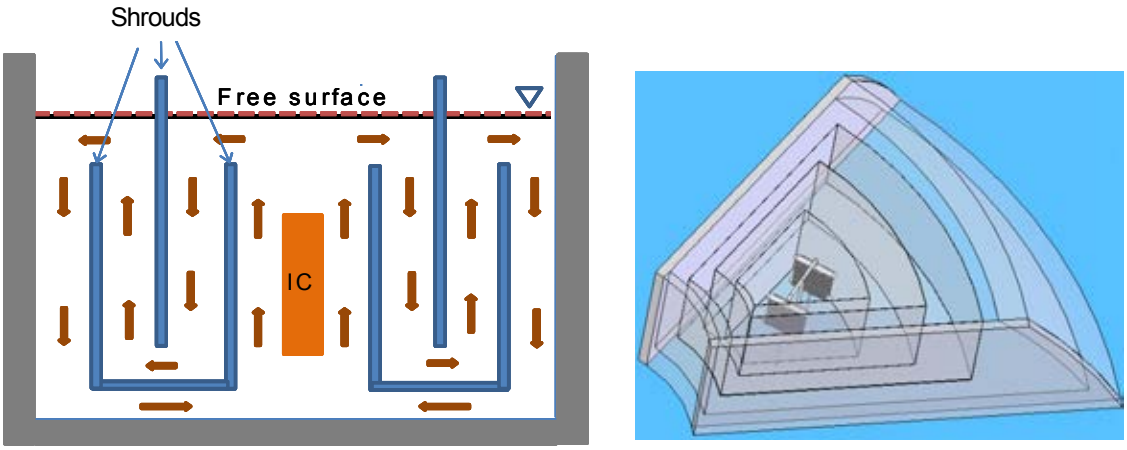

FIG. 69. A typical arrangement of shrouds in GDWP.

The heat transfer by natural convection to large pools with relatively small heat exchangers poses the problem of thermal stratification. These problems can be overcome by incorporation of shrouds around the heat exchangers in the pool. Shrouds lead to formation of relatively hot

and cold legs in the pool, which leads to natural circulation and, hence, mixing of water in the pool thereby utilizing the pool inventory effectively. Similar configuration is envisaged for the GDWP of an AHWR. Due to large size of GDWP in comparison to ICS, it seems appropriate to consider use of multiple shrouds. The effectiveness of a shrouded arrangement depends on the number of shrouds and the inter-shroud flow area. A typical configuration of shrouds in a GDWP with isolation condenser is shown in Fig. 69.

5.2.4.1. Description of different baffle configurations tested

To assess the effectiveness of shrouds to suppress the thermal stratification in a GDWP a shroud configuration of five shrouds is considered and, subsequently, the effect of the number of shrouds is examined by changing the number of shrouds. A GDWP with isolation condenser is simulated using best estimate code RELAP5/MOD3.2. The following assumptions are made for the purpose of this analysis:

- A one-eighth symmetric section of GDWP that forms one compartment of the pool is considered;
- Heat flow from the isolation condenser to pool is modelled as a uniform heat flux source at the centre of the pool;
- Time variation of the heat flux follows the decay power curve;
- The role of the concrete structure of a GDWP in heat transfer and thermal inertia is not considered in view of conservatism;
- Conduction across the shrouds is neglected;
- Inter-shroud regions are considered as pipe with same flow area and appropriate hydraulic diameter to simulate the frictional pressure drops.

5.2.4.2. RELAP5/MOD 3.2 nodalization scheme

RELAP5 nodalization for various arrangements of shrouds is shown in Fig. 70.

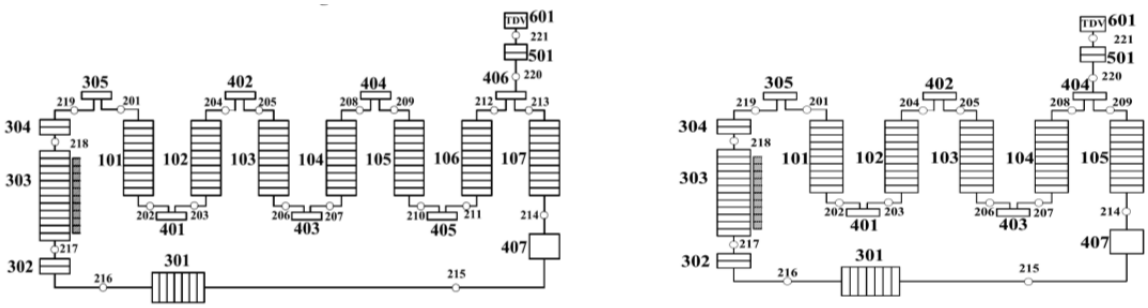

(a) Nodalization diagram for seven shrouds. *(b) Nodalization diagram for five shrouds.*

FIG. 70. Nodalization diagrams for GDWP with structural modification RELAP5/MOD3.2.

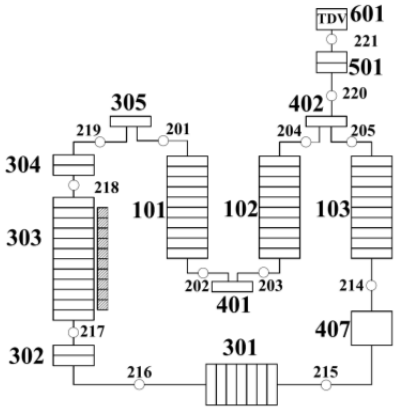

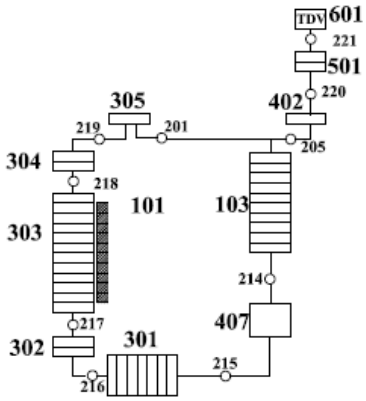

(c) Nodalization diagram for three shrouds. *(d) Nodalization diagram for one shrouds.*

FIG. 70. Nodalization diagrams for GDWP with structural modification RELAP5/MOD3.2.

Figures 71(a) and 71(b) show the mass flow rate through the shrouds and temperature at the locations upstream and downstream of the isolation condenser section. It can be seen from Figure 71(a) that the temperature of the fluid entering and leaving the compartment receiving heat from ICS are fluctuating. This is consistent with the fluctuating nature of flow through the shrouded compartments. Figure 71(b) shows that for most of the transient there is very little flow that leads to accumulation of hot water in the region adjacent to isolation condenser tubes. As the temperature rises and buoyancy force is developed enough to overcome the flow resistance in the outer shrouded compartments, there is a sudden spike in the flow. This sudden rise in flow is followed by mixing of fluid in the pool such that the temperature at the inlet and outlet of first shrouded compartment is nearly equalized and the temperature differential in the adjacent shrouded compartments also nearly vanishes. This phenomenon further results in loss of buoyancy force and hence reduced flow through the compartments. This process is found to occur repeatedly in a cyclic manner. However, with the passage of time, the period of cycle and amplitude of fluctuation are found to increase. It can be attributed mainly to the decaying nature of a heat source that requires a longer period for regeneration of buoyancy force in the system and also slightly increased frictional resistance due to the increased average temperature of the pool water.

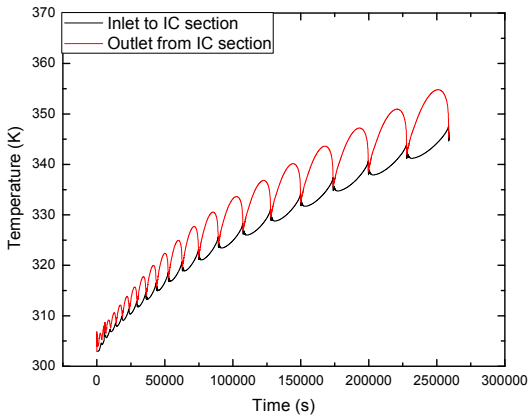

FIG. 71.(a) Temperature at isolation condenser section for five shrouds.

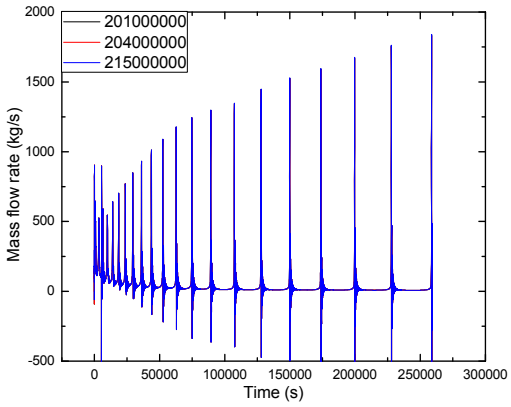

FIG. 71.(b) Mass flow rate through shrouds.

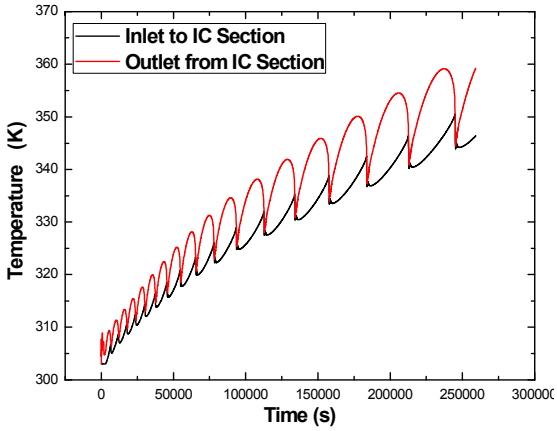

FIG. 72.(a) Temperature at isolation condenser section for seven shrouds.

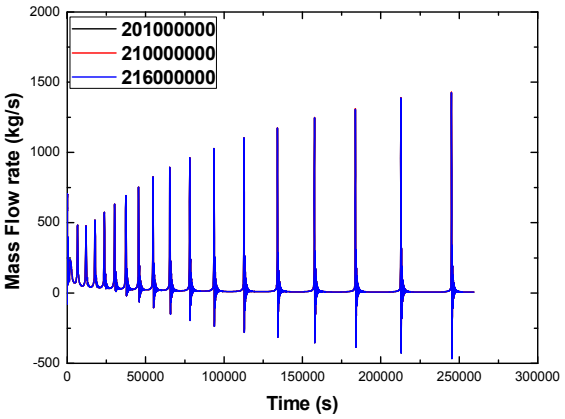

FIG. 72.(b) Mass flow rate through shrouds.

Effect of number of shrouds: Figures 72(a) and 72(b) show the effect of increasing the number of shrouds to seven. It can be seen that maximum temperature of the water in the pool has increased and at the same time, amplitude of temperature oscillations increase. Mass flow rate for the seven-shroud arrangement during stable flow phase is relatively less and having more fluctuation. This is entirely due to increased resistance offered to the flow because of smaller flow area and longer path length of natural circulation loop so formed.

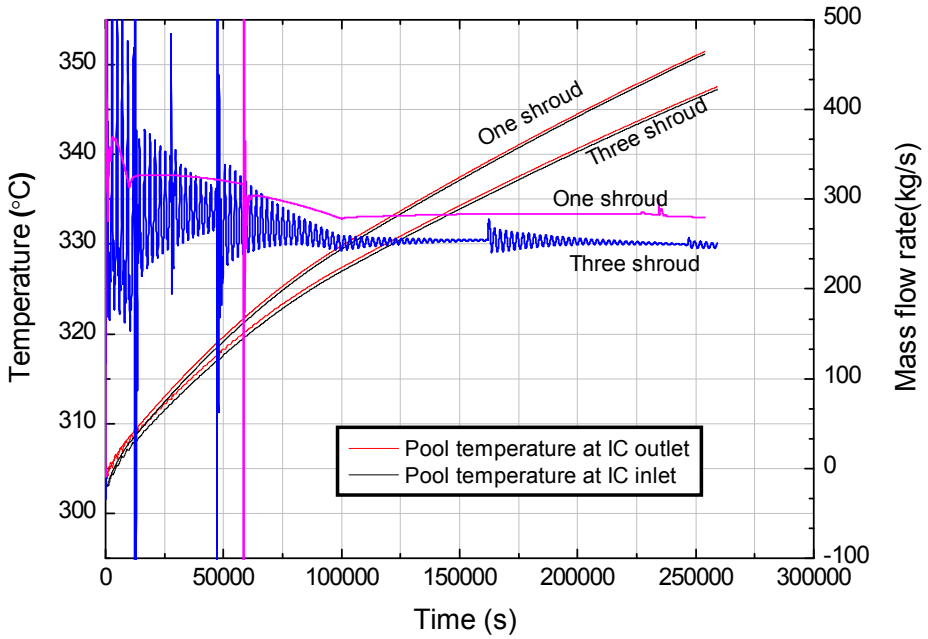

FIG. 73. Comparison of temperature and mass flow rate isolation condenser section for three shrouds and one shroud.

However, as a small number of shrouds can lead to simplified layout and economy, cases of three and one shrouds are also analysed. The comparison of temperature and mass flow rate at an isolation condenser section for arrangements of three shrouds and one shroud is shown in Fig. 73. For one shroud, the flow and temperature transients are non-oscillatory. The simulation shows that fewer shrouds give better performance. However, for such a

configuration, CFD analysis needs to be carried out as 3-D effects can be significant at low velocities.

5.3. CASE STUDIES FOR APR+

5.3.1. Phenomenological studies using CFD code

In design of a heat exchanger in PCCT, two types of heat exchangers were suggested: vertical or horizontal types. This was because the features of natural circulation and heat transfer around heat exchangers differentiate largely along the change of heat exchanger position in a cooling pool. Vertical type heat exchangers have such advantages that it is easier to predict the flow regimes inside the heat exchanger where condensation occurs and that the flow is more stable than that of horizontal types. Inside horizontal type heat exchangers, the condensation process is complex and flow instability or flow oscillation criteria should be considered more in depth. However, the height of PCCT is limited by economics and robustness of plant construction, and horizontal type heat exchangers have advantages here. Two types of heat exchangers showed different behaviour against thermal stratification phenomena. To investigate their characteristics, we performed simple phenomenological studies using commercial CFD code, CFX.

Two cases of heating rods of simple geometry were considered to compare the flow and heat transfer characteristics. The two heating rods are the same size and shape: a single cylinder as shown in Fig. 74. One is placed vertically and the other horizontally in a tank that is of a shape similar to the cooling tank of a separate effect test experiment described in next section.

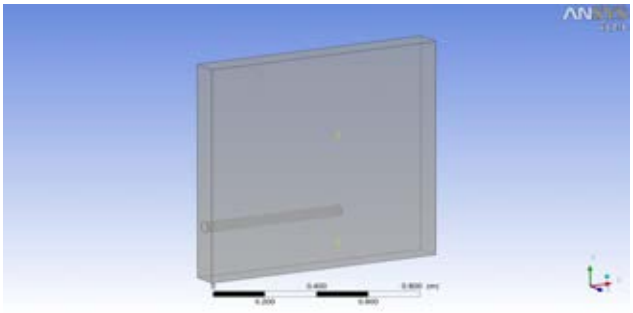

FIG. 74. The geometry of a heating rod in a cooling tank.

The heating rods have constant temperature, 150^{o}C, while the initial water temperature in the tank is given as 30^{o}C. The flow pattern induced by buoyancy is inherently transient. Figure 75 shows the temperature distribution and flow velocity vector field on a middle plane in the tank. In the case of the vertical type heating rod, flow develops along the vertical heating surface and divides into sides at the top surface. The flow vector field is not strong over the inside of the tank. Thereby, water is heated from top to bottom forming temperature layers in height direction. The flow pattern in the horizontal type heating rod is different. The flow vector field is much stronger from inside of tank and a whole circular flow is formed to transport momentum and energy from the heating rod to the cooling water. The temperature field has almost no deviation except for the heated part over the rod. The temperatures of the two heating rods are the same and constant, but heat flux on the rod surface, i.e. the energy transfer rate from the heating surface, is much higher in a horizontal type. Figure 76 shows the ratio of temperature rise to time is greater in the horizontal type. And, temperature difference occurs due to the weak flow mixing in the vertical type. This simulation does not include wall effects of the tank side. The flow pattern is actually affected by the no slip

condition of the walls. In Fig. 77 the temperature stratification appears in the case of the horizontal type. The flow and heat transfer become more complex and unstable when wall effects are considered in a narrow depth tank. It is hard to distinguish the thermohydraulic characteristics caused only by changing the type of heat exchangers from the integrated effects in a real condition. Therefore, it is effective to set apart some conditions in advance of detailed calculations, which is the advantage of CFD analysis.

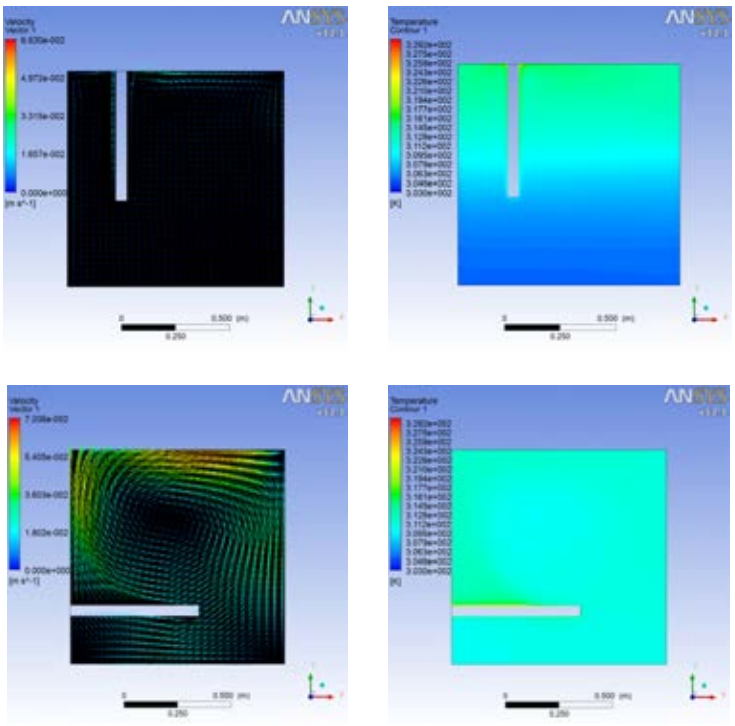

FIG. 75. The temperature distribution and velocity vector field in the cooling tank of heating rods (above: vertical type at 500sec, below: horizontal type at 700sec).

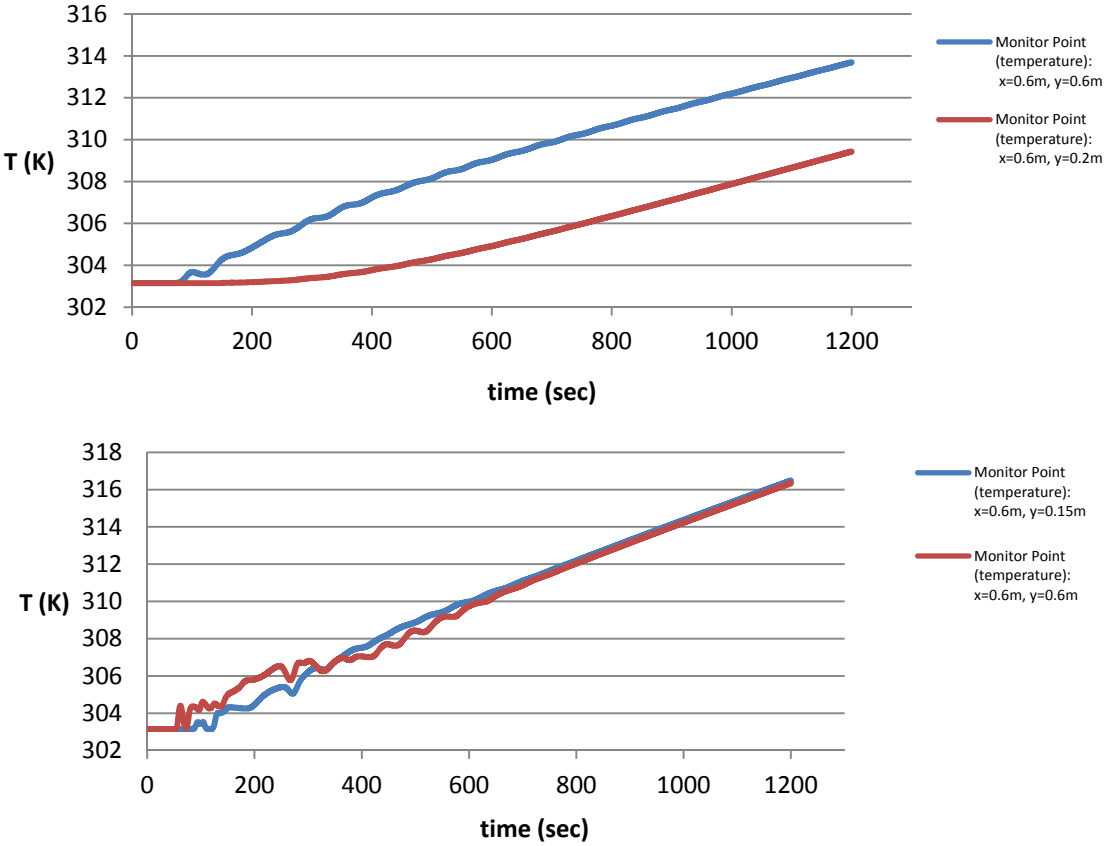

FIG. 76. Temperature changes at monitoring points in the cooling tank of heating rods (above: vertical type, below: horizontal type)

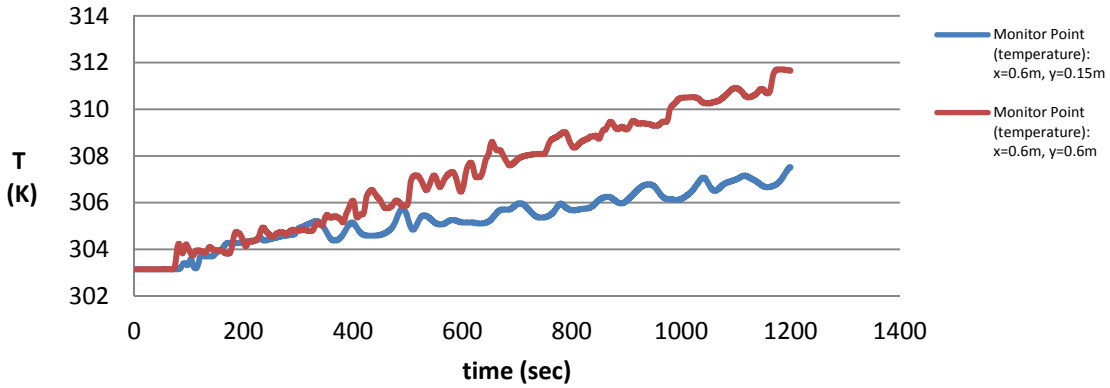

FIG. 77. Temperature changes at monitoring points in the cooling tank of horizontal heating rod considering side wall effects.

5.3.2. RELAP simulations

The purpose of preliminary performance analysis is to make initial sizing of heat exchanger and system configuration and to get intuition for experiments. The other purpose of this evaluation is to confirm the suitability of plant operating and thermohydraulic behaviour in transient conditions. For the preliminary analyses, RELAP5/Mod3.3 codes were used.

5.3.2.1. Modelling of PAFS

A PAFS is composed of two independent trains, and each train covers 100% design capacity. The steam feed line of the PAFS starts from the main steam line upstream of MSIVs, and the steam is condensed in the heat exchanger. The condensed water goes through the return line and finally merges into an economizer line. Isolation valves and check valves are installed for PAFS isolation from the main feedwater system during normal operation. Figure 78 shows the node diagram of APR+ reactor coolant system (RCS). Then the nodalized RCS model was developed in accordance with the design data and system configuration of APR+. The safety systems are connected to the RCS model as a time dependent volume and single junction for safety analysis. The PAFS steam supply line and condensate return line are connected to the main steam line and main feedwater line, respectively. A total 1142 nodes and 635 heat structures are used in this modelling.

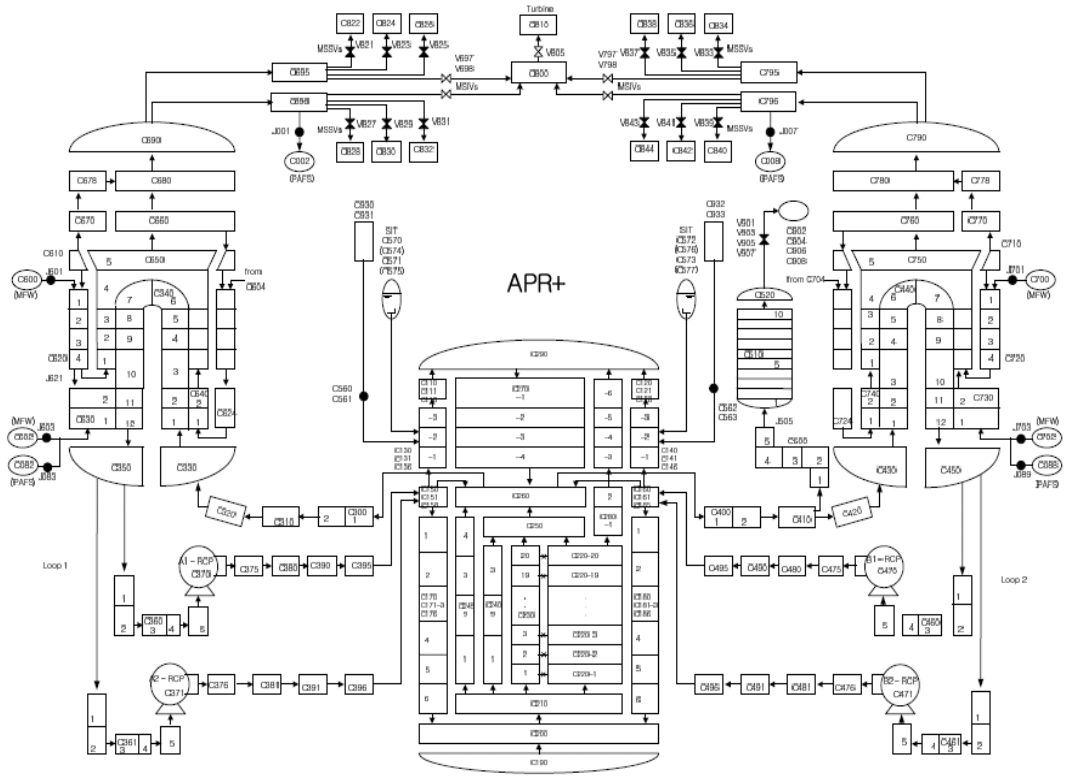

FIG. 78. Nodalization of APR+.

As described earlier, the PAFS consists of a PCCT, a slightly inclined U-tube type heat exchanger, and related valves and pipes. The main thermohydraulic phenomenon inside the heat exchanger is steam condensation and outside the heat exchanger is natural convection in the PCCT. It is well known that RELAP is a one dimensional system code and, thereby, it is deficient in simulating natural convection in a three dimensional water pool. We can consider CFD as a tool for making up this feature of system codes. CFD analysis, however, introduces another problem. It is limited to the simulation of two-phase boiling phenomena. Therefore, we adopted a combined method to resolve these constraints.

The flow pattern under subcooled condition in the PCCT is obtained from CFD analysis. The cooling tank is modelled in RELAP according to the CFD analysis result. If we model PCCT

with a single node, we cannot simulate natural convection inside the tank. So, several two channel multinode methods are suggested as shown in Fig. 79.

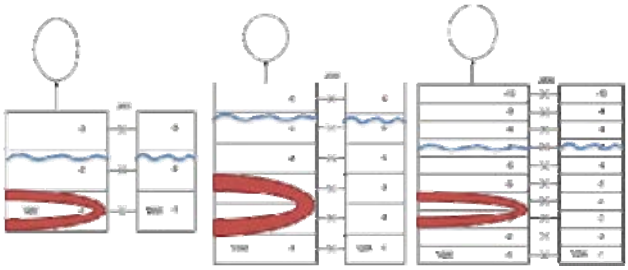

(a) Case I (b) Case II (c) Case III

FIG. 79. RELAP5 nodalization candidates for PCCT.

As the results of RELAP simulations, Case I shows a very different and unphysical result compared to Case II and Case III. The results of Cases II and III are similar to each other as shown in Fig. 80. Finally, Case II is chosen as a standard PCCT nodalization for the reason to reduce computing time. Fig. 80(a) shows vertical water flow for each node. Positive value means upward flow at nodes located at left side of the tank and negative value means downward flow at the right side nodes. Figure 80(b) shows horizontal flow at the junctions between each channel. Positive value means flowing to the right and negative to the left. We can see here that a large circular convection is developed inside the PCCT. This pattern is well matched with the result of CFD analysis described in the next section.

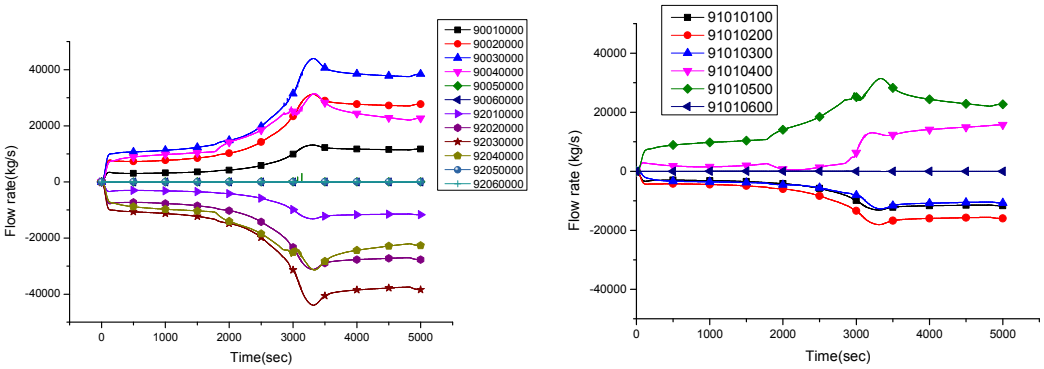

(a) Vertical flow in each channel. *(b) Horizontal flow at junction between two channels.*

FIG. 80. Flow pattern in each nodes of PCCT nodes.

Finally, the PAFS model is developed as shown in Fig. 81. It is attached to the APR+ system model, including nodalization for piping, heat exchanger, and PCCT. The PCCT is divided into six volumes to simulate natural convection in the PCCT. The heat exchanger is divided into 70 volumes in order to analyse the condensation in detail inside the heat exchanger tube. It was assumed that the primary heat load is transferred to the secondary side. Steady state analysis was performed using APR+ conditions.

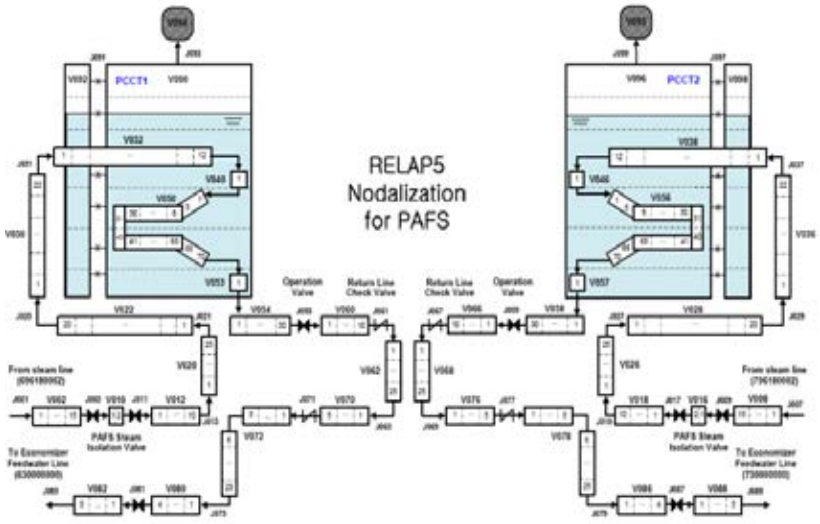

FIG. 81. Nodalization for PAFS model.

5.3.2.2. Performance analysis

Two design basis events — loss of condenser vacuum accident (LOCV) and feedwater line break (FLB) — are selected as basic analysis cases because LOCV and FLB are known to be limiting events for the PAFS. During an LOCV, the two trains of the PAFS are operated while only one train attached to the intact steam generator side is available during FLB.

Following the occurrence of an LOCV, the main feedwater pumps, reactor coolant pumps and the turbine immediately stop due to the loss of off-site power; a reactor trip occurs on the high pressurizer pressure. The pressure of the pressurizer under the LOCV is shown in Fig. 82. As illustrated in the figure, the pressure decreases continuously after reactor shutdown. The results show that the cooling performance of the PAFS is sufficient to remove the decay heat of the reactor core. As illustrated in Fig. 83, the steam generator secondary water level decreases continuously after the reactor trip and the PAFS is actuated when the steam generator water level reaches to the PAFS actuation level. During this period, the heat generated in the reactor core is vented through the main steam safety valve by vapourization of the steam generator secondary water. After the PAFS is actuated, the steam generator water level is maintained at a constant level.

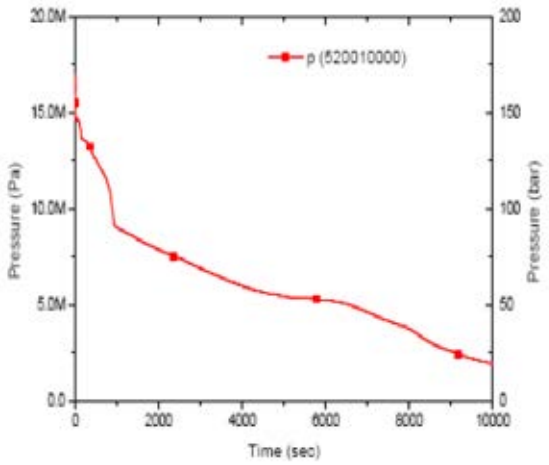

FIG. 82. Pressurizer pressure (LOCV).

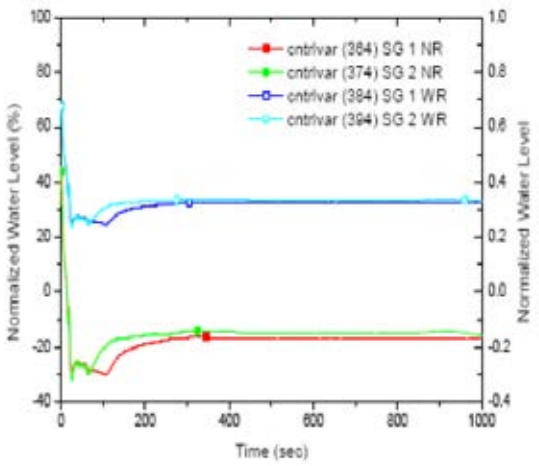

FIG. 83. Steam generator water level (LOCV).

An FLB is initiated by a break in the main feedwater system piping. Depending on the break size and location, its effects can vary. For a conservative analysis, the break location is postulated as being in a feedwater line between the check valve and the steam generator. The fluid of the affected steam generator is discharged through the break. The FLB causes an instant reduction in feedwater flow and a reactor trip under high pressurizer pressure. The pressure of the pressurizer for the FLB is shown in Fig. 84: this graph shows that the single PAFS under FLB has enough cooling performance to accomplish decay heat removal. After the reactor trip, the pressure is continuously decreased and the steam generator secondary water level is continuously decreased. When the water level of the intact steam generator side gets to the PAFS actuation level, the PAFS begins to work.

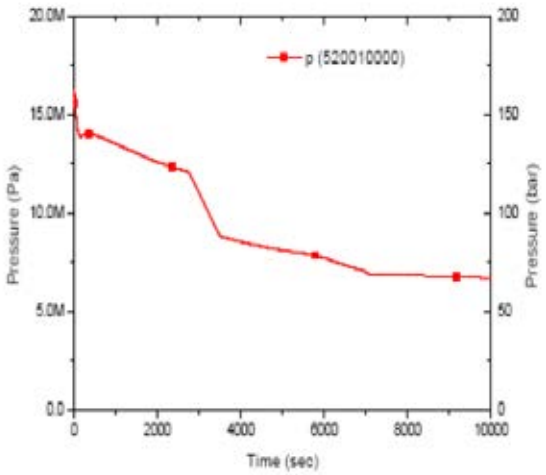

FIG. 84. Pressurizer pressure (FLB).

Thermohydraulic behaviour in a PCCT during accidents is represented in Fig. 80. Natural convection in a PCCT is independent on the accident scenario. Figure 85 shows simple a schematic picture for Fig. 80. As shown in the figure, water in a PCCT makes a large circular flow.

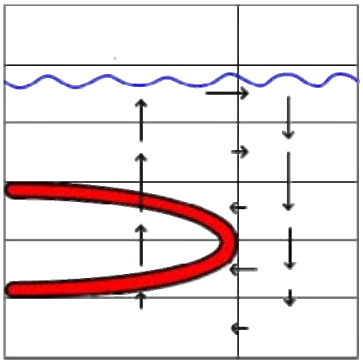

FIG. 85. Water flow in PCCT.

5.3.3. CFD analysis on natural convection in a pool

As mentioned above, PCCT is divided into two channels and six nodes in each channel in order to predict natural circulation in RELAP code. There is, however, limitation of increasing accuracy in analysing heat transfer characteristics of natural convective flow by using system codes, which is rather specialized in CFD analysis. Thermohydraulic phenomenon of PAFS is effectively predicted by system codes. And the following results could provide reasonable boundary conditions of CFD analysis if analysed results do not severely influence the function of total system or if CFD calculation is carried out in link with system code analysis. In this section, preliminary analysis on flow and heat transfer of single heat exchanger cooling tank was performed using CFX, a commercial CFD code.

The simulation in this study is carried out to eventually compare with the results of a PCCT separate effect test experiment. The geometry and dimension come from the experiment plan as shown in Fig. 86. One of the main factors affecting momentum and heat transfer is the boundary condition on the heat exchanger. First, we used temperature distribution along the length of the heat exchanger tube from system code (RELAP) analysis in Fig. 87. RELAP results were gained from the steady state of PAFS operation. The preliminary calculation excluded the subcooled pool boiling for the reason of simplicity in analysis.

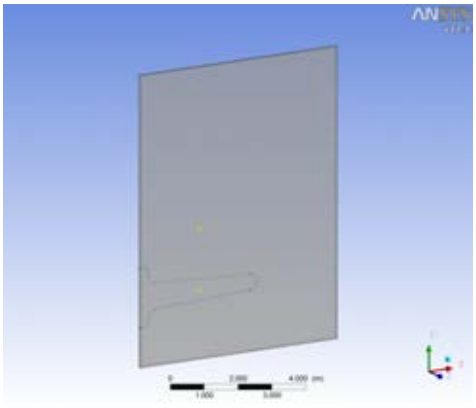

FIG. 86. Flow domain for separate effect test simulation.

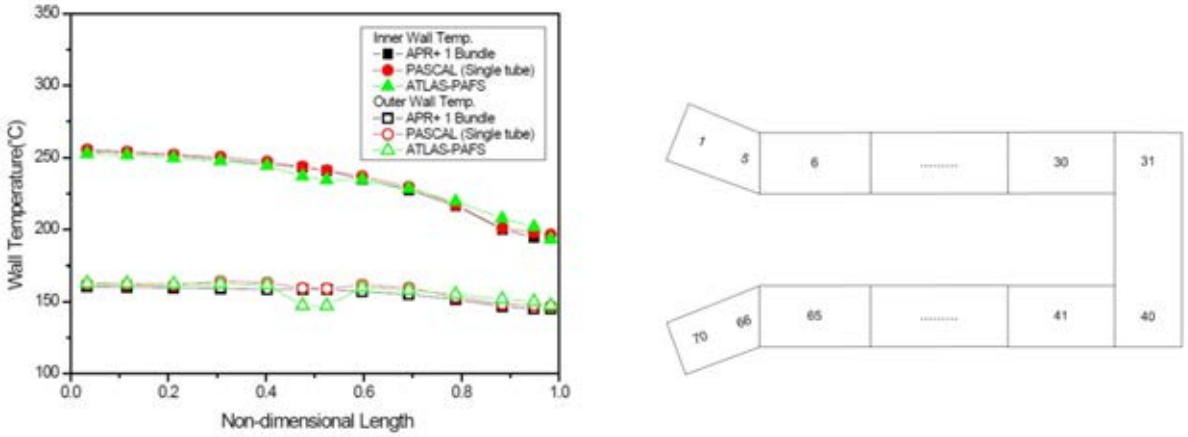

FIG. 87. Inner and outer wall temperature distribution of RELAP steady state results (left) and node model for the single heat exchanger tube used in RELAP calculation (right).

Figure 88 shows the calculated heat flux from the tube surface. The heat flux of the constant temperature condition is about ten times lower than that of the RELAP result. This comes from the scalable wall function used to predict water temperature distribution along the normal direction on the tube could not implement heat flux suitable for the saturation point. Since the temperature deviation resulting from the heat flow through the tube surface brings in driving force of fluid flow and related heat transfer, exact heat flux on the tube is necessary for natural convection analysis. Therefore, it is more reasonable to use heat flux boundary condition before an advanced physical model is applied to the thermal phase changing phenomenon.

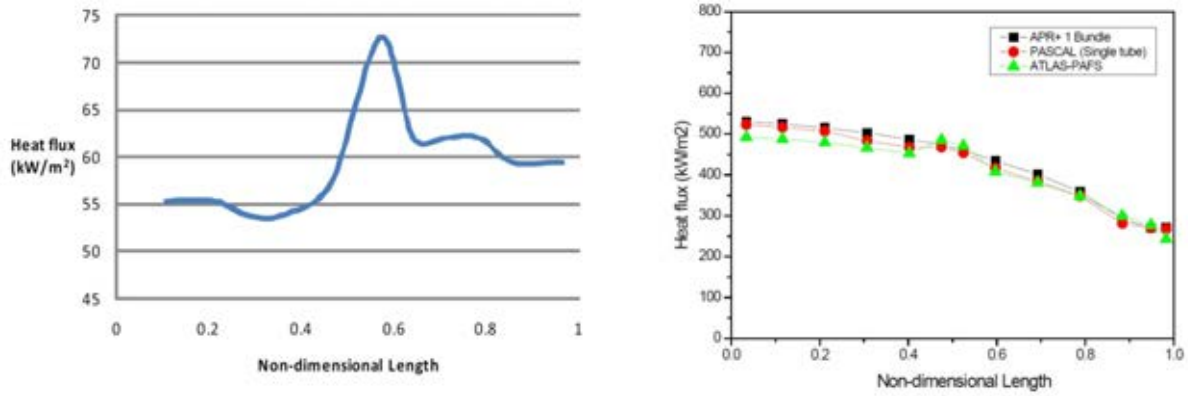

FIG. 88. Heat flux on the single tube of constant temperature boundary condition (left) and RELAP result (right).

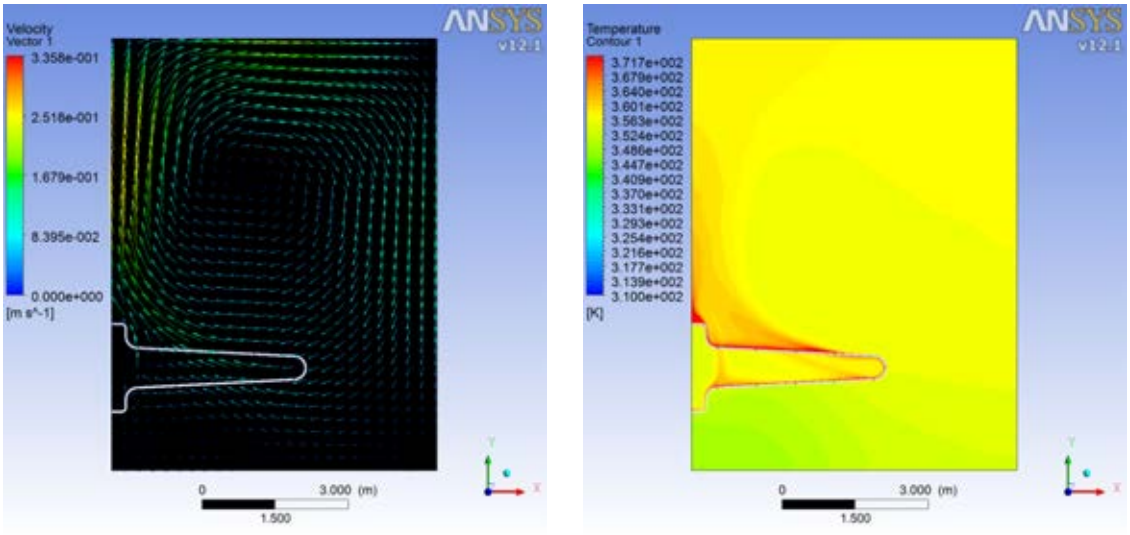

FIG. 89. Flow vector field and temperature distribution of single tube PCCT natural convection at 35 min.

Figure 89 shows the calculated fluid flow vector field and temperature distribution for the case of heat flux boundary condition that is given in Fig. 88. A central eddy flow is driven from the tube surface and transports momentum and thermal energy throughout the cooling tank. This flow pattern develops until the driving force causing fluid circulation and the fluid inertial moment are balanced. In flow pattern development, stability can occur in the flow region around the heat exchanger tube. Figure 90 presents the temperature change at the near-boundary cells of the fluid domain around the tube. The flow pattern changes until about 15 minutes and the turbulence intensity increases abruptly for five to ten minutes. Then the temperature change becomes stable where the flow pattern is established following a regular form. The external forces could be balanced because heat flux on the tube was constant and mass flux out of the tank was excluded in this case. And more, the shear force on the tank wall was not considered. The flow vector field and temperature distribution do not have a regular form as shown in Fig. 91 when no-slip condition is applied to the side walls of the cooling tank. As discussed in the case of a simple horizontal heating rod, stratification in temperature field is observed in the cooling tank flow. The upper region above the single tube is heated almost to the saturation point while the lower region below the tube contains cool water enough cold to have the initial temperature. Stratification seems to be caused mainly by the narrowness of the tube, which can hinder the cooling function of the tank. However, this feature belongs only to the separate effect test facility.

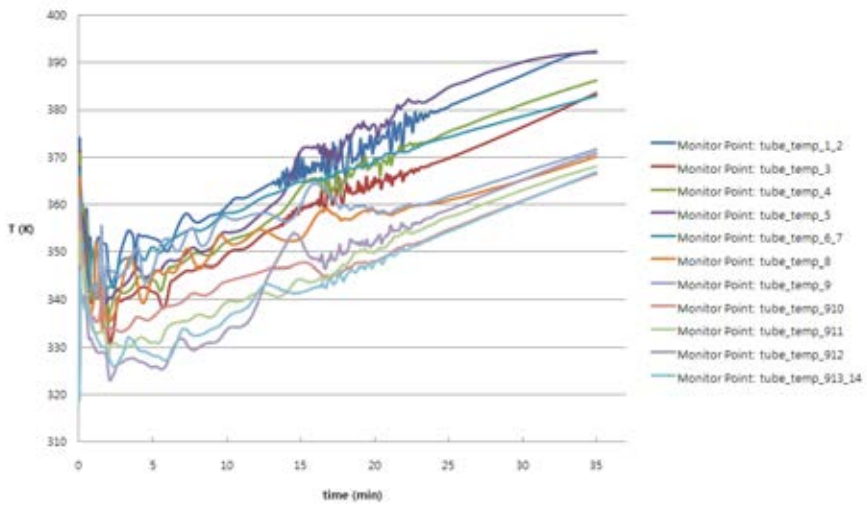

FIG. 90. Temperature change at tube near-boundary cells.

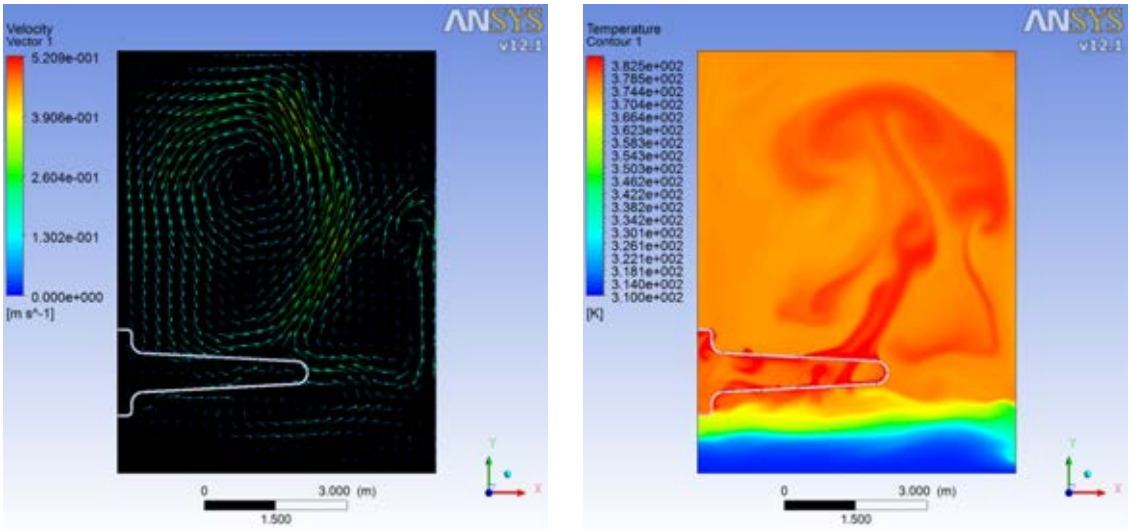

FIG. 91. Flow vector field and temperature distribution of single tube PCCT natural convection at 46 min.

CFD simulation in this study presents fluid flow and heat transfer characteristics of natural convection arising in a single heat exchanger cooling tank. Since only the systematic analysis on the whole PAFS can give a reasonable boundary condition on a specific component of the system, we used RELAP5 results of the tube temperature and heat flux distribution as the boundary conditions for CFD calculation. Also, the heat flux boundary condition is more practical in giving heat source for driving force of natural convection in that prediction of the temperature distribution in normal direction around the tube is limited with the wall function model without concerning thermal phase change. The RELAP result in the previous section matched the flow pattern observed in the cooling tank when the tank side wall effects are neglected. Taking into account the three-dimensional effect like no-slip condition on the side walls would be a big challenge to the current progress of system codes.

5.3.4. Separate effect tests on PAFS

The main driving forces of PAFS are steam condensation inside tubes and two-phase natural circulation. Steam condensation phenomena in slightly inclined tubes are not well known. Models and correlations in the system codes such as RELAP5 are inadequate for this geometry. In order to perform valid and accurate performance analysis for PAFS, adequate steam condensation models or correlations for this geometry should be developed. In PAFS, slightly inclined tubes are immersed in the bottom of the PCCT. The key phenomenon in a PCCT is natural convection. If natural convection is well developed, the water inside the PCCT is well mixed. If not, water near the heat exchangers may be boiled although the bulk temperature of the pool is still subcooled. For these purposes, we perform separate effect tests. Steam condensation heat transfer coefficients and flow regime inside the tubes and natural convection inside the pool will be identified using separate effect tests [27].

PAFS adopts a slightly inclined U-tube heat exchanger, which has been designed with an inclination of 3 degrees against the horizontal to prevent water hammering. The purpose of separate effect tests is to measure the condensation heat transfer coefficient inside the tube, to identify flow regime along the tube, to identify non-condensable gas effect, to measure natural circulation capability in the pool, and to measure flow instability.

Figure 92 shows the test facility. In order to obtain satisfactory assessment results in this separate effect test, the volume scaling method is used for this facility. Height is conserved as a critical parameter for natural circulation and, in the same way, area is reduced to 1 over 240. For the water pool, geometric shape is conserved to measure natural convection. The number of heat exchanger tubes is reduced to 1 over 240. However, tube area is conserved to measure the actual heat transfer coefficient and flow regime.

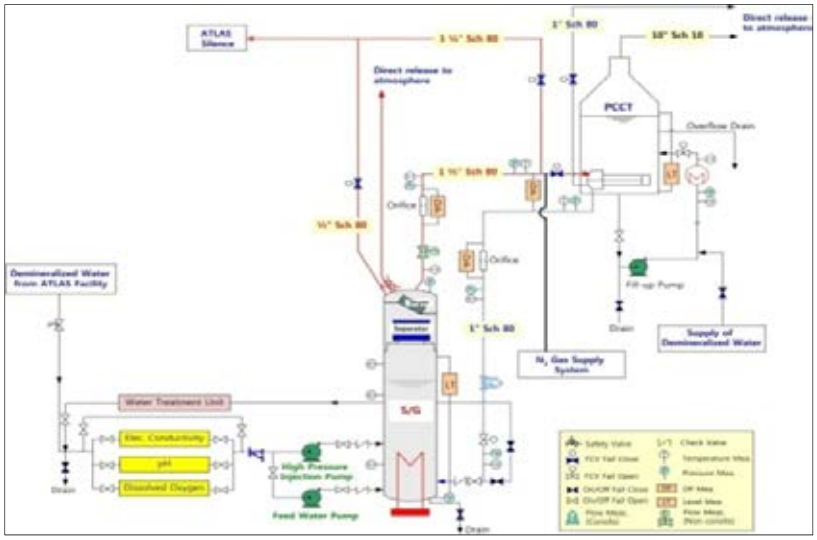

FIG. 92. Separate effect test facility.

As shown in Fig. 92, the test facility is composed of the steam generator, the PAFS heat exchanger, the PCCT, the pressure control system, the steam dump system, and the PAFS tank filling and heating system. The facility has a degassing system. The heating capacity of steam generator is 0.8 MW. This is determined on the basis of decay heat at 5 min after reactor trip. In order to improve the efficiency of the test, we consider several significant tests

such as steady state test, startup test, non-condensable gas effect test, PCCT water level test and main steam safety valve open/close transient test.

In the PCCT, there are 99 thermo-couples to measure natural circulation. Water temperature near the tube is important on heat transfer between tube and the pool. Also, 100 void fraction sensors and visual windows are installed to check pool boiling phenomena. These features are shown in Fig. 93.

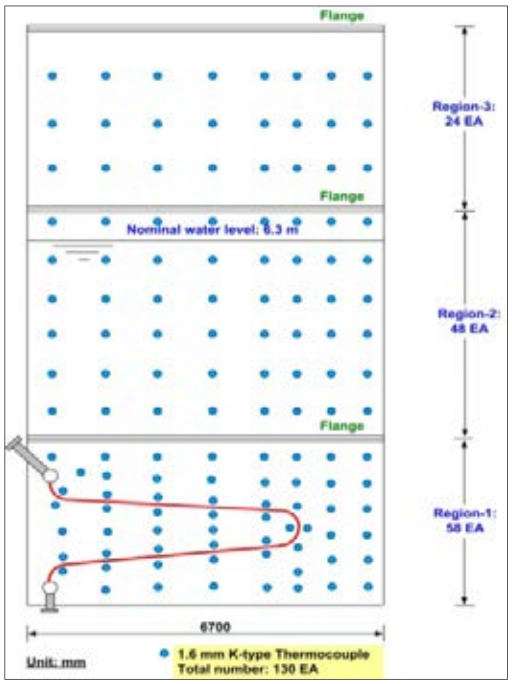

FIG. 93. Measurement system.

Figure 94 shows actual view of a PCCT. It has 6.6 m width and 11 m height.

Among the various tests which have been performed to verify the performance of PAFS, a steady state heat removal test and a natural convection transient test are described in this report because focusing on this report is natural convection inside the PCCT.

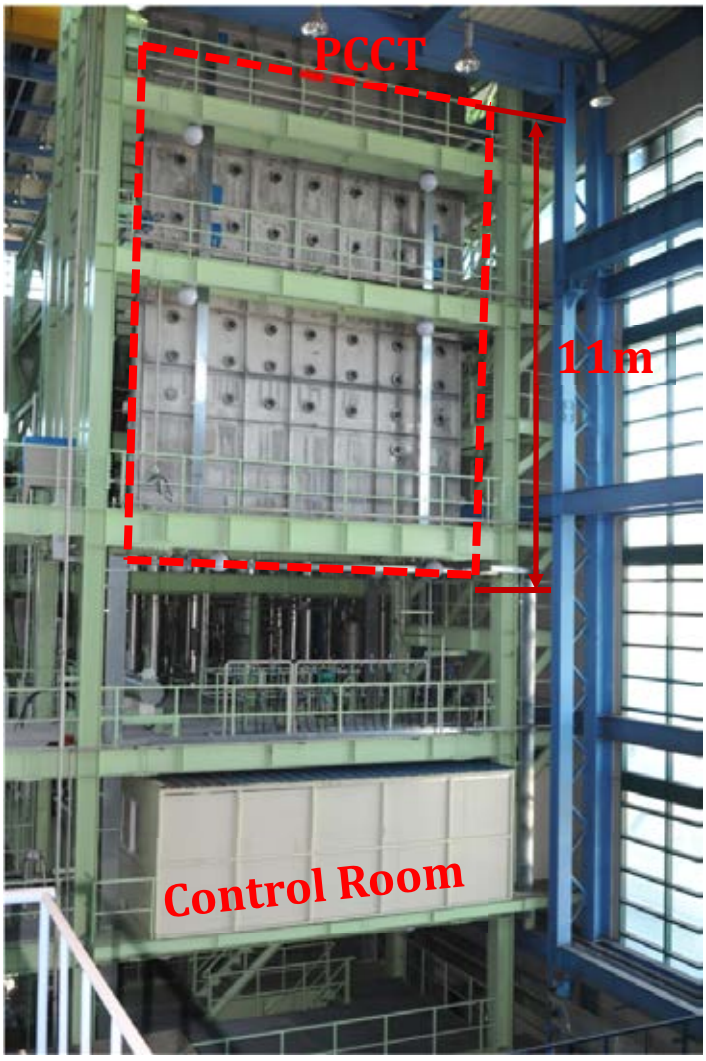

FIG. 94. Actual view of a PCCT.

5.3.4.1. Steady state heat removal test

Before a natural circulation test, we performed steady state heat removal test [28] to verify the heat removal capability of a heat exchanger. Test conditions are as follows:

- Initial water level in PCCT: 4 m (half of full water level);
- Initial water temperature in PCCT: saturation temperature at atmospheric pressure;
- Power in a steam generator: 540 kW.

Based on the above initial conditions, the test procedures are as follows:

- The heater power in the steam generator is preset to 540 kW;
- An operator turns on the heat power and opens the control valve located at the steam line;
- The control valve remains open. The system pressure and the heated power are varying to find steady state condition;
- After a steady state is reached, steady state data are logged.

According to the test results, the steady state system pressure is 2.5 MPa at 15 000 sec after the control valve is opened.

The main observation results are as follows:

- There are no adverse effects such as water hammering, condensation oscillation, or any other effects;
- There is no bulk boiling inside the PCCT. The vapours generated near the heat exchanger are collapsed in the pool;
- The water in the PCCT is slightly subcooled because the water level is 4 m. The generated vapours may be condensed inside the pool because of its subcooling;
- The stratified flow condition is well maintained inside the tube;
- The steady state is well maintained. There is no need to adjust control valve to maintain steady state condition;
- The condensation heat transfer coefficients inside the tube are distributed from 10°000W/m2K to 30 000 W/m2K along the tube. These values are much higher than the predicted heat transfer coefficients by the system codes such as the RELAP5 code.

5.3.4.2. Natural convection transient test

The procedure for the natural convection transient test is similar to that of the steady state test. The only difference is that the initial water temperature is maintained at subcooling condition. Figure 95 shows the temperature distribution at initial state and final state.

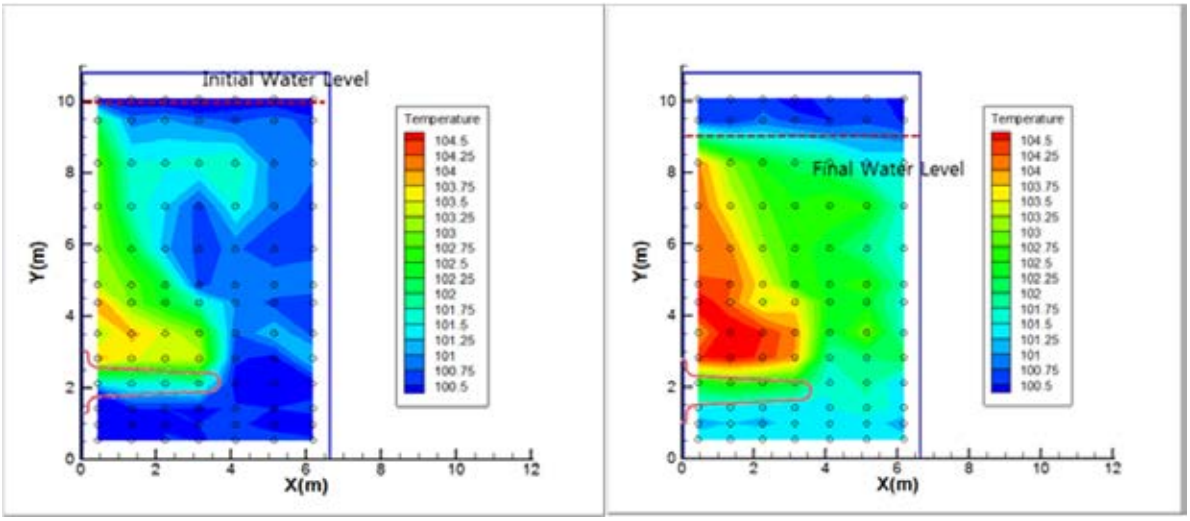

(a) Initial state. *(b) Final state.*

FIG. 95. Temperature distribution inside the PCCT.

As shown in Fig. 95, overall natural circulation is well established and the water inside the pool is well mixed. This test result is well matched to the simulation results. For example, the temperature distributions of Fig. 91 and Fig. 95(b) are very similar: Figure 91 is temperature distribution by CFD simulation and Fig. 95 is temperature distribution by the test.

6. CONCLUSIONS

India, Argentina, and the Republic of Korea actively participated in implementing the INPRO collaborative project on *Advanced Water Cooled Reactor Case Studies in Support of Passive Systems*. According to the Terms of Reference, each country successfully conducted an assigned case study associated with natural circulation and thermal stratification phenomena. During the past three years, extensive experimental and theoretical investigations of steady state, stability and startup of natural circulation in AHWR and CAREM units were performed. In the field of thermal stratification, phenomenological experiments using both simple test facilities and an integral test facility representing AHWRs were performed along with their simulation using the RELAP5 computer code. Also, the thermal stratification phenomenon in the PAFS of the APR+ was investigated using separate effect tests and simulations carried out using CFX and RELAP5 codes.

The major findings and conclusions from this project are presented below.

6.1. AHWR

- The startup procedure for AHWR with stage-wise external pressurization up to nominal operating pressure was validated in ITL. The predictions made using the computer code RELAP5/MOD3.2 were found to be compatible with experimental data. Therefore, the codes could be used for simulating the startup procedure of the AHWR prototype plant.

- Experimental investigations on stability threshold were carried out using four different mechanical gadgets, including a spool piece with helical coil and bellows. It was found that all gadgets were able to suppress the instability in the loop and especially that the spool piece with helical coil caused the least reduction in mass flow rate and increased the instability threshold highest among all the gadgets. Therefore, it could be concluded that the helical coil was an effective tool to suppress instability in single-phase natural circulation systems.

- Experimental investigations with nanoparticles showed that the instabilities got suppressed in both single-phase and two-phase natural circulation systems in the presence of nanoparticles in water. The enhancement in flow rate was brought about by the enhancement of the thermal expansion coefficient resulting from the addition of nanoparticles. The increase in loop flow rate in the presence of nanoparticles was found to be proportional to the concentration of nanoparticles. Highest flow rate was observed with CuO nanoparticles followed by TiO_2, Al_2O_3 and SiO_2 in that order.

- The single-phase natural convection flow pattern in a heated rectangular enclosure was studied using aluminum particles and PIV system. CFD calculations were in close agreement with experimental PIV data. Scaled isolation condenser performance was tested and it was found that thermal stratification observed in isolation condenser pool did not significantly degrade the heat transfer to pool if isolation condenser tubes were submerged.

- RELAP5/ MOD3.2 code adequately simulated the isolation condenser performance but, due to 1-D nature of the code, the thermal stratification in isolation condenser pool was not adequately simulated. The study carried out using shrouds in one sector of the GDWP by RELAP5/MOD3.2 code showed boiling suppression and participation of bulk pool inventory in heat transfer process. The use of fewer shrouds gave higher flow rate and

improved inventory utilization. However, multidimensional effects were not accounted for in the simulations with RELAP5 code. Therefore, further studies on the effect of shrouds based on integral simulation with ICS and CFD simulation are required.

6.2. CAREM

- Under the hypothesis of the HUARPE model, it was possible to show the CAREM-25 reactor's stability performance for a wide range of operational conditions. At nominal conditions, the stabilizing effects of the neutronic feedback and reactor pressure were verified. In addition, an unstable area was found to be located at relatively low condensation powers. It was also confirmed that the unstable region was induced by instabilities generated by density waves that travel along the reactor chimney.

- A wide area in the stability map was detected at condensation power values close to 0.75 MW in which the stability margins were considerably incremented. This region offered excellent conditions to guarantee reactor stability for a wide range of operational conditions. Preliminary estimations showed that incrementing the condensation power up to 0.75 MW would be enough to increase the reactor stability margins and thus optimize the plant safety.

- It was corroborated that the flashing phenomenon was of crucial importance for the stability analysis in the range of pressures, core powers and condensation powers relevant for CAREM reactor. This result emphasizes the need to use tools which consider the pressure variation by hydrostatic height.

- The stability maps shows that a stable condidtion could reach regardless of the core powers value by incrementing the system pressure. Therefore, it is suggested to begin the pressurization stage with the RPV pressure at 4.7 MPa.

- It was found that the maps presented in the reactor power-system pressure plane did not show any significant changes when incrementing the condensation power from 0.75 MW to 1.0 MW. These maps also showed that the reactor could be operated from a condition of low pressure and low reactor power to a nominal condition without passing through unstable regions.

- According to the implemented model, it is observed that it is possible to pressurize the reactor without encountering instabilities if a condensation power of at least 0.75 MW can be guaranteed. This important result indicates the reactor could be started up without encountering instabilities of thermohydraulic origin.

6.3. APR+

- As per simple analyses using CFX code for vertical and horizontal heater rods, the horizontal heater rod showed better performance with regard to thermal stratification in large pools. The reason was that the horizontal heater rod provided a larger driving force for natural convection and hence higher circulation rates than a vertical heater rod.

- Using the separate effect test facility, a steady state heat removal test and a natural convection transient test were performed. It was observed that there were no adverse effects such as water hammering, condensation oscillation and bulk boiling. High circulation flow was observed during the test without pool thermal stratification phenomenon.

- Natural convection simulations using CFX code were performed. The calculation results are in good agreement with the test results.

- Coupled calculations using CFX code and the RELAP5 system code were performed. As well known, the RELAP5 code was deficient in handling multidimensional phenomena such as natural convection in a large pool, and CFX code was deficient in handling two-phase fluid. To deal with the deficiencies of both codes, simulation results for two-phase flow in a tube obtained from RELAP5 code were given as the tube boundary conditions for CFX code calculation. The obtained flow behaviour in a pool from CFX code was used to refine the simulation results of RELAP5 code. The results of the coupled calculation with RELAP5 and CFX codes showed very similar behaviour with the test results. Finally, it was confirmed that RELAP5 code could be used to simulate natural convection behaviour in a pool.

REFERENCES

[1] INTERNATIONAL ATOMIC ENERGY AGENCY, Natural Circulation in Water Cooled Nuclear Power Plants Phenomena, Models and Methodology for System Reliability Assessments, IAEA-TECDOC-1474, IAEA, Vienna (2005).

[2] SINHA, R.K., KAKODKAR, A., Design and development of AHWR – the Indian thorium fuelled innovative nuclear reactor, Nuclear Engineering and Design, Volume **236**, Issue 7–8 (2006).

[3] KHNP Central Research Institute, Standard Safety Analysis Report for APR+, a Licensing Document submitted to Nuclear Safety and Security Commission in the Republic of Korea, Seoul, Republic of Korea (2011).

[4] GOMEZ, S., Development activities on advanced LWR designs in Argentina, Technical Committee Meeting on Performance of Operating and Advanced Light Water Reactor Designs, Munich, Germany (2000).

[5] DELMASTRO, D., Thermohydraulic aspects of CAREM reactor, IAEA TCM on Natural Circulation Data and Methods for Innovative Nuclear Power Plant Design, Vienna, Austria (2000).

[6] RAO, G.S.S.P., VIJAYAN, P.K., JAIN, V., BORGOHAIN, A., SHARMA, M., NAYAK, A.K., BELOKAR, D.G., PAL, A.K., SAHA, D., SINHA, R.K, AHWR integral test loop scaling philosophy and system description, BARC Report, BARC/2002/E/017 (2002).

[7] GARTIA, M.R., VIJAYAN, P.K., PILKHWAL, D.S., A generalized flow correlation for two-phase natural circulation loops, Nuclear Engineering and Design, Vol. **236**, Issue 17, (2006) 1800–1809.

[8] NAYAK, A.K., VIJAYAN, P.K., SAHA, D., VENKAT R.V. and ARITOMI, M., Study on the stability behaviour of a natural circulation pressure tube type boiling water reactor, Nuclear Engineering and Design, Volume **215** (2002) 127-137.

[9] Design Basis Report on Start – up, Project: AHWR Engineering Development, AHWR/DBR/33110/rev 3, BARC (2004).

[10] BAGUL, R. K., SHARMA, M., PILKHWAL, D.S., VIJAYAN, P.K., SINHA, R.K., An overview of thermohydraulic design validation studies for AHWR, Int. Conf. Future of HWRs, Ottawa, Ontario, Canada, (2011).

[11] BAGUL, R.K., BODKHA, K., PILKHWAL, D.S., PAL, A.K. and VIJAYAN, P.K., Validation of AHWR Startup Procedure in Integral Test Loop, BARC Report, BARC/2009/E/017 (2009).

[12] BODKHA, K., KUMAR, N., VIJAYAN, P.K., SAHA, D., Investigations on role of mechanical gadgets in controlling flow instability in single-phase natural circulation loops, Proceedings of the 20th National and 9th International ISHMT-ASME Heat and Mass Transfer Conference, Mumbai, India (2010).

[13] NAYAK, A.K., GARTIA, M.R. and VIJAYAN, P.K., Nanofluids: A novel promising flow stabilizer in natural circulation systems, AIChE Journal Volume **55**, Issue 1 (2009), 268–274.

[14] NAYAK, A.K. KULKARNI, P.P., VIJAYAN, P.K., Study on the transient and stability behaviour of a boiling two-phase natural circulation loop with Al2O3 nanofluids, Applied Thermal Engineering Volume **31**, Issue 10 (2001) 1673-1681.

[15] BOURE, J.A., BERGLES, A.E. and TONG, L.S., Review of two-phase flow instability, Nucl. Eng. Des., **25** (1973) 165.

[16] LAHEY, R.T. Jr., MOODY, F.J., The Thermohydraulics of a Boiling Water Nuclear Reactor, American Nuclear Society, LaGrange Park, Illinois (1979).

[17] FUKUDA, K., KOBORI, T., Classification of two-phase instability by density wave oscillation model, Journal of Nuclear Science and Technology **16**, v2 (1979) 95-108.

[18] MARCEL, C.P., Experimental and Numerical Stability Investigations on Natural Circulation Boiling Water Reactors. IOS press (2007).
[19] ZANOCCO, P., GIMENEZ, M., DELMASTRO, D., Modeling Aspects in Linear Stability Analysis of a Self-Pressurized Natural Circulation Integral Reactor, Nuclear Engineering and Design, **231** (2004) 283–301.
[20] ZANOCCO, P., DELMASTRO, D., GIMENEZ, M., Linear and Nonlinear Stability Analysis of a Self-Pressurized, Natural Circulation, Integral Reactor, ICONE12, International Conference on Nuclear Engineering, Washington, DC (2004).
[21] ROHDE, M., MARCEL, C.P., VAN der HAGEN, T.H.J.J., MANERA, A., SHIRALKAR, B., Investigating the ESBWR stability with experimental and numerical tools: A comparative study, Nuclear Engineering and Design **240** (2010) 375–384.
[22] MARCEL, C.P., ROHDE, M. and VAN der HAGEN, T.H.J.J., Experimental Investigation on the ESBWR stability performance, Nuclear Technology Volume **164** (2008).
[23] FURUYA, M., INADA, F., VAN der HAGEN, T.H.J.J.,. Regional stability estimation of natural circulation BWRs using SIRIUS-N facility. J. Nuclear Science and Technology, **42** (2005) 341.
[24] The Conceptual Design Report for PAFS of APR+, S07NJ06-E-TR-006, KHNP Central Research Institute (2009).
[25] KIM, H.G., et al., The Development of a Passive Auxiliary Feedwater System in APR+", ICAPP 2010, San Diego, USA (2010).
[26] SHARMA, M., PILKHWAL, D.S., VIJAYAN, P.K. SAHA, D., Experimental Investigations on the Isolation Condenser performance in Integral Test Loop, ICONE 16 - 48600, Orlando, Florida (2008).
[27] BAE, B.E., et al., Scaling Analysis of Separate Effect Test Loop (PASCAL) for PAFS, NTHAS7, Seoul, Republic of Korea (2010).
[28] Korea Atomic Energy Research Institute, Quick look report on the cooling performance test (SS/PL-540-02) with the PSACAL, 9-017-A599-002-049, Seoul, Republic of Korea (2011).

ABBREVIATIONS

AFWS	auxiliary feed water system
AHP	analytical hierarchical process
AHWR	advanced heavy water reactor
APR+	advanced power reactor plus
AWCR	advanced water cooled reactor
BARC	Bhabha Atomic Research Centre
BWR	boiling water reactor
CAREM	Central Argentina de Elementos Modulares
CFD	computerized fluid dynamics
CMT	core make-up tank
CP	INPRO collaborative project
CRP	coordinated research programme
DWO	density wave oscillation
ECCS	emergency core cooling system
ESBWR	economic simplified boiling water reactor
FCS	fuel channel simulator
FLB	feedwater line break
FP	full power
GDWP	gravity driven water pool
GEN III+	third-generation plus
GIF	Generation IV International Forum
ICS	isolation condenser system
IGCAR	Indira Gandhi Centre for Atomic Research
INPRO	International Project on Innovative Nuclear Reactors and Fuel Cycles
ITL	integral test loop
KHNP	Korea Hydro & Nuclear Power Co. Ltd
LEU	low enriched uranium
LOCA	loss of coolant accident
LOCV	loss of condenser vacuum accident
LWR	light water reactor
MASLWR	multi-application small light water reactor
MHTS	main heat transport system
MSIV	main stem isolation valve
PAFS	passive auxiliary feed water system
PCCT	passive condensation cooling water tank
PFBR	prototype fast breeder reactor
PHWR	pressurized heavy water reactor
PIV	particle image velocimetry
PWR	pressurized water reactor
R&D	research and development
RCS	reactor coolant system
RPV	reactor pressure vessel
SBO	station blackout
TEM	transmission electron microscope

SYMBOLS

Latin alphabet

a	Amplification factor
A	Reference cross section in the loop
C_p	Heat capacity
f	Distributed friction coefficient
F	Force
g	Gravity acceleration
h	Enthalpy of the liquid
K	Localized friction coefficient
L	Length
$\dot{m}$	Coolant flow in the circuit
N_{PCH}	Phase change number
N_{Sub}	Subcooling number
P	Pressure at the steam dome
Q	Power
T	Temperature
v	Local fluid velocity
z	Refers to position within the loop

Greek letters

$\bullet$	Expansion coefficient
λ	Flashing-boiling boundary length
ρ	Density
χ	Thermo-dynamic equilibrium quality

Subscripts

0	Reference value
Cond	Refers to the condensation in the steam dome
Ch	Refers to the chimney section
e	Refers to exit location
fg	Refers to liquid vapour phase change
i	Refers to inlet location
L	Refers to liquid
Nuc	Refers to core section
Sat	Refers to saturation
SG	Refers to the steam generators
v	Refers to vapour

CONTRIBUTORS TO DRAFTING AND REVIEW

Beatty, R.	International Atomic Energy Agency
Choi, J.H.	International Atomic Energy Agency
Khartabil, H.	International Atomic Energy Agency
Kim, H.G.	Korea Hydro & Nuclear Power Co., Ltd, Republic of Korea
Kim, S.B.	International Atomic Energy Agency
Marcel, C.	National Atomic Energy Commission, Argentina
Meyer, L.	International Atomic Energy Agency
Park, P.H.	International Atomic Energy Agency
Vijayan, P.K.	Bhabha Atomic Research Centre, India

Consultants Meetings

Vienna, Austria: 10–11 November 2008, 10–11 November 2008,
5–6 November 2010, 5–6 December 2011.

IAEA
International Atomic Energy Agency

Where to order IAEA publications

In the following countries IAEA publications may be purchased from the sources listed below, or from major local booksellers. Payment may be made in local currency or with UNESCO coupons.

AUSTRALIA
DA Information Services, 648 Whitehorse Road, MITCHAM 3132
Telephone: +61 3 9210 7777 • Fax: +61 3 9210 7788
Email: service@dadirect.com.au • Web site: http://www.dadirect.com.au

BELGIUM
Jean de Lannoy, avenue du Roi 202, B-1190 Brussels
Telephone: +32 2 538 43 08 • Fax: +32 2 538 08 41
Email: jean.de.lannoy@infoboard.be • Web site: http://www.jean-de-lannoy.be

CANADA
Bernan Associates, 4501 Forbes Blvd, Suite 200, Lanham, MD 20706-4346, USA
Telephone: 1-800-865-3457 • Fax: 1-800-865-3450
Email: customercare@bernan.com • Web site: http://www.bernan.com

Renouf Publishing Company Ltd., 1-5369 Canotek Rd., Ottawa, Ontario, K1J 9J3
Telephone: +613 745 2665 • Fax: +613 745 7660
Email: order.dept@renoufbooks.com • Web site: http://www.renoufbooks.com

CHINA
IAEA Publications in Chinese: China Nuclear Energy Industry Corporation, Translation Section, P.O. Box 2103, Beijing

CZECH REPUBLIC
Suweco CZ, S.R.O., Klecakova 347, 180 21 Praha 9
Telephone: +420 26603 5364 • Fax: +420 28482 1646
Email: nakup@suweco.cz • Web site: http://www.suweco.cz

FINLAND
Akateeminen Kirjakauppa, PO BOX 128 (Keskuskatu 1), FIN-00101 Helsinki
Telephone: +358 9 121 41 • Fax: +358 9 121 4450
Email: akatilaus@akateeminen.com • Web site: http://www.akateeminen.com

FRANCE
Form-Edit, 5, rue Janssen, P.O. Box 25, F-75921 Paris Cedex 19
Telephone: +33 1 42 01 49 49 • Fax: +33 1 42 01 90 90
Email: formedit@formedit.fr • Web site: http://www. formedit.fr

Lavoisier SAS, 145 rue de Provigny, 94236 Cachan Cedex
Telephone: + 33 1 47 40 67 02 • Fax +33 1 47 40 67 02
Email: romuald.verrier@lavoisier.fr • Web site: http://www.lavoisier.fr

GERMANY
UNO-Verlag, Vertriebs- und Verlags GmbH, Am Hofgarten 10, D-53113 Bonn
Telephone: + 49 228 94 90 20 • Fax: +49 228 94 90 20 or +49 228 94 90 222
Email: bestellung@uno-verlag.de • Web site: http://www.uno-verlag.de

HUNGARY
Librotrade Ltd., Book Import, P.O. Box 126, H-1656 Budapest
Telephone: +36 1 257 7777 • Fax: +36 1 257 7472 • Email: books@librotrade.hu

INDIA
Allied Publishers Group, 1st Floor, Dubash House, 15, J. N. Heredia Marg, Ballard Estate, Mumbai 400 001,
Telephone: +91 22 22617926/27 • Fax: +91 22 22617928
Email: alliedpl@vsnl.com • Web site: http://www.alliedpublishers.com

Bookwell, 2/72, Nirankari Colony, Delhi 110009
Telephone: +91 11 23268786, +91 11 23257264 • Fax: +91 11 23281315
Email: bookwell@vsnl.net

ITALY
Libreria Scientifica Dott. Lucio di Biasio “AEIOU”, Via Coronelli 6, I-20146 Milan
Telephone: +39 02 48 95 45 52 or 48 95 45 62 • Fax: +39 02 48 95 45 48
Email: info@libreriaaeiou.eu • Website: www.libreriaaeiou.eu

JAPAN
Maruzen Company Ltd, 1-9-18, Kaigan, Minato-ku, Tokyo, 105-0022
Telephone: +81 3 6367 6079 • Fax: +81 3 6367 6207
Email: journal@maruzen.co.jp • Web site: http://www.maruzen.co.jp

REPUBLIC OF KOREA
KINS Inc., Information Business Dept. Samho Bldg. 2nd Floor, 275-1 Yang Jae-dong SeoCho-G, Seoul 137-130
Telephone: +02 589 1740 • Fax: +02 589 1746 • Web site: http://www.kins.re.kr

NETHERLANDS
De Lindeboom Internationale Publicaties B.V., M.A. de Ruyterstraat 20A, NL-7482 BZ Haaksbergen
Telephone: +31 (0) 53 5740004 • Fax: +31 (0) 53 5729296
Email: books@delindeboom.com • Web site: http://www.delindeboom.com

Martinus Nijhoff International, Koraalrood 50, P.O. Box 1853, 2700 CZ Zoetermeer
Telephone: +31 793 684 400 • Fax: +31 793 615 698
Email: info@nijhoff.nl • Web site: http://www.nijhoff.nl

Swets and Zeitlinger b.v., P.O. Box 830, 2160 SZ Lisse
Telephone: +31 252 435 111 • Fax: +31 252 415 888
Email: infoho@swets.nl • Web site: http://www.swets.nl

NEW ZEALAND
DA Information Services, 648 Whitehorse Road, MITCHAM 3132, Australia
Telephone: +61 3 9210 7777 • Fax: +61 3 9210 7788
Email: service@dadirect.com.au • Web site: http://www.dadirect.com.au

SLOVENIA
Cankarjeva Zalozba d.d., Kopitarjeva 2, SI-1512 Ljubljana
Telephone: +386 1 432 31 44 • Fax: +386 1 230 14 35
Email: import.books@cankarjeva-z.si • Web site: http://www.cankarjeva-z.si/uvoz

SPAIN
Díaz de Santos, S.A., c/ Juan Bravo, 3A, E-28006 Madrid
Telephone: +34 91 781 94 80 • Fax: +34 91 575 55 63
Email: compras@diazdesantos.es, carmela@diazdesantos.es, barcelona@diazdesantos.es, julio@diazdesantos.es
Web site: http://www.diazdesantos.es

UNITED KINGDOM
The Stationery Office Ltd, International Sales Agency, PO Box 29, Norwich, NR3 1 GN
Telephone (orders): +44 870 600 5552 • (enquiries): +44 207 873 8372 • Fax: +44 207 873 8203
Email (orders): book.orders@tso.co.uk • (enquiries): book.enquiries@tso.co.uk • Web site: http://www.tso.co.uk

On-line orders
DELTA Int. Book Wholesalers Ltd., 39 Alexandra Road, Addlestone, Surrey, KT15 2PQ
Email: info@profbooks.com • Web site: http://www.profbooks.com

Books on the Environment
Earthprint Ltd., P.O. Box 119, Stevenage SG1 4TP
Telephone: +44 1438748111 • Fax: +44 1438748844
Email: orders@earthprint.com • Web site: http://www.earthprint.com

UNITED NATIONS
Dept. I004, Room DC2-0853, First Avenue at 46th Street, New York, N.Y. 10017, USA
(UN) Telephone: +800 253-9646 or +212 963-8302 • Fax: +212 963-3489
Email: publications@un.org • Web site: http://www.un.org

UNITED STATES OF AMERICA
Bernan Associates, 4501 Forbes Blvd., Suite 200, Lanham, MD 20706-4346
Telephone: 1-800-865-3457 • Fax: 1-800-865-3450
Email: customercare@bernan.com · Web site: http://www.bernan.com

Renouf Publishing Company Ltd., 812 Proctor Ave., Ogdensburg, NY, 13669
Telephone: +888 551 7470 (toll-free) • Fax: +888 568 8546 (toll-free)
Email: order.dept@renoufbooks.com • Web site: http://www.renoufbooks.com

Orders and requests for information may also be addressed directly to:

Marketing and Sales Unit, International Atomic Energy Agency
Vienna International Centre, PO Box 100, 1400 Vienna, Austria
Telephone: +43 1 2600 22529 (or 22530) • Fax: +43 1 2600 29302
Email: sales.publications@iaea.org • Web site: http://www.iaea.org/books

13-08501

INTERNATIONAL ATOMIC ENERGY AGENCY
VIENNA
ISBN 978–92–0–139810–9
ISSN 1011–4289